

ANNUAL REPORT
JULY 1964

UNPUBLISHED PRELIMINARY DATA

ADHESION BETWEEN ATOMICALLY PURE METALLIC SURFACES PART III

By

D. V. KELLER, JR.

Associate Professor of Metallurgy

Department of Chemical Engineering & Metallurgy

W. M. FRANKLIN, JR., Research Assistant

D. HAUSER, Research Assistant

OTS PRICE

XEROX

MICROFILM

\$

\$

FACILITY FORM 102

N64-29217

(ACCESSION NUMBER)

(PAGES)

CR-58714

(NASA CR OR TRX OR AD NUMBER)

N64-29216

(THRU)

(CODE)

18

(CATEGORY)

Prepared for

NATIONAL AERONAUTICS AND SPACE ADMINISTRATION
OFFICE OF GRANTS AND RESEARCH CONTRACTS; CODE SC
WASHINGTON, D. C.
Grant No. NSG-483

SYRACUSE UNIVERSITY RESEARCH INSTITUTE

Department of Chemical Engineering and Metallurgy

Met. 1100-647A

FINAL REPORT

ADHESION BETWEEN ATOMICALLY PURE METALLIC SURFACES

PART III

Prepared For

National Aeronautics and Space Administration

Office of Grants and Research Contracts; Code CS

Washington, D.C.

Submitted by

Douglas V. Keller, Jr., Director

Wilbur Mitchell Franklin, Jr., Research Assistant

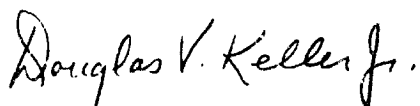
Daniel Hauser, Research Assistant

This report was produced under a sponsored contract. The conclusions and recommendations expressed are those of the Author(s) and are not necessarily endorsed by the Sponsor. Reproduction of this report, or any portion thereof, must bear reference to the original source and Sponsor.

SYRACUSE UNIVERSITY RESEARCH INSTITUTE

DEPARTMENT OF CHEMICAL ENGINEERING AND METALLURGY

Approved by:



Douglas V. Keller, Jr.
Project Director

Sponsored by:

N.A.S.A.
NsG-483

BRIEF

Enclosed in the following 1963-4 annual report to the National Aeronautics and Space Administration on the NSG-483 program at Syracuse University is one complete doctoral dissertation on the Surface Energy of Solid Silver (Part 1) and a portion of a master's thesis (Part 2). Since these two works comprise the two major efforts for the past year at Syracuse they are included in their entirety. The theoretical study and experimental data from the surface energy dissertation is to be presented to the open literature as a publication within the following year. Upon completion of the master's thesis, this work will also be published.

N64-29218

PART I

SURFACE ENERGY OF SOLID SILVER

by

Wilbur Mitchell Franklin, Jr.

(Doctoral Dissertation)

THE SURFACE ENERGY OF SOLID SILVER

by

Wilbur Mitchell Franklin, Jr.

B.A. - The College of Wooster, 1954

B.S. - Case Institute of Technology, 1957

M.S. - Yale University, 1962

ABSTRACT OF DISSERTATION

Submitted in partial fulfillment of the requirements for
the degree of Doctor of Philosophy in Solid State Science
and Technology in the Graduate School of Syracuse University,
July, 1964

Approved _____

Date _____

29218

ABSTRACT

A three dimensional atomic model of solid surfaces is developed and the origins of surface stress are explained. It is shown how the strain energy in solid surfaces can be incorporated into the equilibrium thermodynamic equations of surfaces. A relation between gradients of surface quantities is derived.

A new, direct experimental approach to the determination of surface energy of atomically clean surfaces was developed. The technique involves the evaporation in ultra-high vacuum of a solid sample to form a thin film of very large surface area. The surface area is measured by a physical adsorption (Brunauer, Emmett, Teller) technique. The surface energy is obtained from measurements of the energies of evaporation and condensation and from the surface area determination. The energy of condensation was measured in an isothermal liquid nitrogen calorimeter of new design. The technique applied to pure elemental silver yielded a surface energy value of 3500 ergs/cm^2 at 77°K .

auth

THE SURFACE ENERGY OF SOLID SILVER

by

Wilbur Mitchell Franklin, Jr.

B.A. - The College of Wooster, 1954

B.S. - Case Institute of Technology, 1957

M.S. - Yale University, 1962

DISSERTATION

Submitted in partial fulfillment of the requirements for
the degree of Doctor of Philosophy in Solid State Science
and Technology in the Graduate School of Syracuse University,
July, 1964

Approved _____

Date _____

TABLE OF CONTENTS

	Page
Acknowledgement	ii
List of Tables and Illustrations	iv
I. Introduction	1
II. Theory	3
A. Gibbs Surface	3
B. Surface Tension and Free Energy	4
C. Surface Stress and Atomic Spacing	9
D. Effects of Adsorbed Layers	28
E. Irreversible Processes and Equilibrium of Surfaces	34
III. Other Experimental Techniques	41
IV. Experimental Procedure and Systems Analysis	53
A. General Outline of Technique	53
B. Evaporation Procedure and Ultra-High Vacuum (UHV) Technique	57
C. Power Measurement System	65
D. Calorimeter System	69
E. Surface Area Measurement	74
V. Results and Discussion	79
VI. Conclusions and Recommendations	84
Appendices	
A. List of Symbols	86
B. Heats Involved in the Evaporation of the Silver Sample ...	89
Bibliography	92
Biographical Note	98

LIST OF TABLES AND ILLUSTRATIONS

	Page
Table 1 - Surface Tensions	43
Figures:	
1 - Gibbs Surface	5
2 - A Typical Two-body Potential Curve	12
3 - The Sum of Two-body Potential Curves for a Linear Chain of Three Atoms	14
4 - The Potential Energies of Atoms in a Finite Linear Chain	17
5 - Two Dimensional Lattice of a Finite Crystal Showing Displacements of Surface Atoms	18
6 - Three Effects on Spacing of Surface Atoms in a Section from the Middle of a Side of a Finite Two Dimensional Crystal Assuming Nearest and Next-Nearest Neighbor Interactions	19
7 - Tensor Components of Stress Vectors Acting in a Surface	23
8 - Region of a Crystal Near a Free Surface Showing Surface Traction	26
9 - Schematic of Entire Apparatus	58
10 - Filament Assembly Designs	59
11 - Diagrammatic Sketch of Ultra-High Vacuum System	62
12 - Power Measurement Apparatus	66
13 - Plots of Voltage, Amperage and Power Taken From an Experimental Run	68
14 - Liquid Nitrogen Calorimeter	71
15 - Gas Burette	73
16 - Surface Area Measurement Apparatus	77
17 - A Plot of the Energies Involved Versus Temperature in the Condensation of a Silver Film	90

Surfaces of solid condensed phases have great importance in many technologies and both the amount of research and the variety of models concerning surfaces are growing at an increasing rate. Often more information about crystals can be obtained from experiments on surfaces than from those dealing with the bulk of the crystal. The role of surface tension^{*} in the overall field of surfaces and interfaces is of paramount importance since it is a basic parameter of all surfaces.

To this date, no low temperature experimental determinations of the surface tension of atomically clean solid surfaces have been published. Generally, measurements of surface tension appearing in the current literature involved interfaces of the type solid-poor vacuum, inert gases, liquids, etc. Surface tension measurements utilizing the high temperature technique of field electron emission^{**} did study atomically clean surfaces. It would be possible to adapt some of the other experimental techniques to ultra-high vacuum and, thereby, obtain measurements for clean surfaces. The difficulties which might arise in such experiments are also discussed.

This study introduces a new experimental approach to the determination of surface tensions of solids and provides a critical survey of the other techniques currently in practice. An attempt is made to condense, unify, and extend some of the current and classical phenomenological descriptions of surfaces emphasizing thermodynamic and atomistic concepts rather than quantum mechanics. Since the experimental work involves the solid surface-vacuum interface, the scope of this study was

* See Section on Theory for definitions

**See Section on Other Experimental Techniques

limited in general to only this interface or to those concepts which are generally applicable.

The low temperature technique developed herein is applicable to a number of solid elements and compounds with differing degrees of amenability. The procedure consists of measuring the difference in the heats of evaporation and condensation of a metal in an isothermal calorimeter under conditions in which the area of the sample is several magnitudes smaller than that of the condensate. The change in area is then determined by standard Brunauer, Emmett, Teller (BET) techniques.

II. THEORY

The terminology used to describe surface parameters is extremely varied and often difficult to correlate with other uses of the same terms. In some cases a misunderstanding of concepts and definitions has led to confusion in the literature. This is particularly true of the terms, surface tension (γ), surface free energy (F_s) and surface stress ($\tau_{\mu\nu}$). Therefore, an attempt to consolidate and elucidate precise definitions of terms and concepts will be given here. The role played by point defects and dislocations in surface studies is certainly important but, since a good understanding of the defect free surface is required before attacking defect-surface interactions, the theory is generally limited to simple defect free surfaces.

A. Gibbs' Surface

The concept of surface quantities given by Gibbs (1) defines an excess quantity due to the presence of an interface between two bulk quantities such as phases or magnetic or electric domains. The bulk quantities are considered homogeneous throughout up to a region called the surface. A dividing surface which is a mathematical and conceptual convenience, may be chosen in the surface region somewhere between the two homogeneous bulk states to pass through all points having the same environment with respect to the adjacent matter. Thus, the dividing surface is a surface having no thickness which may separate the surface regions of two bulk phases. The location of the dividing surface is rather arbitrary and could be chosen, for example, for a solid-gas interface, as a surface outside the outermost layer of atoms in the solid in which the electron density is equal and homogeneous throughout.

For any extensive thermodynamic quantity, X , (such as energy, entropy, or volume of a system)

$$X = X_a + X_b + (X_a^s + X_b^s) \quad (1)$$

where X_a and X_b are bulk quantities for homogeneous bulk regions a and b extending through the volumes of regions a and b and through the surface regions on the a and b sides up to the dividing interface. X_a^s and X_b^s are the surface excess quantities which are due to the disturbed layers near the interface and are just the difference between the quantity, X , in the surface volume and the homogeneous quantities, X_a and X_b , in the surface region. For flat surfaces the surface region can be considered as a section of a cylinder or prism and for curved surfaces, as a frustrum of a cone or pyramid as shown in Figures 1a and 1b.

The beauty of Gibbs' definition lies in its simplicity and in the concept of the surface in terms of excess extensive quantities and of three dimensions. Nonetheless, unambiguous definitions of and distinctions between surface tension, free energy, stress, and atomic spacing require a more detailed examination of the system.

In the following, the normal to the surface will, in general, be considered the $|z|$ direction and a flat surface will lie in the $|xy|$ plane as suggested by Wood (2) in a discussion of surface crystallography.

B. Surface Tension and Free Energy

Consider first a one component system initially at chemical equilibrium and having no applied fields. Then the surface tension, γ , is defined (3) as an intensive quantity equal to the

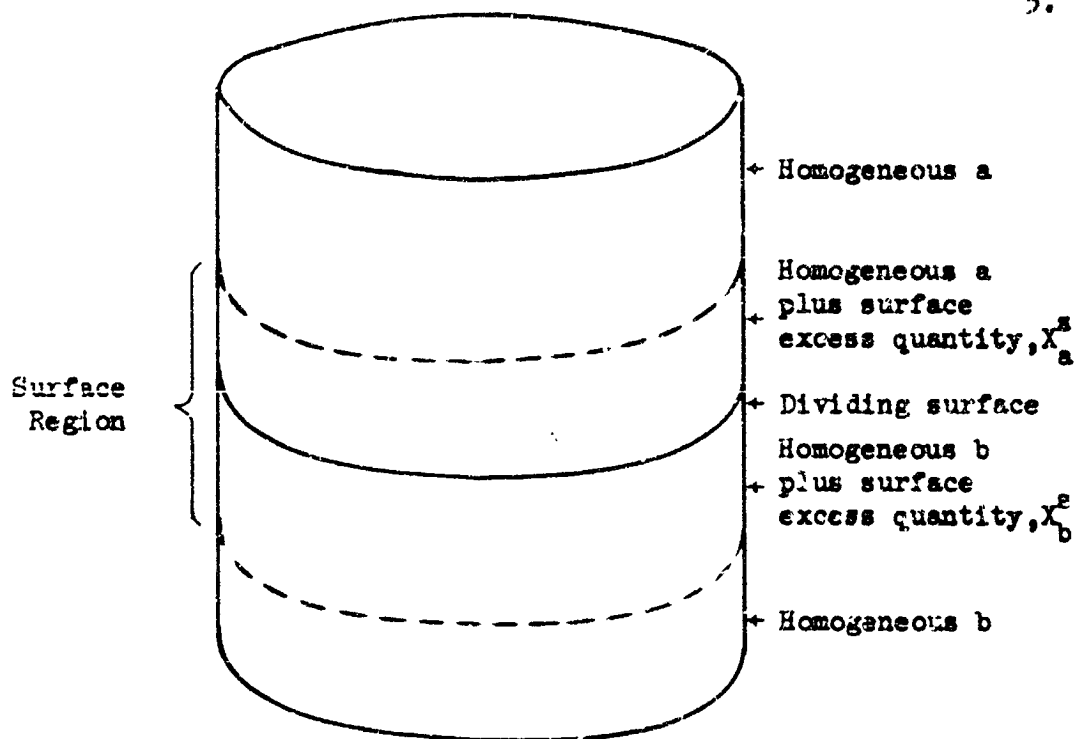


Figure 1a - Surface Excess Region Showing a Planar Dividing Surface

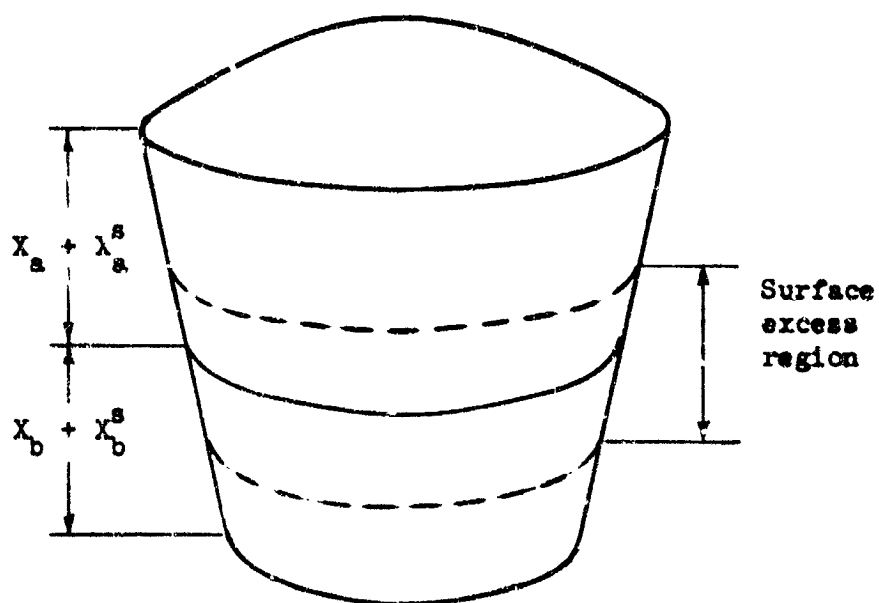


Figure 1b - Surface Excess Region Showing a Curved Dividing Surface

reversible work required to form a unit of new surface area from material in the bulk state under the constraints of constant temperature (T), volume (V), and chemical potential (μ)^{*}:

$$\gamma = \left(\frac{dW}{dA} \right)_{T,V,\mu} \quad (2)$$

where W = reversible work done and A = area. Thermal, pressure, and atomic reservoirs are needed to ensure constant temperature, volume, and chemical potential since all three of these quantities can change with respect to the bulk state during formation of new surface. Under these conditions for a one component system, surface tension and specific surface free energy (an intensive quantity) are equal:

$$\gamma = G_s = E_s - T S_s + P V_s \quad (3)$$

where G_s , E_s , S_s , P , and V_s are the specific surface Gibbs free energy, internal energy, entropy, pressure and volume respectively. These quantities represent differences between bulk and surface states for a number of atoms per unit area. The $P V_s$ term of Equation (3) is normally neglected as it is in Equation (2) since volume is generally considered constant and since, in actuality, the volume change in bringing an atom from the bulk state into the surface is probably quite small. This pressure is the ambient pressure above the surface and Frank (4) arrived at an order of magnitude value of the $P V_s$ term of about 10^{-2} ergs/cm² for atmospheric pressure. However, the pressure that an atom

^{*}cf., the section on Irreversible Processes and Equilibrium of Surfaces.

moving toward the surface of a solid is subjected to, includes the internal pressure in the surface stress system which may be considerably greater than atmospheric and possibly of a different sign. For example, the diagonal components of the stress tensor give the three possible internal pressures in the surface. The pressure perpendicular to the surface is affected by the external fluid pressure. Under certain circumstances, e.g. vacuum, the external pressure exerted on the surface may be effectually zero. In lattice thermodynamics the stress and strain due to internal forces constitute the strain energy and appear, therefore, in the internal energy of Equation (3). The external pressure needed to restore surface atoms to their bulk lattice positions is given by Kaplan (5) for a linear chain of atoms interacting by two-body potentials. For further discussion of this subject see the section, "Surface Stress and Atomic Spacing".

The variation of surface tension with crystallographic orientation has been studied rather exhaustively (6) and, therefore, further discussion, of this subject seemed unnecessary. Maximum variations of surface tension with orientation of 10% to 15% are commonly reported.

With the above idealized definition of γ in mind, the terminology used for surface quantities can now be clarified. Gibbs (1; p. 315), Herring (7; p. 8) and Mullins (3; p. 18) point out some of the ambiguities in the use of the term "surface tension" which is a scalar energy quantity in units of ergs/cm^2 . Surface tension is not a vector or a stress tensor quantity. Surface

stress is represented by a second rank tensor and is given in units of dynes/cm. Under certain circumstances, the surface stress can equal surface tension as pointed out later in the section "Surface Stress and Atomic Spacing". Specific surface free energy, G_s , is an energy per unit area term as is γ but can equal γ only under certain special conditions as stipulated below. Thus, for the general case, γ is neither a free energy nor a stress but under certain conditions can be equal in every way to the specific surface free energy and can be equal in magnitude to the surface stress, but not in units or in meaning.

Since E_s and S_s of Equation (3) represent differences in energy and entropy upon changing atoms from the homogeneous bulk state to the surface state as in an ideal cleavage (following the constraints stipulated in the definition of γ), the effect of preferential concentration of certain atomic species on the surface of compound crystals must also be accounted. If an ideal cleavage is performed on a compound crystal and, subsequently, atomic migration allowed to occur such that equilibrium in the system is attained, the atomic concentrations of surface atoms may be quite different from concentrations in the bulk due to the lowering of surface tension (1). Thus, in compound crystals and in crystals with adsorbed atoms or molecules:

$$\gamma = E_s - TS_s - \sum_i \mu_i \frac{N_i^s}{A} \quad (4)$$

where μ_i is the chemical potential of the i^{th} adsorbed species on the crystal and N_i^s/A are the changes from bulk concentration of

molecules on the surface.

If there is an adsorbed layer on the original sample, before forming the new surface area, the composition or electronic state of the surface may differ considerably from that of the bulk. That is, a chemical potential gradient or other gradient may exist between surface and bulk states such that there is a quasi-equilibrium situation^{*}. If the surface tension of the original sample is desired, the state of the newly formed surface must be identical to that of the original. Thus, reservoirs of atoms, electric fields, magnetic fields, etc. are necessary in the general case to ensure that chemical, electric, magnetic, and other potentials are identical in the newly formed surface. In a quasi-equilibrium situation the potential gradients perpendicular to the dividing surface must, therefore, remain constant throughout the experiment. Also, potential gradients parallel to the dividing surface must vanish for our definition of surface tension to hold. In addition to potential reservoirs, thermal and mass reservoirs are required to ensure constant temperature and volume, both of which may change slightly upon formation of new surface.

C. Surface Stress and Atomic Spacing

Surface tension, γ , was defined as the work required to form unit area of new surface under certain constraints while surface stress is defined by the work required to deform a surface parallel to the surface. Surface stress might be defined, at a particular point, more precisely, as the difference in stress

^{*}See section on Irreversible Processes and Equilibrium of Surfaces.

states between a point in the surface phase relative to a point in a standard state of zero stress in the bulk phase. For small deformations Hooke's law may be assumed such that stress is a linear function of strain; but for large deformations non-linear terms should be included (8). If the atoms in surface layers do not reside on the bulk lattice sites the surface stress would be equal to that applied stress necessary to remove the surface strain, e.i., to restore the surface atoms to their bulk lattice positions. It is important to realize that a surface stress will exist for a system in complete equilibrium having no external applied forces. The surface strain which we are considering here, is not plastic in nature, e.g. a layer of dislocations and, in addition, does not follow some of the usual concepts of elastic strain. In the fully annealed equilibrium state with no applied forces, a stress and strain will still exist.

Presentations of surface stress as a two dimensional quantity have been given by Herring (7,9), Shuttleworth (10), and Mullins (3). The spacings of surface atoms considering certain types of atomic interaction potentials have been studied by Lennard-Jones and Dent (11) and Kaplan (5). Since the many-body problem is a highly complex mathematical model and quite difficult to interpret, a consideration of the spacing of surface atoms in terms of two-body interaction potentials will provide some insight to the problem even though there are many inherent limitations to this technique.

Consider a crystal with no external or internal stress to be

an infinite lattice at equilibrium and homogeneous throughout. The introduction of a surface to this system will result in displacements of the atoms in and near the surface. The reasons are as follows: the removal of atoms constituting neighbors to the surface atoms and, consequently, their interaction potentials above the newly formed surface layers and, secondly, the modification of interaction potentials of the atoms within the surface layer. The stress corresponding to the displacement of atoms in and near the surface is the surface stress and may act both parallel and/or perpendicular to the surface and may include shears. In terms of bond strengths and electron densities, the electrons in the broken bonds at a surface may increase the electron density in adjacent bonds in the surface layer, if such electron states are available.

Since lattice strain energy can be formulated in terms of two-body potentials for many types of atomic bonding (12), we can consider the following equation in which the repulsive exponent, m , and attractive exponent, n , may vary with the type of bonding considered (e.g. ionic, metallic, covalent, etc.).

$$\phi(r) = \frac{a}{r^m} - \frac{b}{r^n} \quad (5)$$

This equation gives the potential energy of interaction, $\phi(r)$, between two atoms at a distance, r , and gives the equilibrium diatomic molecule spacing, r_2 , at $\frac{d\phi}{dr} = 0$ and $\frac{d^2\phi}{dr^2} > 0$. We are interested in the location of the nearest neighbor (NN) and next-nearest neighbor (nNN) atomic spacings in the bulk lattice and in surface layers on this potential curve, as shown in Figure 2.

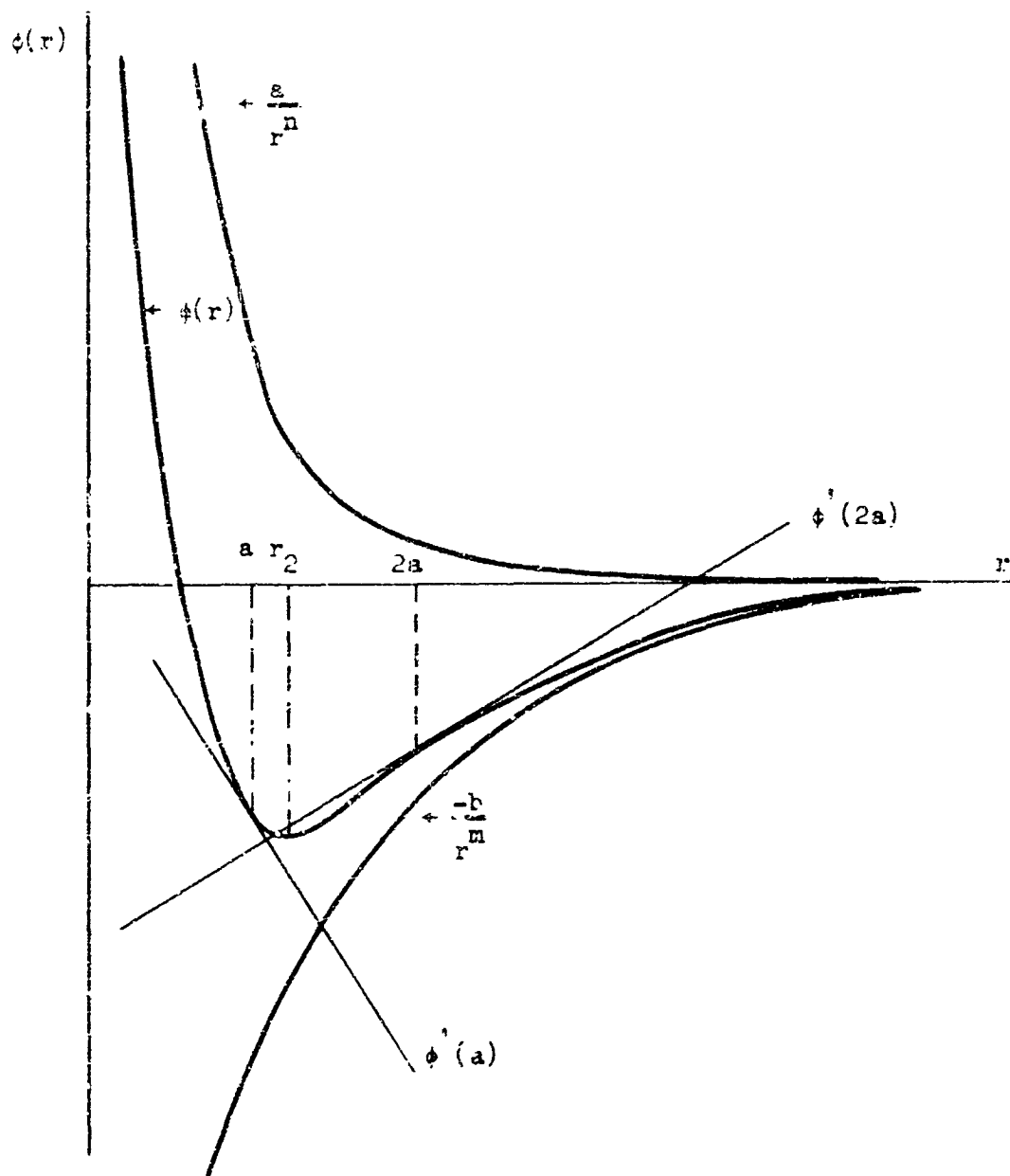


Figure 2 - A typical two-body potential curve, $\phi(r)$, and its repulsive (a/r^m) and attractive ($-b/r^n$) components showing the locations of equilibrium spacings in the diatomic molecule (r_2), and nearest neighbor (a) and next nearest neighbor ($2a$) distances well within a linear chain.

Lattice summations of any reasonable type of potential curve resembling that shown in Figure 2 show that the NN distance in a lattice is smaller than the atomic spacing in a diatomic molecule. This is obvious from consideration of Figure 3. If only NN and nNN interactions are considered here, the effect of adding a third atom to a diatomic molecule is to make the interatomic spacing smaller due to the positive slope of the nNN potential of the third atom such as atom C in Figure 3. In the triatomic molecule, the potential of each atom is the sum of two interaction potentials as shown in Figure 3. The sum of the two-body potentials gives a triatomic molecule spacing, $r_3 < r_2$. In many lattices only NN and nNN interactions are important and, hence, the analogy between the lattice interactions and the triatomic molecule is obvious. However, the same argument holds for more distant neighbor interactions. We have assumed here for simplicity that the two-body interaction potential curve does not change as more and more atoms are added to the diatomic molecule. However, this is obviously not true and a knowledge of a two-body potential within the matrix of a lattice or for an adsorbed atom on a surface would be much more useful.

In terms of two-body potentials Kaplan (5) demonstrated that the atoms at the ends of a linear chain are spaced very slightly farther apart than atoms in the bulk. This was accomplished using a new method accounting for the equilibrium pressure in a lattice. In the Born and Huang (13) formalism of lattice dynamics a relation for the pressure in lattice equilibrium is missing since, at

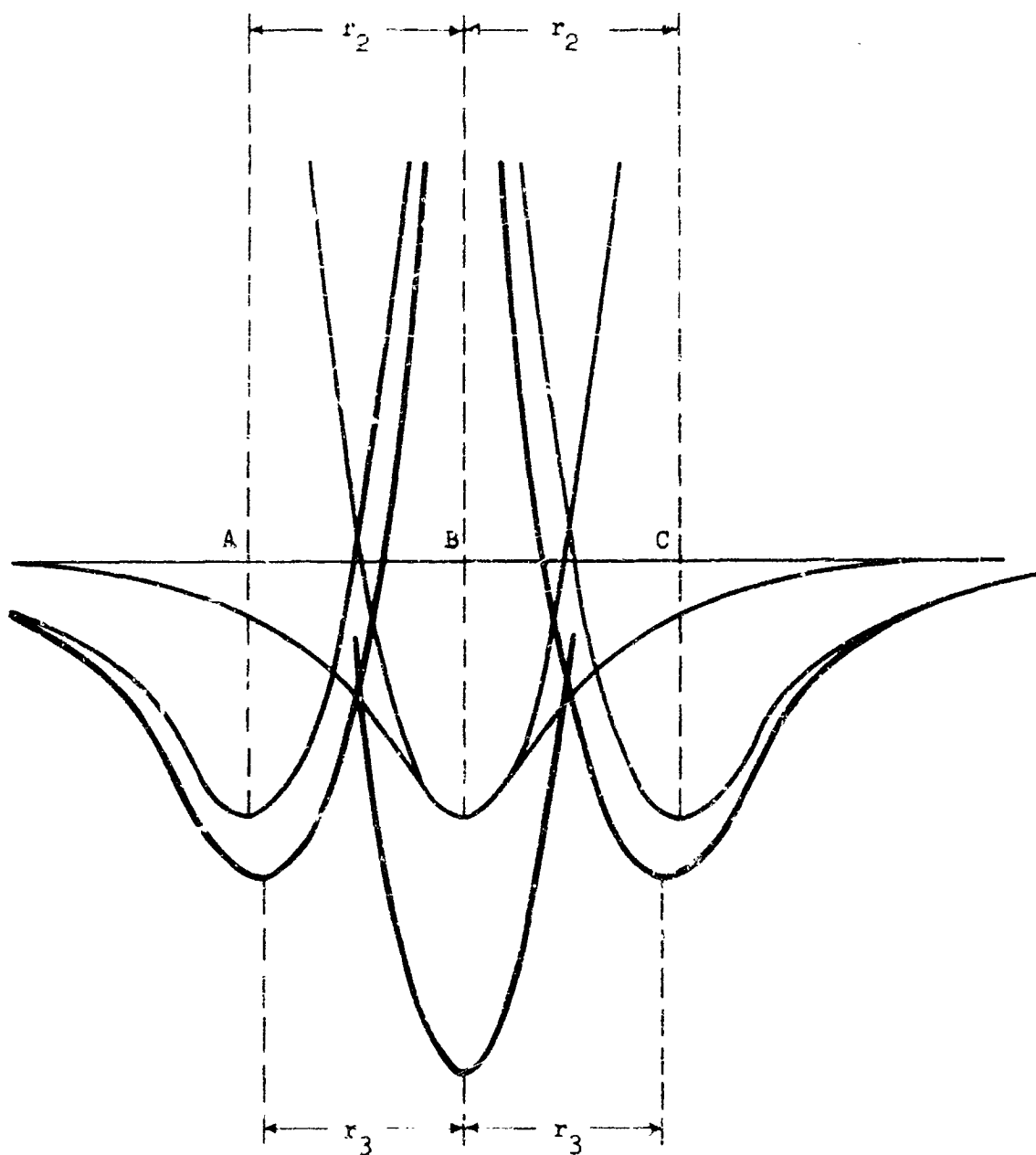


Figure 3 - The sum of two-body potentials for a linear chain of three atoms initially spaced at the diatomic molecule distance, r_2 . The new equilibrium spacing, r_3 , is less than r_2 . The light lines represent the four two-body potential curves and the heavy lines are the sums of these.

the equilibrium position in its potential well, an atom has no force acting on it as $(\frac{d\phi}{dr})_{r=a} = 0$ for a potential well exhibiting a minimum at the equilibrium lattice spacing. This difficulty was surmounted by using a potential where $(\frac{d\phi}{dr})_{r=a} \neq 0$ as for a diatomic molecule potential for a linear chain. Kaplan expands the two-body potentials for NN $\phi(X_n - X_{n-1})$ and nNN $\phi(X_n - X_{n-2})$ assuming small deformations so that a series expansion is valid:

$$\phi(X_n - X_{n-1}) = \phi(a) + K_1(X_n - X_{n-1}) + \frac{\lambda_1}{2}(X_n - X_{n-1})^2 \quad (6)$$

$$\phi(X_n - X_{n-2}) = \phi(2a) + K_2(X_n - X_{n-2}) + \frac{\lambda_2}{2}(X_n - X_{n-2})^2 \quad (7)$$

where X_n is the position of the n^{th} atom ($X_n = na + x_n$), a is the lattice spacing well removed from a surface, x_n is the displacement from the bulk lattice position of the n^{th} atom, and the force constants K_1 and K_2 are the first derivatives of the two-body potential curve at the NN and nNN distances respectively and λ_1 and λ_2 are the second derivatives $K_1 \equiv \phi'(a)$, $K_2 \equiv \phi'(2a)$, $\lambda_1 \equiv \phi''(a)$, $\lambda_2 \equiv \phi''(2a)$.

These force constants can be obtained from diatomic molecule potential curves. If they are assumed constant even for surface atoms, the displacement of atoms in a finite linear chain with no applied forces was derived by Kaplan as:

$$X_n - X_{n-1} \approx \left| \frac{(K_1 + K_2)}{\lambda_1} \right| (\lambda_2/\lambda_1)^{n-1} \quad (8)$$

The important aspect of this equation is that it shows that the

displacements of atoms from their equilibrium bulk values fall off extremely rapidly with distance from the surface. For instance, if we use realistic values for $\left| \frac{K_1 + K_2}{\lambda_1} \right| \approx 0.1a$ and $\left| \lambda_2/\lambda_1 \right| \approx 0.01$ for short range potentials, then the first, second, and third atoms in the linear chain are displaced by $0.1a$, $10^{-3}a$ and $10^{-5}a$ respectively from their bulk lattice sites. The obvious shortcoming of Equation (8) for crystals with strong bonding is that the force constants of surface atoms were assumed identical to those for bulk atoms. Even with this correction, the displacements within the chain approaches zero as $\left| \lambda_2/\lambda_1 \right|^n$ which is very rapid for short range potentials. For long range Coulombic potentials, important in ionic crystals, the extent of atom displacement is much deeper into the lattice (14). However, for metals it is expected that the displacements of surface atoms would be large enough to be observed only for the first atomic layer. The difficulty in determining the spacing of even the first layer of atoms is apparent from the conflicting reports of MacRae and Germer (15) and Farnsworth (16) utilizing low energy electron diffraction experiments.

Some simple examples will help to clarify the origin of surface stress and of the stress in layers immediately beneath the surface. Figure 4 shows a linear chain in which the first and second atoms of the chain have larger radii than the internal atoms. Figure 5 shows this situation for a two dimensional lattice in which the compression of the first two rows of surface atoms is obvious. Figure 6 portrays the two-fold origin of the

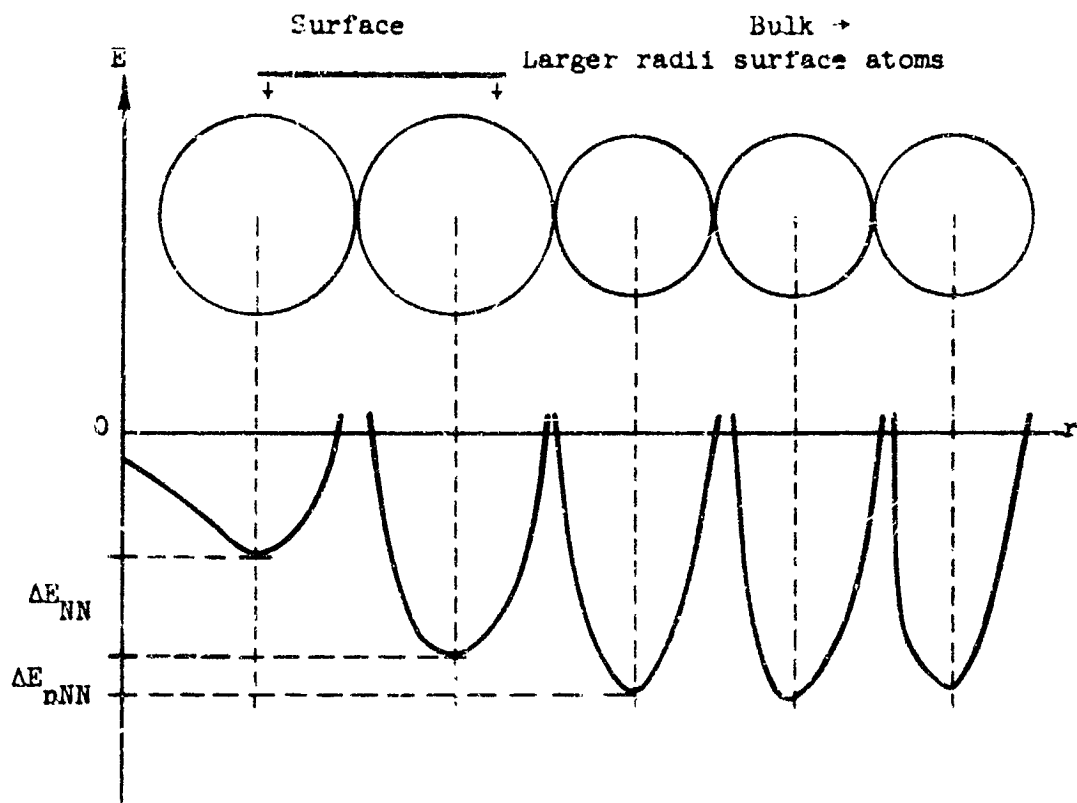


Figure 4 - The potential energies of the surface and bulk atoms are shown for NN and nNN interactions in a linear chain when $E = 0$ at infinite separation of atoms. The excess internal energy of the surface, E_s , is $\Delta E_{NN} + 2\Delta E_{nNN}$ plus the strain energy (see pp. 38 and 39).

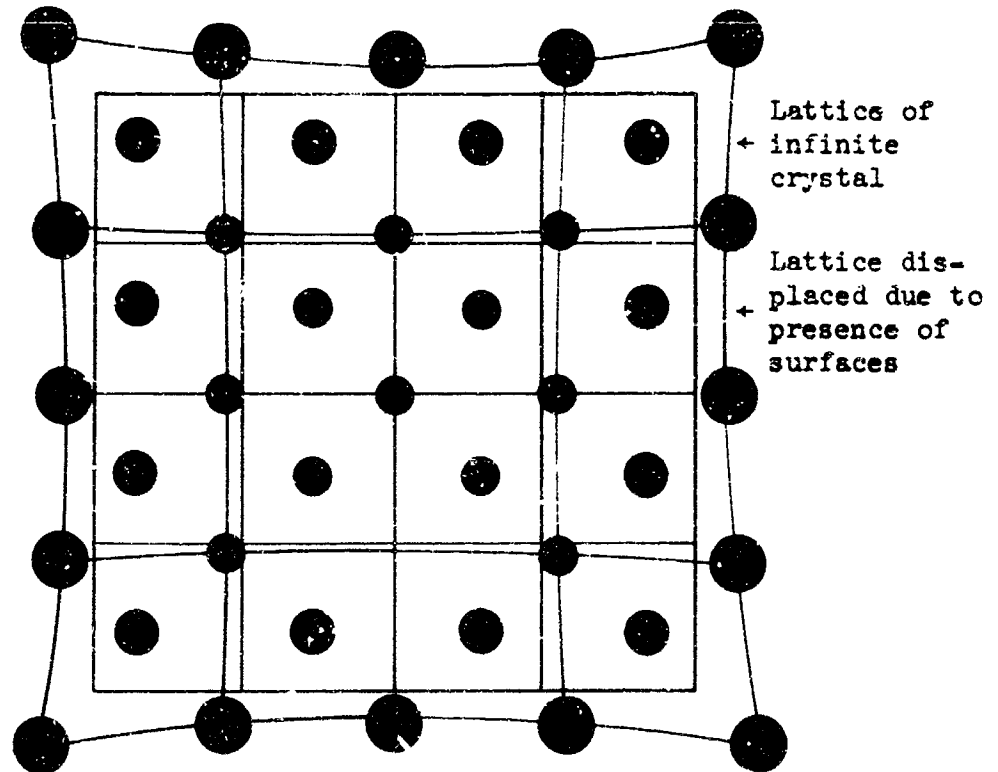


Figure 5 - Two dimensional lattice of a finite crystal showing displacements of surface atoms due to compression in first two rows resulting in tension in deeper rows assuming NN and nNN interactions. The forces in the first two layers are due to the missing interaction potentials and increased repulsion modifications of the force constants in the first two rows. Compare this with Figure 6d.

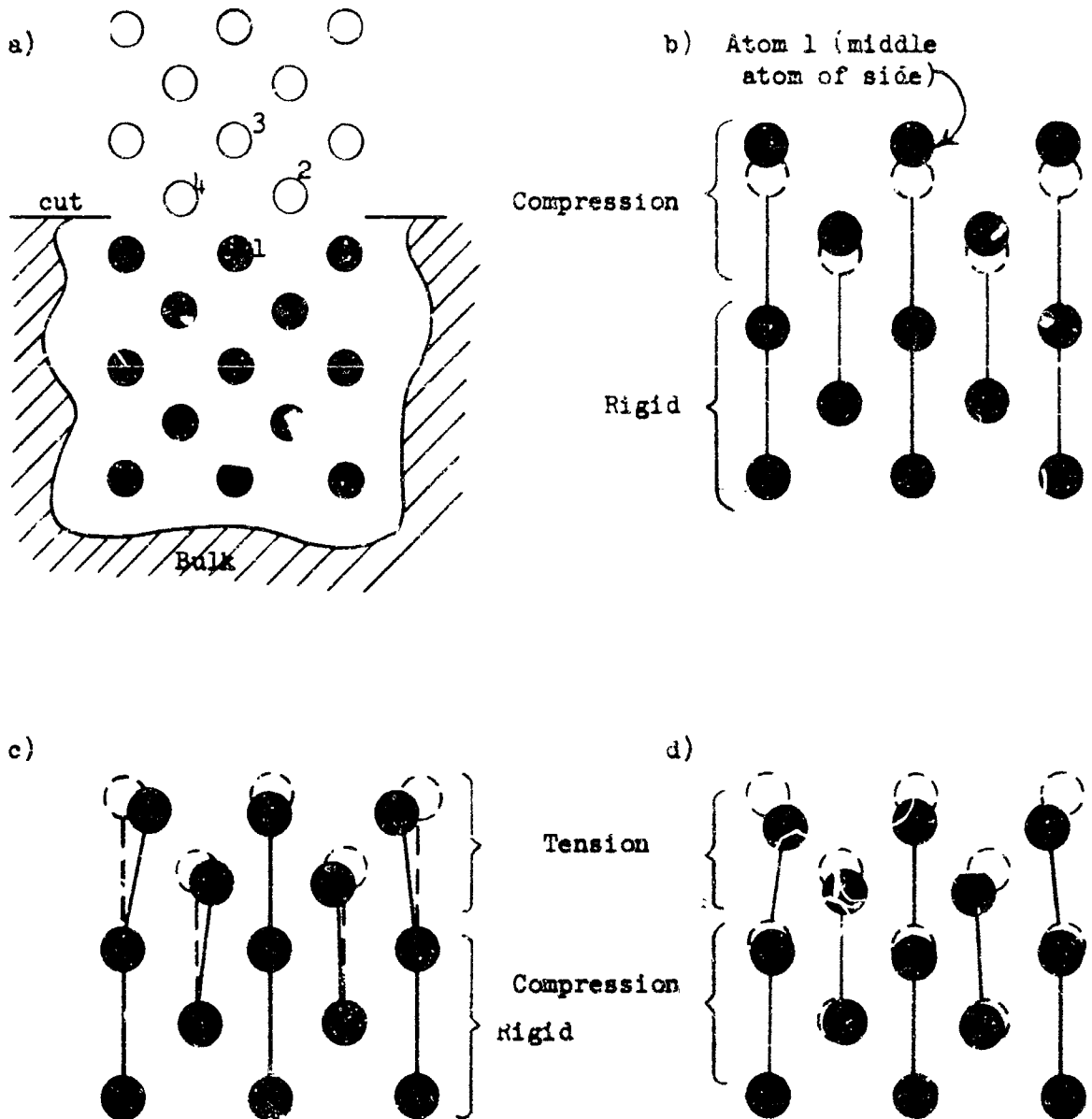


Figure 6 - Three effects on spacing of surface atoms in a section of a finite two dimensional crystal assuming NN and nNN interaction. a) Far from crystal sides showing location of cut to make surface shown in b), c) and d); b) Displacements of surface atoms due to the effect of the missing two-body interaction potentials above the surface; c) Displacements of b) plus those due to the effect of a modification of the two-body interaction potential for surface atoms giving larger attractions in the surface; d) Displacements of rows deeper than the first two due to stresses in the first two rows. In b) and c) the deeper rows were assumed rigid.

displacements of atoms in the immediate surface layers resulting in a net tension and of the displacements of deeper atoms caused by movement of the surface layers. Simultaneous reference to Figures 4-6 will aid in the explanation presented here. For most lattices other than ionic, NN and nNN interactions are sufficient to account for observable effects in atom spacing. For simplicity of portrayal, therefore, the effect of missing atoms above a surface is assumed to be "felt" only by atoms in the first and second layers. However, displacements of atoms in the first two layers due to forces upon them will cause movement of atoms in lower layers and this is portrayed in Figure 5 and Figure 6d. The forces on the first two layers are of two types mentioned above. Firstly, the effect of missing interaction potentials above a surface is to cause displacements in only the z direction for a lattice in which every atom is a center of symmetry. Referring to Figure 6a, the forces in the (xy) plane exerted on atom 1 by atoms 2 and 4 cancel each other so that removal of the NN atoms 2 and 4 and the nNN atom 3 can result in a force only in the (z) direction on atom 1. (This would not hold true, however, if each atom were not a center of symmetry). The result is a compressive force acting between the surface layers and a rigid bulk as depicted in Figure 6b. The surface layers are restrained by the bulk from expanding outwards as far as they would like to go and this effect actually causes a tension between atoms below the first two layers. The second effect on atoms in the immediate surface layers is the variation of the interaction potentials between atoms in the surface from

potentials in the bulk. This may be due to exchange interactions as a result of relaxation of broken surface bonds and results in alteration of electron densities within bonds in the surface layers and consequent changes in force constants. This can obviously result in forces within the (xy) plane as well as in the (z) direction as portrayed for tension in Figure 6c. Displacements of atoms in the first two layers due to the two effects mentioned are restrained by atoms in deeper layers. Consider a thin sheet two atoms thick having a larger atomic spacing in the (xy) plane than in the bulk. If this sheet is attached epitaxially to a bulk lattice substrate having bulk lattice atomic spacings, then the thin sheet will be in compression in the (xy) plane and the first few layers of the bulk will be in tension. This is the situation shown in Figures 5 and 6d for the third and deeper layers. It is interesting to note that displacements in the (xy) plane will be negligible because of the restraining force of the bulk for a semi-infinite crystal or for a large crystal face; and, measureable atomic strains in the (xy) plane are not expected except for the very smallest crystallites. This has been observed for Ni by MacRae and Germer (15). The (z) direction spacing of the first layer of (111) and (110) planes was found to be about 5% greater than bulk spacings (15). Farnsworth (16) has indicated, however, that these results may be in error and that surface layer spacing may be identical to bulk layer spacing. In Ge, Si, and diamond (17,18,19) the surface strain is inhomogeneous and consists of vertical displacements of a fraction of the surface atoms which has

been explained by Haneman (20). Surface stresses can be increased tremendously by such things as concentration gradients of impurities, point defects, and dislocations and by large curvatures. Therefore, although the stress in flat, perfect, atomically clean metallic surfaces may be small, the subject of surface stress is important.

From the above discussion it is obvious that a three dimensional stress tensor is needed for surface atoms. Assuming continuum linear elasticity theory and following the notation of Sokolnikoff (21) we can write the stress vectors \vec{T}_x , \vec{T}_y and \vec{T}_z acting the x, y, and z planes at a point in terms of components:

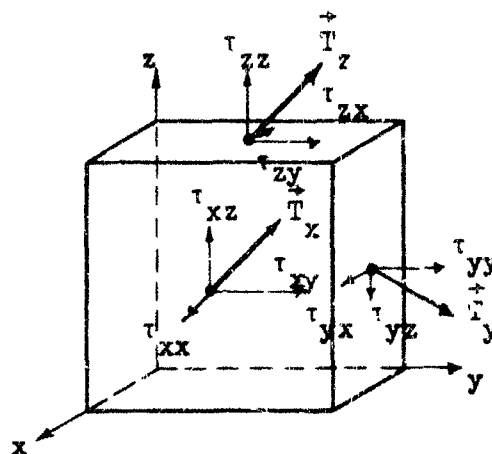
$$\begin{aligned}\vec{T}_x &= \vec{i} \tau_{xx} + \vec{j} \tau_{xy} + \vec{k} \tau_{xz} \\ \vec{T}_y &= \vec{i} \tau_{yx} + \vec{j} \tau_{yy} + \vec{k} \tau_{yz} \\ \vec{T}_z &= \vec{i} \tau_{zx} + \vec{j} \tau_{zy} + \vec{k} \tau_{zz}\end{aligned}\tag{9}$$

where \vec{i} , \vec{j} , and \vec{k} are unit vectors along the axis and τ_{ij} are the components of the stress tensor. The situation is portrayed graphically in Figure 7a. Note that the stress vectors, \vec{T}_i , have units of force/area but that the relations in Equation (9) can apply at a point. Using the Einstein summation convention Equation (9) can be written:

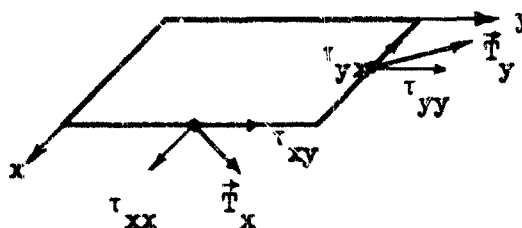
$$T_i = \tau_{ij} q_j\tag{10}$$

where $q_j = \vec{i}, \vec{j}, \vec{k}$. Applying the equilibrium conditions the stress tensor becomes symmetric and $\tau_{ij} = \tau_{ji}$ reducing the number of

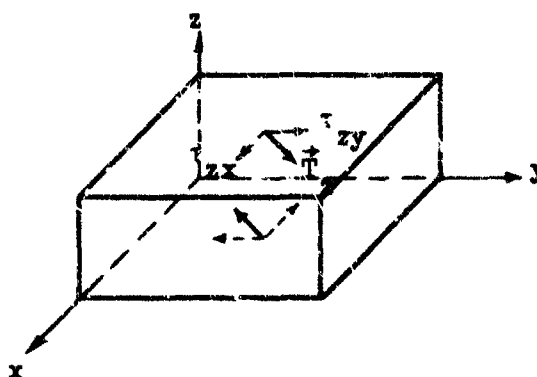
Figure 7



- a) Force vectors \vec{T}_i acting on x, y, z planes and broken into components portraying the usual 3-D stress tensor τ_{ij} .



- b) Two dimensional stress vectors, \vec{T}_i , and tensor, τ_{ij} .



- c) Rotation couple in Equation (12) which must vanish for equilibrium (see Sokolnikoff, p. 5).

independent components from nine to six. The planar two dimensional stress vectors acting on line elements can be written for planes perpendicular to z :

$$\begin{aligned}\vec{T}_x &= \vec{i} \tau_{xx} + \vec{j} \tau_{xy} \\ \vec{T}_y &= \vec{i} \tau_{yx} + \vec{j} \tau_{yy}\end{aligned}\tag{11}$$

and is portrayed in Figure 7b. The surface stress tensor, g_{ij} , of Herring (7,9) reduces to the above when the equilibrium conditions are applied. Because of possible misconceptions this will be clarified. Herring considered that forces could act in all three directions on line elements x and y in a surface perpendicular to z . Thus, his stress tensor for the surface, g_{ij} , allows $i = x, y, z$ and $j = x, y$, and the stresses on unit line elements can be written:

$$\begin{aligned}\vec{T}_x &= \vec{i} g_{xx} + \vec{j} g_{xy} \\ \vec{T}_y &= \vec{i} g_{xy} + \vec{j} g_{yy} \\ \vec{T}_z &= \vec{i} g_{zx} + \vec{j} g_{zy}\end{aligned}\tag{12}$$

The components g_{zx} and g_{zy} acting on a z (xy) plane could just as well be included in g_{xx} and g_{yy} respectively and, therefore, would be redundant. Also, if the components of g_{ij} are considered as acting on a three dimensional body, then g_{zx} and g_{zy} would have to vanish in order to satisfy the equilibrium conditions as portrayed in Figure 7c. Otherwise, a rotational couple would

exist which could accelerate the body. The point of the above discussion is that, to avoid confusion in surface stress, it appears best to utilize ordinary three dimensional elasticity theory.

Following the notation and argument of Herring (9) we can briefly relate the stress tensor, $\tau_{\mu\nu}$, to the surface tension, γ . We shall now use the three dimensional form of the stress tensor and arrive at an expression similar to that given by Herring for the relation between surface stress and tension. Consider the stress vectors of Equation (9) applied to a surface of a homogeneous body as a surface traction as shown in Figure 8 for an arbitrary direction. The surface stress acts through some depth, h , as shown in Figures 5 and 6; and, if an average over h is taken, homogeneous stress can be assumed. The surface traction is counterbalanced by body forces, which extend to some depth, d . An equation of equilibrium is then:

$$\vec{T}_\mu = \int_0^{z=h} \sum_\nu \tau_{\mu\nu} q_\nu dz = - \int_0^{z=d} \sum_\nu p_{\mu\nu} q_\nu dz \quad (13)$$

where q_ν are the three components of a unit vector, \vec{q} , normal to the x , y , and z faces, and $p_{\mu\nu}$ are the components of a bulk stress tensor. The bulk and surface stress tensors are assumed homogeneous throughout their respective depths and, therefore, Equation (13) can be integrated to yield:

$$\sum_\nu \tau_{\mu\nu} q_\nu h = - \sum_\nu p_{\mu\nu} q_\nu d \quad (14)$$

or

$$\tau_{\mu\nu} h = - p_{\mu\nu} d$$

noting that the coefficients of q_ν must vanish separately. Now we

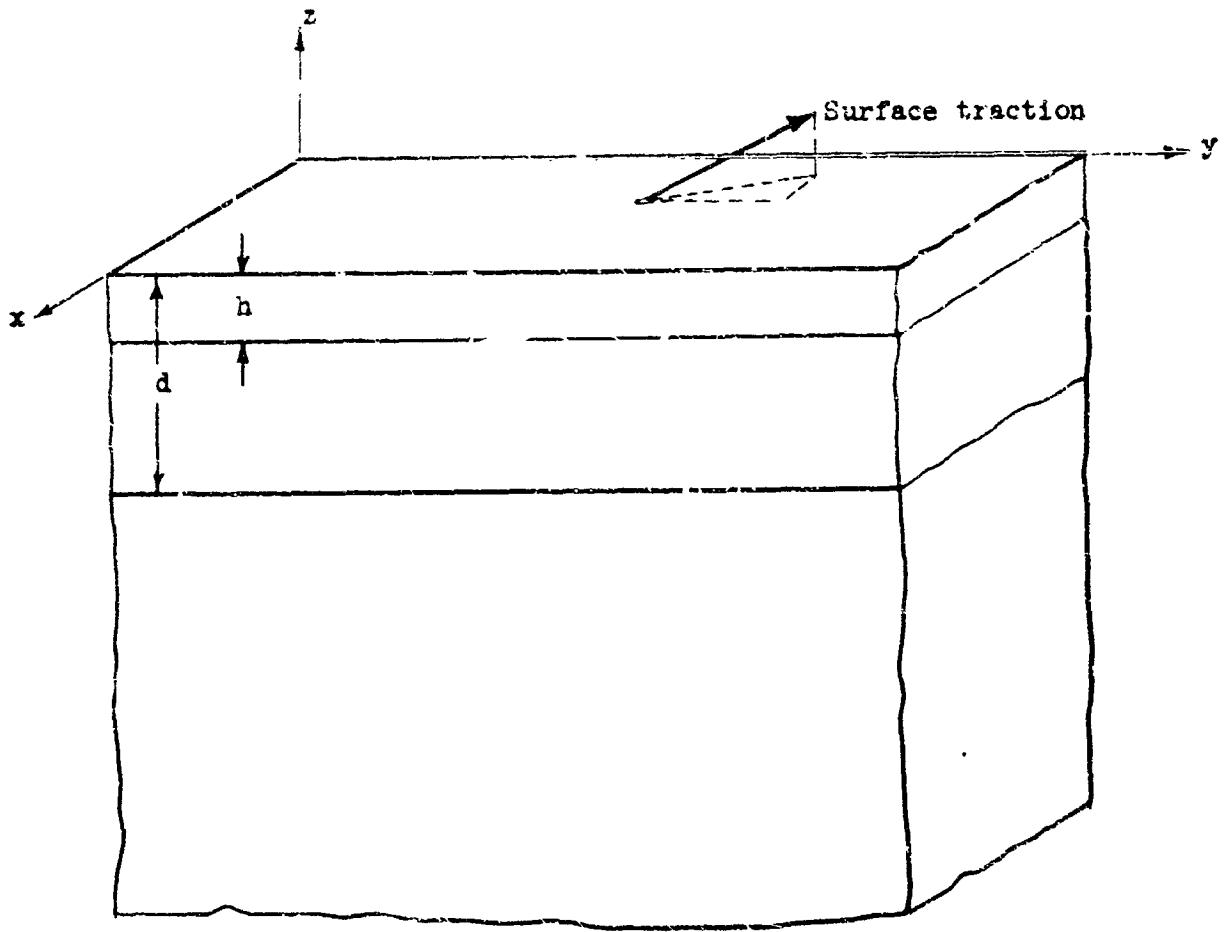


Figure 8 - Region of a crystal near a free surface showing a surface traction and the depths of surface stress, h , and counterbalancing body stresses, d .

can consider the changes in bulk and surface free energy due to the application of an arbitrary strain. If the strain tensor is denoted by $u_{\mu\nu}$, the strain energy is given by $\frac{1}{2} \sum_{\mu,\nu} p_{\mu\nu} u_{\mu\nu}$ for the bulk stress per unit volume and we can write for any virtual deformation:

$$\frac{Ad}{2} \sum_{\mu,\nu} p_{\mu\nu} u_{\mu\nu} = - \frac{Ah}{2} \sum_{\mu,\nu} \tau_{\mu\nu} u_{\mu\nu} \quad (15)$$

using Equation (14). This is the strain energy due to homogeneous virtual deformations.

In order to conform with a three dimensional stress tensor, we can also define a three dimensional surface tension, γ , in units of ergs/cc. With this definition the surface free energy is γAh and the change in surface free energy with strain is:

$$\sum_{\mu,\nu} \frac{\partial(\gamma Ah)}{\partial u_{\mu\nu}} u_{\mu\nu} = Ah \sum_{\mu,\nu} \frac{\partial\gamma}{\partial u_{\mu\nu}} u_{\mu\nu} + \gamma h \sum_{\mu,\nu} \frac{\partial A}{\partial u_{\mu\nu}} u_{\mu\nu} + \gamma A \sum_{\mu,\nu} \frac{\partial h}{\partial u_{\mu\nu}} u_{\mu\nu} \quad (16)$$

Now the changes in scalar and strain free energy with strain are equal and using Equations (15) and (16) we can write:

$$\frac{Ah}{2} \sum_{\mu,\nu} \tau_{\mu\nu} u_{\mu\nu} = Ah \sum_{\mu,\nu} \frac{\partial\gamma}{\partial u_{\mu\nu}} u_{\mu\nu} + \gamma h \sum_{\mu,\nu} \frac{\partial A}{\partial u_{\mu\nu}} u_{\mu\nu} + \gamma A \sum_{\mu,\nu} \frac{\partial h}{\partial u_{\mu\nu}} u_{\mu\nu} \quad (17)$$

or, noting that the coefficients of each $u_{\mu\nu}$ in the sum must vanish separately:

$$\tau_{\mu\nu} = 2 \frac{\partial\gamma}{\partial u_{\mu\nu}} + \frac{2\gamma}{A} \frac{\partial A}{\partial u_{\mu\nu}} + \frac{2\gamma}{h} \frac{\partial h}{\partial u_{\mu\nu}} \quad (18)$$

Equation (18) gives us a relation between the scalar three dimensional surface tension, γ , and the three dimensional stress tensor,

$\tau_{\mu\nu}$. Both of these quantities will vary with distance perpendicular to the surface and both are excess quantities to a depth h .

In very small KCl crystals Walton (22) has shown that the surface energy, γ , can be more than one and one half times the surface energy of a semi-infinite crystal using a lattice sums technique. This is due to the fact that the ionic displacements of many of the ions in very small crystals are quite large because of their proximity to corners (see Figures 5 and 6). This provides a very graphic example of the inter-relation between surface energy and surface strain (and stress) as well as the importance of a three dimensional picture of the surface.

D. Effects of Adsorbed Layers

The effects of adsorbed layers on solids and of solid surfaces on two dimensional equations of state of the adsorbed films have received much experimental and theoretical attention in the last 30 years. Only recently, however, has there been direct experimental evidence concerning adsorption of less than a monolayer on clean surfaces. From this evidence a true picture of real surfaces is being developed. In this section the Gibbs' adsorption equation is discussed and the status of development of adsorption isotherm equations is reviewed. The effects of an atomic model of a dynamically varying surface on adsorption are also discussed.

Sorption in general includes both ab- and adsorption; the former defines solution of foreign atoms within the bulk lattice and the latter concerns those atoms limited to a layer on the surface. It is important to realize that many sorbed species are

soluble in the substrate material and diffuse into it - the solubility depending on chemical affinity, temperature, pressure, entropy considerations, etc. (cf. 23). The simplified picture of uniform homogeneous adsorption is evidently far from reality in most cases as exemplified by low energy electron diffraction studies showing adsorption of oxygen on alternating rows of surface nickel atoms and consequent raising of rows of metal atoms (24) and by field electron emission studies of inert gases adsorbed on refractory metals which show nucleated clusters of adsorbed atoms on high index crystal faces of the emitter tips (25,26).

The universal decrease of surface tension of a pure solid (or liquid) phase due to adsorption of foreign gas atoms on the surface is exemplified by the Gibbs adsorption equation (1,27):

$$\pi = \gamma_0 - \gamma(p) = kT \int^p \Gamma(p) d \ln p \quad (19)$$

where γ_0 is the surface tension of the atomically clean solid and γ is the surface tension after adsorption and equilibration of gas at pressure, p . $\Gamma(p)$ is surface concentration expressed as number of adsorbed molecules per unit area, N/A . $\Gamma(p)$ may also be expressed by $\Gamma(\theta) = \frac{1}{\sigma} = \frac{\theta}{\sigma_0}$ (28) where α is the area per molecule at fractional surface coverage, θ , and σ_0 is the limiting area per molecule at complete monolayer coverage. For Equation (19) to apply to a system the following must be true or assumed:

- 1) equilibrium between adsorbed molecules and gas molecules
- 2) constant temperature
- 3) the chemical potentials of the gas and adsorbed molecules are equal
- 4) the gas is ideal so that $\mu(\text{gas}) = \mu(\text{adsorbed molecules}) = RT d \ln p$

It is questionable that all of these constraints can be satisfied in many adsorption experiments. Assuming that they can be, however, the adsorption isotherm obtained experimentally and relating the surface coverage, θ , to pressure, p , can be integrated graphically to obtain values for π at various pressures. Olivier and Ross (28) have done this for argon adsorption on carbon black at 90.1°K and compared the result with those obtained using isotherm equations such as the Langmuir and Volmer equations. The important thing to note here is that the Gibbs equation provides a good test for various theoretical isotherm equations since, if the listed assumptions hold, the Gibbs equation can be evaluated accurately by graphical analysis and then compared with the results obtained using theoretical isotherms. As an example, substitution of the Brunauer, Emmett, and Teller (29) isotherm into the Gibbs equation gives an infinite value for π at the saturated gas pressure as discussed by Hill (27). The status of development of isotherm equations leaves much to be desired in their applicability to the Gibbs adsorption equation.

The generalized Gibbs equation (1)

$$d\gamma = -S_g dT - \sum_1 \Gamma_1 du_1 \quad (20)$$

is applicable to any interface between phases at equilibrium and must, therefore, be applicable to non-ideal gases, to both physical and chemical adsorption and to all possible interfaces between condensed phases and between a condensed and gaseous phase. In the case of strong chemisorption on clean metal surfaces it would seem difficult to obtain p - θ adsorption isotherms at

coverages of less than a monolayer since almost every atom striking the clean surface would be expected to stick. However, both adsorption and desorption of gas atoms is thought to involve a multiple phonon interaction so that, even at fairly low temperatures, desorption of strongly bound atoms is possible as suggested by Ehrlich (25). Further experimental work is needed concerning the effects of less than a monolayer of chemisorbed molecules on the surface tension of initially clean surfaces in order to evaluate the Gibbs adsorption equation.

The general process of adsorption has been described by Ehrlich (25) and by Hirth and Pound (30) and is summarized briefly here. The attraction of an incoming molecule by a surface depends on the potential energy well at the surface and on the polarizabilities of both the surface and incoming atom. The direction and speed (temperature) of the incoming molecule affect sticking probability such that, for a perfectly flat surface, molecules of certain energies and angles of incidence may be specularly reflected or adsorbed. The energy of the incident molecule must be dissipated by the lattice; otherwise, elastic reflection will occur. The molecule may or may not be dissociated at some stage in the adsorption process. The energy is dissipated by molecular dissociation and production of a single or multiple phonons depending on the gas molecules' energy and on the phonon energies available in the lattice. After an atom is adsorbed, it may remain in an excited vibrational state within its potential well and continue to dissipate phonons until equilibrated thermally with the lattice or it may diffuse, which is the more likely possibility if the

potential energy well is not too deep. If adsorption occurs initially on a flat surface, subsequent surface diffusion to more stable corner or ledge sites will increase the probability of the atom's sticking. Otherwise, re-evaporation may occur due to interaction with one or more lattice phonons before a more stable site is reached. The stability and, hence, heat of adsorption of an atom on a surface depends on both vertical (gas atom - surface) interactions and on horizontal (gas atom - gas atom) interactions. Because of the horizontal interactions and the higher stability on rough surfaces, nucleation and growth processes of clusters of adsorbed atoms are important. Moazed and Pound (31) and Duell and Moss (32) have observed the nucleation and growth of silver crystallites on tungsten field emitter tips and noted preferential growth on high index (rough) lattice planes. The fact that thin films deposited from the vapor onto low temperature substrates have very high surface areas (33) may be explained for polycrystalline substrates on the basis of the nucleation and growth of very small crystallites and their inability to coalesce due to low surface diffusion at low temperatures (see Swaine and Plumb (34)). The above description is important in the understanding of the thin silver films produced in this study for the determination of surface tension.

Since the surface tension is decreased by adsorbed layers, it is important to know the status of the initial surface such as its temperature, ratio of ledge to flat surface sites, surface defect concentration, state of strain, etc. in order to assess the amount of decrease in surface energy for each effect. This has

not been done for atoms adsorbed on silver and only a very rough estimate can be obtained. Allen (35) has reported an approximate heat of adsorption of oxygen on silver of 10.5 kcal per gram-atom showing that silver is a relatively inert metal since this adsorption energy is close to the range usually designated for physical adsorption (less than 10 kcal per gram-atom). This is larger than the heat of formation of Ag_2O (6.7 kcal/gm atom) and, thus, follows the general observation that heats of adsorption are larger than heats of formation of the compound (36). This is evidently due to the fact that the surface is in a highly reactive state such that its energy can be reduced more than the bulk by chemical reaction.

The existence of electrically charged surface layers should be mentioned since the dipole or double layer of a clean surface is modified by adsorbed layers. The existence of surface dipoles on clean surfaces is due to two effects as explained by Herring (37). In the first place, the electron density may tend to "spill out" into the surrounding vacuum and secondly, the electrons in a surface may tend to fill in the valleys between surface ions thus leaving protruding positive ions with negative valleys between them (with respect to the bulk lattice). In the adsorption of an atom on the surface, dispersion forces are always active and tend to redistribute the electronic charge, even for inert atoms, due to the Hellmann-Feynman theorem (38,39). Very large changes in work function have been observed (see Ehrlich (25)) for adsorption of inert gases on tungsten thus indicating substantial changes in electron density distribution which has normally been unexpected for physical adsorption. In chemical adsorption, on the other

hand, it has long been known that the electron density tends to concentrate in the adsorbed atom or in the surface thus forming dipoles with the negative or positive side, respectively, outward (40).

E. Irreversible Processes and Equilibrium of Surfaces

An interface region between two homogeneous bulk phases constitutes an inhomogeneous layer even when complete equilibrium exists. When a non-equilibrium status exists, as is commonplace in surface studies, irreversible flows must occur to attain equilibrium. In this section the status of surfaces at equilibrium is considered as well as the flows involved in irreversible processes. A typical example of a non-equilibrium situation is the case of an adsorbed surface layer. Irreversible diffusion of the adsorbed atoms into the substrate can take place if the temperature is sufficiently high. This inward diffusion will continue until equilibrium is attained; i.e. until the bulk concentration is homogeneous and until the system energy is at a minimum with respect to any virtual change of system variables between the surface and bulk states at constant temperature. The important variables to be considered here are the gradients of the intensive quantities such as concentration, stress, temperature, electrochemical potential, and the densities of energy and entropy.

It is important to realize that all of the above gradients except that of temperature may exist at complete thermal equilibrium between surface and bulk phases. Cahn and Hilliard (41) and Hart (42) have analysed the thermodynamics of inhomogeneous systems emphasizing surface considerations. The conditions for

equilibrium obtained by Hart show how the chemical potentials, concentrations, first and second derivatives of concentration and the pressure depend on each other and how they vary with position in a system having stipulated boundary conditions. Their analysis can include all possible internal and experimental variables for fluids or "fully equilibrated" solids with no applied electromagnetic fields. They considered the situation, therefore, when the stress tensor reduced to hydrostatic pressure at equilibrium and did not include electromagnetic potentials. It would be interesting to extend their arguments for anisotropic solids at temperatures where diffusion could not relieve the non-hydrostatic stresses in reasonable lengths of time and to include the effects of electric and magnetic fields.

If a state of quasi-equilibrium for solids and viscous fluids can be defined for temperatures where atomic diffusion is negligible, then the system variables other than concentration and concentration derivatives can attain equilibrium with respect to each other and the boundary conditions (i.e. temperature, total masses, and state of strain). In this case, the equilibrium thermodynamics of inhomogeneous systems can be applied keeping in mind that irreversible flows of matter will occur if the temperature is raised sufficiently high.

The scope of irreversible thermodynamics concentrates on flows or currents due to forces or affinities and their interdependence and, therefore, the conditions at a point within the system can be described by the steady state or time dependent formalisms depending on the boundary conditions. As an example,

the irreversible mechanisms operative in the condensation of a thin film from the vapor onto a surface containing planar, ledge, and corner sites (see the preceding section) could include net atomic fluxes toward ledge and corner sites because of their greater stability, heat flow away from the surface, current flow if ions are deposited, and the establishment of charge and stress gradients due to the concentration gradient set up by the deposited layer. If thermal equilibrium is subsequently established such that evaporation and condensation rates are equal and no net flows exist between surface, bulk, and gas phases, then equilibrium thermodynamics (thermostatistics) can be applied even though an extremely high concentration gradient may exist between the adsorbed layer and substrate.

Utilizing the arguments of irreversible thermodynamics (43,44) we can show how the forces and fluxes in surfaces are related and, if the fluxes vanish, how gradients may remain and balance each other. A comprehensive analysis of irreversible processes including both chemical and electric potentials has been given by deGroot and Tolhoek (45). Since their arguments are applicable to surfaces and to solids we can utilize their results and extend them to describe surface phenomena.

In the general case, they treated a system in which the irreversible processes of diffusion, electric conduction, heat conduction and a number of chemical reactions could take place. An electrochemical potential, $\tilde{\mu}_k$, is considered to be the sum of a chemical, μ_k , and electric, $e_k \phi$, part for the k^{th} component:

$$\tilde{\mu}_k = \mu_k + e_k \phi \quad (21)$$

The external force, \vec{F}_k , acting on the k^{th} component consists of an electric force, $-e_k \text{ grad } \phi = -e_k \vec{E}$, and a non-electrical part, \vec{F}_k^{ne} :

$$\vec{F}_k = \vec{F}_k^{\text{ne}} - e_k \text{ grad } \phi \quad (22)$$

The phenomenological equations obtained relate fluxes of matter, \vec{J}_i ; energy, \vec{J}_q ; and chemical reactions, J_j^c , to the appropriate forces:

$$\vec{J}_i = \sum_k \tilde{L}_{ik} \left[\vec{F}_k - T \text{ grad } \left(\frac{\tilde{\mu}_k}{T} \right) \right] - \tilde{L}_{iq} \frac{\text{grad } T}{T} \quad (23)$$

$$\vec{J}_q = \sum_k \tilde{L}_{qk} \left[\vec{F}_k - T \text{ grad } \left(\frac{\tilde{\mu}_k}{T} \right) \right] - \tilde{L}_{qq} \frac{\text{grad } T}{T} \quad (24)$$

$$J_j^c = -\sum_m \tilde{L}_{jm}^c \sum_k \mu_k \nu_{km} \quad (25)$$

In the above equations, the L 's are the phenomenological coefficients which follow the appropriate Onsager relations and ν_{km} are the stoichiometric coefficients. Equation (23) relates diffusion to electrochemical potential and temperature gradients and to other externally applied forces, \vec{F}_k . Equation (24) includes the flow of both thermal and electrical energy while Equation (25), which is a scalar equation and does not couple with Equations (23) and (24), describes the dependence of chemical reactions on each other. Note that all subscripts in the above equations refer to chemical components.

Equations (23)-(25) are useful for both dynamic situations,

when flows and forces exist, and static situations, when one or more flows or forces may vanish. If we consider the static case when there are no flows and no thermal gradients or external forces, the situation is quite simple and the phenomenological equations require that the gradients of electrochemical potential must vanish:

$$\sum_k \text{grad } \tilde{\mu}_k = \sum_k \text{grad } (\mu_k + e_k \phi) = 0 \quad (26)$$

In order to include the effects of energy, volume and entropy gradients which exist in interfaces, the chemical potential can be written as:

$$\mu = u + pv - T_s \quad (27)$$

for a single component. In Equation (27), u , v , and s are intensive quantities and actually consist of sums of homogeneous bulk quantities and surface excess quantities such as $u = \frac{U}{n} + E_s$.

In an interface region, only the surface excess quantities have gradients and gradients of the homogeneous bulk portions of u , v , and s vanish by definition. Thus, assuming that gradients of external pressure, p , and temperature T , vanish, we can write:

$$\begin{aligned} \text{grad } \mu &= \text{grad } u + p \text{ grad } v - T \text{ grad } s \\ &= \text{grad } \left(\frac{U}{n} + E_s \right) + p \text{ grad } \left(\frac{V}{n} + V_s \right) - T \text{ grad } \left(\frac{S}{n} + S_s \right) \\ &= \text{grad } E_s + p \text{ grad } V_s - T \text{ grad } S_s \\ &= \text{grad } \gamma \quad (\text{by Equation 3}) \end{aligned} \quad (28)$$

The excess internal energy, E_s , in an interface region can consist of a strain energy portion, $\frac{1}{2} \sum_{\mu, \nu} \tau_{\mu\nu} u_{\mu\nu}$, if strains exist, and of

potential energy excesses not due to strain, E_s^i , as portrayed in Figure 4. The gradient of surface internal energy then becomes:

$$\text{grad } E_s = \text{grad } E_s^i + \frac{1}{2} \text{grad } \sum_{\mu, \nu} \tau_{\mu\nu} u_{\mu\nu} \quad (29)$$

Combining Equations (26), (28), and (29) for a one component system we obtain:

$$\text{grad } E_s^i + \frac{1}{2} \text{grad } \sum_{\mu, \nu} \tau_{\mu\nu} u_{\mu\nu} + p \text{ grad } v - T \text{ grad } s = - e \text{ grad } \phi \quad (30)$$

With no external pressure, such as a surface-vacuum interface, the $p \text{ grad } v$ term vanishes and, if we assume a flat surface with no gradients parallel to the surface, then

$$\frac{dE_s^i}{dz} = \frac{1}{2} \frac{d}{dz} \left(\sum_{\mu, \nu} \tau_{\mu\nu} u_{\mu\nu} \right) = T \frac{ds}{dz} - e \frac{d\phi}{dz} \quad (31)$$

The important aspect of Equation (31) is that it shows the interaction of gradients of surface quantities which can exist at equilibrium, i.e. when fluxes, entropy flows, temperature gradients, etc., vanish.

The magnitude of the variation of internal energy, E_s^i , strain energy, entropy, and electric potential with distance beneath the surface depends on the material. An electric potential gradient can exist in a space charge region when the electrochemical potential is separable into its electrical and chemical portions as shown by de Groot and Tolhoek (45). Insulators and semiconductors exhibit space charge regions whereas metals do not. In adsorbed layers or oxides on metals, however, space charge regions may exist and have high electric potential gradients.

What we have attempted to show in the above analysis is that

standard irreversible thermodynamics can be applied to fluxes and forces in solid interfaces. When one or more fluxes or forces vanish, Equations (23), (24), and (25) are still applicable and for the static case, the interesting relation, Equation (30), provides a graphic picture of the gradients which may remain.

III. OTHER EXPERIMENTAL TECHNIQUES

At the present time about 14 different techniques have been proposed for measuring surface tensions of solids. These methods are listed in Table 1 together with the respective references. Experimental results have been reported for ten of these and are also included in the table. Since Inman and Tipler (46) have reviewed the more important of these techniques and listed the experimental results for most metals and alloys, only a very brief description and critique of each method will be presented here. In addition, some data for non-metallic elements and compounds is presented.

Probably the most widely used technique for obtaining the surface tension of solid metals involves a measurement of the force in thin foils and wires tending to reduce the surface area. In effect, the high surface area sample is exposed to a temperature above $0.75 T_m$ (melting point temperature) at which sufficient thermal energy is available to allow creep and the resulting surface area reduction to take place at an observable rate. In the experimental procedure, a counterbalancing mechanical load which is utilized to prevent surface area reduction, i.e. zero creep rate, is related to the surface tension. Nabarro (47) and Herring (48) have explained the creep mechanism in terms of diffusion fluxes, surface and grain boundary tensions, and applied load.

In 1909 Chapman and Porter (49) reported the first creep experiments on thin foils which was followed by surface tension measurements on thin foils by Sawai and Nishida (50) and Tammann and Boehme (51). Contemporary investigators (52-60) have improved the technique and used small diameter wires as well as thin foils.

Since the creep rate in this type of experiment is a diffusion

TABLE 1 - SURFACE TENSIONS

Method 1) - Creep of Thin Wires or Films				
Material (Plane)	Surface Tension in ergs/cm ²	Temp. °K	Atmos.	Ref.
Cu (avg)	1650	1357	Vac.	52
Cu (avg)	1770	1123	He	57
Cu (avg)	1740	1323	H or He	58
Ag (avg)	1130	1234	He	53
Ag (avg)	400	1123	Air	59
Au (avg)	1350	1336	He	54
Au (avg)	1650	1336	?	51
Ni (avg)	1725	1725	A	55
δ-Fe (avg)	1914	1780	A	46
Sn (avg)	685	488	Vac.	60
Nb (avg)	2100	2523	Vac.	56
Method 2) - Cleavage				
Zn(0001)	105	77	Liq. N ₂	69
Zn(0001)	90	77	Liq. N ₂	74
Zn(0001)	87	R.T.	Air	74
Graphite(basal)	1750	R.T.	UHV	73
Fe-3% Si(100)	1360	24	Liq. N ₂	69
Si (111)	1240	77	Liq. N ₂	69
Zn-.1% Cd(0001)	1000	77	Liq. N ₂	69
KCl (100)	110	R.T.	Air	66
Mg O (100)	1150	R.T.	Air	67
Mg O (100)	1200	77	Liq. N ₂	69
LiF (100)	340	77	Liq. N ₂	69
Ca F ₂ (111)	450	77	Liq. N ₂	69
Pa F ₂ (111)	280	77	Liq. N ₂	69
Ca CO ₃ (1010)	230	77	Liq. N ₂	69
Mica (001)	310	R.T.	Air	70
Mica (001)	375	R.T.	Air	65
Mica (001)	4500	R.T.	Vac.	65
Mica (001)	10250	R.T.	UHV	72

(Continued)

TABLE 1 (Continued)

(Method 2) - Cleavage (Continued)				
Material (Plane)	Surface Tension in ergs/cm ²	Temp. °K	Atmos.	Ref.
Muscovite (001)	1100-1200	R.T.	Dry Air	71
Phlogopite (001)	2000-3000	R.T.	Dry Air	71
Polystyrene	7.13×10^5	R.T.	Air	75
Poly(methyl methacrylate)	1.40×10^5	R.T.	Air	75
Method 3) - Heats of Solution				
Ni (avg)	3700	R.T.	Soln.	81
Co (avg)	3580	R.T.	Soln.	81
Mg O (avg)	1090	R.T.	Soln.	79
NaCl (avg)	276	R.T.	Soln.	80
Ca O (avg)	1310	R.T.	Soln.	80
Ca(OH) ₂ (avg)	1180	R.T.	Soln.	80
Siloxane	259	R.T.	Soln.	80
Silanol	129	R.T.	Soln.	80
KCl (avg)	252	R.T.	Soln.	80
Method 4) - Liquid-Solid Interface				
Na (110)	220	361	Melt	85
Li (110)	430	459	Melt	85
Cu (111)	1417	1356	Melt	85
Ag (111)	1056	1234	Melt	85
Au (111)	1267	1336	Melt	85
Pt (111)	2060	2047	Melt	85
Pb (111)	498	501	Melt	85
Method 5) - Heat of Immersion				
Graphite (basal)	119	R.T.	Air	86
Teflon (basal)	56-69	R.T.	Air	86
Method 6) - Field Emission				
W (avg)	2900	2000	UHV	87

(Continued)

TABLE 1 (Continued)

Method 7) - Helium Bubbles				
Material (Plane)	Surface Tension in ergs/cm ²	Temp. °K	Atmos.	Ref.
Be (avg.)	1000	973	He	88
Method 8) - Wedge Grooving				
Cu (avg)	1550	1223	Dry H	93
Method 9) - Dihedral Angles. known γ (liq.)				
Cu (avg)	1800	1025	H or A	94
Method 10) - Chemical Potential of Particles in Solution				
Ag (avg)	5500	R.T.	Ionic soln.	92

controlled process, surface tension measurements can be made only in a temperature range where the Nabarro-Herring steady state creep mechanism can be observed within the time limits of the experiment and for the small mechanical loads required. Allen (59) was able to make measurements with silver at temperatures as low as 650°C which is 0.75 T_m , which appears to be the lower limit for most metals.

The atmosphere was found to affect the results drastically and most experimenters utilized inert gases in heating chambers made of the same material as the sample. Allen (59) obtained a surface tension of 400 ergs/cm² for silver in air at 950°C and Funk et al (53) obtained 1140 ergs/cm² for the same material at the same temperature in a helium atmosphere. Experiments in vacuum at pressures below 3×10^{-5} Torr have not been reported. For many metals the high evaporation rate in vacuum in the temperature range necessary for the experiment precludes the use of high vacuum and, therefore, limits the use of the technique to surface tension measurements in inert gas atmospheres.

The relation of the surface tension data obtained from the typical creep experiments on the sample-atmosphere interface may be any number of percent of the value for the pure metal (cf. Effects of Adsorbed Layers section) to that of the true vacuum-solid interface is most difficult to ascertain. A number of experiments (cf. 61,62) have indicated that the elimination of adsorbed surface layers of chemisorbed gases by simple high temperature evaporation in vacuum or inert gas atmospheres is almost impossible. For that matter, difficulties are encountered in obtaining a clean surface even when the most careful ion bombardment cleaning techniques are utilized as pointed out by Farnsworth et al (62) who studied the surface layer directly with low-energy electron diffraction. Therefore, it is apparent that the creep type experiment, as well as most other surface tension techniques which are used in practice today, involve some form of impure surface which holds little resemblance to the truly clean surface.

The second method of surface tension determination involves the measurement of the strain energy required to extend a cleavage crack on a particular lattice plane. This follows the Griffith (63) criterion for crack initiation and is based on a balance of strain energy and surface energy. The classical experiments on mica by Obreimoff (64) and by Orowan (65) have been improved upon and the method utilized for metals and for organic and inorganic compound crystals by a number of more recent workers (66-75).

The well known difficulties encountered in determining a true surface tension from cleavage experiments include the possible plastic energy of deformation and cleavage step energies. Also, if vacancy concentration in a surface at thermal equilibrium differs from that of the

bulk, the surface tension and surface stress would not be equilibrium values for cleavage experiments. After cleavage occurs, thermal rearrangement of surface atoms may occur in order to attain the equilibrium surface vacancy concentration and surface atom displacement. Cleavage experiments do not, therefore, measure the energy of a surface but measure the energy required to break the bulk lattice bonds. The magnitude of this effect is difficult to ascertain until more is known about surface point defect concentrations and surface atom displacements.

The effect of gaseous environment on crack propagation has been discussed by Snowden (76) and Westwood (77). Gilman (69), who performed his cleavage experiments in liquid nitrogen, stated that the tip of the cleavage crack was probably so sharp that liquid nitrogen molecules could not get very close to the tip. However, the effect of adsorbed layers on opening up cracks and increasing crack tip radii has been reported by Westwood. A very large effect of the atmosphere on cleavage energies was observed by Bryant et al (72,73) who reported a value of $10,250 \text{ ergs/cm}^2$ for mica in an ultra-high vacuum of 10^{-13} Torr and 300 ergs/cm^2 in air. It is obvious, therefore, that the environment in cleavage experiments has a very pronounced effect on the results. While the effect in mica is a special case involving surface charge layers, it is, nonetheless, expected that cleavage energies for metals in an ultra-high vacuum environment would be higher than those reported for other environments.

Another technique for the determination of surface tensions involves the difference in heat of solution between a material of fine particle size and in bulk form. Lipsett et al (76) were the first to report data utilizing this technique. In their experiments on NaCl, the

surface area of the powder was measured microscopically. More recently Jura and Garland (79) and others (80,81) have utilized the heat of solution technique but have applied more sophisticated methods for surface area determination of the powder by a monolayer adsorption technique such as the Brunauer, Emmett, Teller (BET) (29) and Harkins, Jura (82) techniques. Many aspects of the heat of solution method of measuring surface tension are similar to the method developed in this laboratory.

It is interesting to compare the results of the heat of solution technique with those of others.

	in ergs/cm ² from heats of solution	Ref.		in ergs/cm ² by other techniques	Ref.
MgO	1090	(79)	1150	cleavage	(67)
			1200	cleavage	(69)
			1200-1300	cleavage-UVHV	(68)
KCl	252	(80)	110	cleavage	(66)
Ni	3700	(81)	2600	wire creep	(55)

These results were obtained at room temperature except for the 1200 ergs/cm² value for MgO and the 2600 ergs/cm² for Ni which were extrapolated to room temperature using a surface entropy (see Equation 3) of -0.5 ergs/cm²/°C. The results for MgO are in remarkable agreement. However, the results from the heat of solution technique for KCl and Ni are, respectively, 2.3 and 1.4 times the values obtained from other techniques. In the heat of solution method, the effect of using a powder surface area smaller than actually exists is to increase the value of surface tension obtained. If good BET practice is utilized, however, even for powders having very small pore sizes (see section on Experimental Procedure), the surface area obtained generally correlates

well with values obtained from other techniques of determining surface area. This technique of surface tension measurement could be adapted to ultra-high vacuum since the initial powders are vacuum degassed before dissolution. The quantity that is actually determined is the solid-vacuum surface tension, not the solid-liquid tension as reported by Inman and Tipler (46).

An interesting technique first used by Meissner (83) utilizes the difference between the melting point of a flat solid and one with a sharp radius of curvature. This difference in melting point is proportional to the solid-liquid interfacial energy. Assuming the Dupré equation ($\gamma_s = \gamma_l + \gamma_{ls}$) and known values of the surface tensions of liquids such as those given by White (84), the surface tension of the solid, γ_s , is just the sum of the surface tension of the liquid, γ_l , and the interfacial tension, γ_{ls} . This approach has been expanded by Skapski (85). Again in this technique, as in the method of creep, one is limited to temperatures very close to the melting point. The results are listed here for the noble metals at the melting point and are remarkably close to values obtained from thin wire creep experiments.

	γ in ergs/cm ² by the ΔT_m technique	Ref.	γ in ergs/cm ² by the creep technique	Ref.
Cu	1417	(85)	1650	(52)
Ag	1056	(85)	1130	(53)
Au	1267	(85)	1350	(54)

In this technique, the values of the surface tension of the liquid would be affected considerably by the surrounding atmosphere and would be higher in ultra-high vacuum, thereby giving higher values for the solid surface tension.

Another interesting technique was developed by Hood, et al (86) and

makes use of the increasingly available heats of immersion of solids.

The technique is adaptable to various temperatures and to vacuum as is the heat of solution technique. The results of Good, et al (86) for graphite are about a factor of ten low as shown by Bryant, et al (73) due to unclean surfaces. The energy of the surface, c_s , is calculated from the equation:

$$c_s = \frac{(e_{lv} - h_{i(sl)})^2}{4 e_{lv} \phi^2} \quad (32)$$

where e_{lv} is the surface energy of the wetting liquid and $h_{i(sl)}$ is the heat of immersion. The quantity ϕ is given by the expression:

$$\phi = \frac{\gamma_{sv} + \gamma_{lv} - \gamma_{sl}}{2 \gamma_{sv} \gamma_{lv}} \quad (33)$$

and is often close to or equal to one.

The pulsed field electron emission technique of Barbour, et al (87) was the first to ensure an atomically clean surface. Field emitter tips are heated to a temperature at which atoms can migrate from the tip to the shank to reduce surface area and this tendency is reduced to zero by applying a known DC electric field. Surface tension is assumed proportional to the square of the applied field. An additional field is required for observation of the emitter tip on the fluorescent screen and was applied in pulses to eliminate the effect of the second field on atomic migration. One objection to this technique would be the strain in the surface region of the emitter tip caused by the applied field which might affect the value of surface tension obtained. However, this could probably be accounted for as shown in the section on Theory.

A very interesting technique developed recently by Barnes and collaborators (88) involves equating the force of surface tension acting in the walls of a cavity in a solid to the force exerted by gas pressure in the cavity at equilibrium. Barnes, et al did this by injecting helium atoms into beryllium via α -particle bombardment in a cyclotron or fast neutron bombardment in an atomic pile. Subsequently, samples were annealed such that the supersaturation of vacancies formed during the bombardment could agglomerate to form cavities in which the helium gas collected. If helium adsorption on a clean surface is assumed not to affect the surface tension significantly, this method would appear to be quite useful for temperatures below the melting point and for materials not amenable to other techniques.

It would be possible to measure surface tensions in many solids quite simply without utilizing bombardment techniques by determining the gas pressure in equilibrated cavities within the crystal. Amelincynx, et al (89) determined pressures inside crystal cavities by observing the bubble size of the gas released during etching of the sample. They were also able to analyse the gas with a mass spectrometer. If the cavity size and gas pressure and analysis could be determined, then the solid surface tension under a known atmosphere could be measured.

Other techniques for the determination of surface tensions of solids include measurements of surface stresses in ultra-high vacuum by bending very thin plates and comparing the bending stresses required to those known for thicker plates as suggested by Haneman (90). Frazer (91) proposed a technique involving the measurement of curvatures of surface steps between precipitated particles. Borel (92) has recently reported a very high value for the surface tension of silver (5500 ergs/cm^2)

obtained from measurements of the chemical potential of silver in an ionic solution containing very small crystals of silver of known radii. The variation of chemical potential with radius is well known (9) and suggests another technique which has not, as yet, been utilized for surface tension determinations; that is, the equilibrium vapor pressure, which depends on chemical potential and, hence, on crystal radius, could be measured as a function of particle size in an ultra-high vacuum. Using the Herring (9) equations, surface tensions could then be obtained. Another technique utilized recently by Shewmon (93) involves measuring the angle of a groove made in a flat surface by a wedge. Bailey and Watkins (94) used very good experimental techniques in obtaining the surface tension of copper via the Dupré equation by measuring dihedral angles on single crystals, liquid-solid interface angles, and using the known surface tension of liquid copper.

Due to the ever increasing profusion of ideas concerning surfaces and techniques for measuring surface tensions, the very reasonable question might be raised as to why develop another approach to surface energy determination? The answer can be found in the objections raised to the techniques described above and in the fact that none of the techniques form a direct approach to the problem, and as such, rely on secondary mechanisms which in themselves are suspect. In addition, the applicability of many of the methods listed is limited to certain materials. None of the techniques reported in the literature thus far, except for the field emission method, has utilized ultra-high vacuum; and, hence, the true solid metal-vacuum interface has not as yet been studied. And until field emission is adapted to low melting point materials, only such materials as tungsten can be studied by this method.

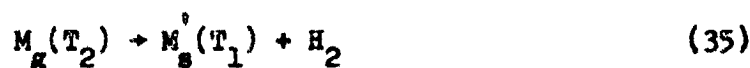
It is true that the cleavage method could be adapted to ultra-high vacuum; however, the other objections which were raised above still leave this approach in question. The solid-liquid interface and heat of immersion techniques both depend on available data for the surface tensions of liquids which are also not yet available in ultra-high vacuum environment. Measuring the gas pressure inside cavities in crystals obviously will not yield values for the solid-vacuum interface. Of the important techniques developed, to this time, the heat of solution technique seems most adaptable even though this has not as yet been utilized in ultra-high vacuum. In view of the large discrepancies in the surface tension data shown in Table 1, one may assume either that the methods for the determination of the surface tension or the experimental procedure or both are at fault. Most of the techniques utilized for solids are subject to large experimental errors and have taken many years to develop. The adaptation of these techniques to an ultra-high vacuum environment would involve a great deal of effort and complex equipment. The need for a direct approach to the problem of measuring surface tensions of solids in ultra-high vacuum utilizing established techniques in a range of temperatures below $0.75 T_m$ and not specifically limited to the type of material studied is apparent.

IV. EXPERIMENTAL PROCEDURE AND SYSTEM ANALYSIS

A. General Outline of Technique

The technique developed in this laboratory for the determination of the surface tension of a solid involves the measurement of electrical energy required to evaporate a mass of solid and a calorimetric measurement of the heat evolved from the condensation of the resulting vapor. The approximate difference in surface area between condensed vapor and the initial mass is a factor of about 10^4 . If the temperature of the sample is identical at the start and at the completion of a run, then the difference between power input used for evaporation and heat given off to the calorimeter is essentially the surface tension times the difference in area between the initial sample and the thin film. When this process is carried out for a pure elemental substance in ultra-high vacuum, it is possible to obtain a thin film with an atomically clean surface.

The determination of surface tension by this technique involves, effectively, the following process:



in which the only essential difference between the starting mass of solid, $M_s(T_1)$, and the product of the reaction, $M'_s(T_1)$, is the surface area. The energy, ΔH_1 , required to heat and evaporate the sample is greater than the heat given off to the calorimeter, ΔH_2 , during condensation of the vapor, $M_g(T_2)$, because of the energy tied up in the large surface area of the deposited thin

film. The difference, $\Delta H_1 - \Delta H_2$, is essentially the surface tension of the material times the surface area of the film (γA) (see Results and Discussion). The similarity between the approach presented here and the heat of solution technique utilized by Jura and Garland (79) should be apparent (see Other Experimental Techniques). Since the recorded values of the surface tension are so small (100-3000 ergs/cm² for most metals) in comparison to heats of sublimation per cc, the major requirement of this experiment is that the change in area between M_g and M_g' must be very large. This was accomplished by evaporation onto a substrate maintained at a low temperature.

According to Allen, et al (33) the surface area resulting from the ultra-high vacuum vaporization of copper onto a glass substrate was an inverse function of substrate temperature. Thin films deposited at room temperature had a surface area of about 8m²/gm whereas an area of 39.6 m²/gm was obtained for films deposited at liquid oxygen temperature (90°K). Liquid nitrogen temperature (77.32°K) was utilized for the temperature of the substrate in our experiments. Areas of thin films evaporated in vacuum (but not in ultra-high vacuum) onto room temperature substrates have been reported by Brennan (95) for a number of metals while Swaine and Plumb (34) discuss some of the experimental variables influencing the surface areas obtained for evaporated films. Many factors, such as substrate temperature, angle of incidence of the vapor during deposition, substrate cleanliness, vacuum, purity of the sample, etc., affect the surface areas of

vacuum deposited thin films. The techniques of surface area measurement vary considerably and present another possible error in many of the reported surface area values as will be discussed later. Until data are available for a group of metals evaporated in ultra-high vacuum and utilizing identical experimental conditions it is difficult to draw meaningful conclusions from a comparison of the surface areas of different metals reported in the literature. The surface area is, however, an important factor in determining the amenability of a material to this experimental procedure.

Some other factors influencing the amenability of various materials to this experimental procedure are known or can be estimated. The amenability, Q , is inversely proportional to the difference in heat content, ΔH_1 , between a gas at the temperature of evaporation, T_{ev} , and the solid at the initial temperature. The reason for this is that the total surface energy of the thin film deposited in the experiment must be a measurable percentage of the total energy involved in the experimental run. The total electrical power input energy, ΔH_1 , includes radiation loss, the heat content difference between the material at the initial temperature and the temperature of evaporation, T_{ev} , and the heat of vaporization. The energy received by the calorimeter, ΔH_2 , includes the radiant energy and the heat released due to condensation of the vapor on the substrate. ΔH_1 is equal to ΔH_2 plus the small quantity, γA , the total surface energy of the thin film. Since radiation loss is proportional to T^4 , the amenability is inversely proportional to T_{ev}^4 . The amenability is directly proportional to the surface tension, γ , the surface area per gram of the thin film, A' , and to the

evaporation rate, R , at the temperature of evaporation chosen. Values for evaporation rates of metals are given by Dushman and Lafferty (23). Values for surface tension and surface areas of thin films have been discussed above. The factors influencing amenability of a material to the experimental procedure are grouped together in the following proportionality relation:

$$Q \sim \frac{\gamma A^2 R}{T_{ev}^4 \Delta H_1} \quad (36)$$

In addition to the above, Q is also related to the heat leak rate of the calorimeter and to the precision of the electrical power measurement system since the product γA (where A is the area of the thin film obtained in the experiment) must be considerably larger than both the calorimeter leak rate and the limit of precision in the power measurement system in order to obtain results. Consequently, Q is inversely proportional to either the calorimeter leak rate or the power measurement error, whichever is larger and, therefore, the limiting factor. Also to be considered was the ability of the material to be tested to undergo the preliminary ultra-high vacuum bake-out (up to 450°C) without evaporation. From the above analysis, silver was chosen for this experiment since its amenability was good in comparison to other metals for which data was available and since γA was large enough to be detected experimentally. An additional factor influencing the purity attainable is the fact that the oxides of silver are relatively unstable and, therefore, easy to dissociate and remove through ultra-high vacuum procedures. The experimental procedure developed here would,

however, be amenable to other materials, both metallic and non-metallic.

In the following sections the techniques necessary for vacuum evaporation and for obtaining an atomically clean thin film surface are discussed together with the calorimetry and power measurement systems and the (BET) method of surface area measurement. Figure 9 portrays diagrammatically the various components of the experimental apparatus.

B. Evaporation Procedure and Ultra-High Vacuum (UHV) Technique

Since the surface tension varies with adsorbed atoms, the requirement of a clean surface was stipulated for the experimental measurement of the surface tension of silver. The utilization of ultra-high vacuum (UHV) evaporation procedures was, therefore, mandatory. In this section the UHV technique is described as well as the filament assembly design and evaporation procedure. Since the surface tension of the evaporated film is a very small percentage of the heat liberated to the calorimeter, an evaporation temperature of 1600°K was chosen to optimize the energetics of the system as explained in Appendix 1.

The sample material chosen for vaporization was 0.005" diameter silver wire of 99.999% purity as obtained from Leytess metal and Chemical Corp. Fourteen coils of about twenty turns each of the silver wire were wound on a 10 mil tungsten - 3% rhenium filament as shown in Figure 10a, which had been degassed for about 10 minutes at 2000°K in a vacuum of at least 10^{-6} Torr. After winding the silver wire on the degassed filament, the whole assembly was degassed further at 10^{-6} Torr for a few hours at

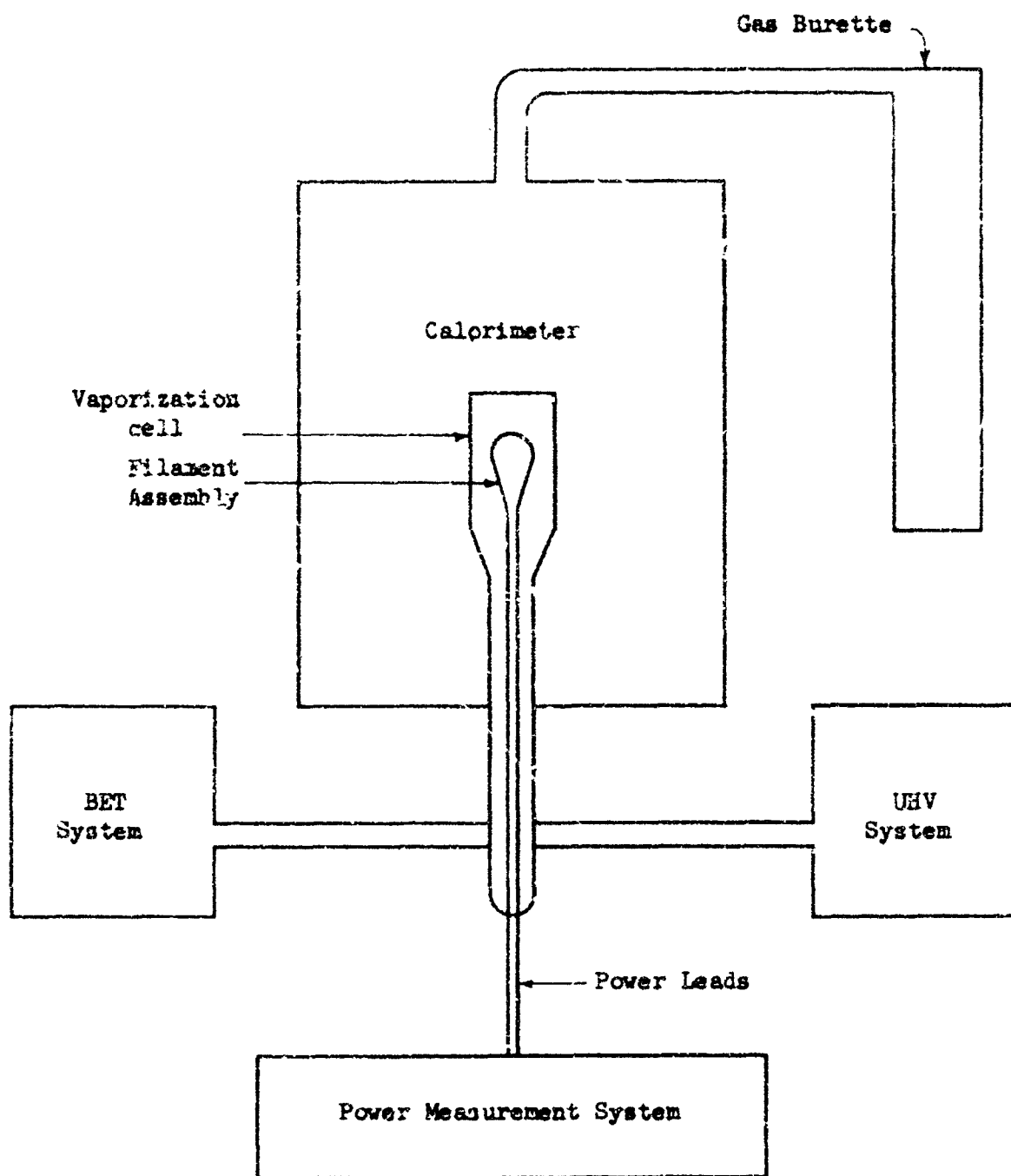


FIGURE 9 - Schematic of Entire Apparatus

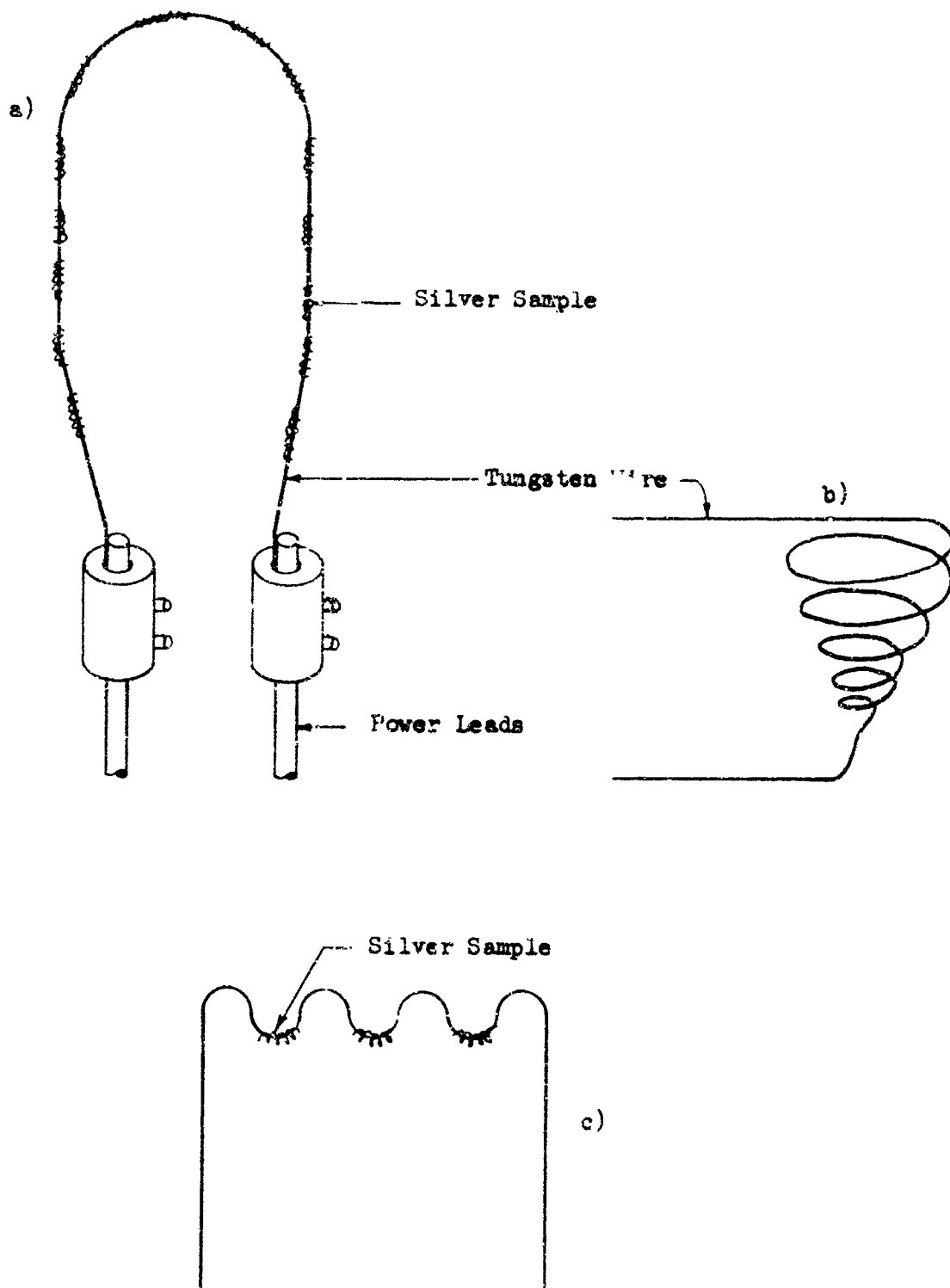


FIGURE 10 - Filament Assembly Designs
(Type a) was used)

about 1000°K. The filament assembly was then incorporated in the experimental apparatus and UHV attained, further degassing was done in the 10^{-8} Torr range until no increase in pressure was observed upon repeated heatings of the assembly to 1000°K.

At the evaporation temperature utilized (1600°K) Rook and Plumb (96) have shown that tungsten contamination of the evaporant is negligible. Because of this and the degassing procedure used, the purity of the silver evaporated during a run was expected to be at least 99.999%. Other filament assembly designs as shown in Figures 10b and c were tested. The crucible type shown in Figure 10b, in which the sample was a small lump of silver, gave a limited evaporation rate since the surface area of the silver exposed during evaporation was very small in comparison to the area available using the design of Figure 10a. The crucible type of filament also produced large fluctuations in power which were difficult to record (see section on Power Measurement System) and which were probably caused by electrical shorting between turns of the filament as the silver melted and vaporized. The design of Figure 10c worked well but the simpler design shown in Figure 10a was possible if a tungsten - 3% rhenium alloy filament was used instead of pure tungsten, since liquid silver wet and adhered to the alloy but not to the pure tungsten.

Since Allen, et al (33) have shown that the surface areas of metals condensed from the vapor in UHV at about 77°K are a linear function of the mass evaporated, the choice of the amount of silver evaporated during an experimental run was not critical. Weights of approximately 0.02 - 0.05 gms were evaporated and, assuming a

surface area of $40\text{m}^2/\text{gm}$, the surface areas obtained for these weights were in the neighborhood of $0.8 - 2.0 \times 10^4 \text{ cm}^2$. Using a value of 1675 ergs/cm^2 for the surface tension of silver obtained by extrapolation to 77°K of data given by Funk, et al (53), the total energy of the thin film surface was expected to be approximately $0.22 - 0.54$ calories or more. Since it was necessary that this small energy be as high a percentage of the total heat received by the calorimeter as possible, an analysis of all the energies involved in an experimental run was made as discussed in Appendix 1. Taking into account the heat released to the calorimeter during condensation of the silver vapor, radiant energy received from the hot filament, and the amount of silver evaporated at various temperatures, it was found that the surface energy of the thin film was the highest percentage of the total energy at about $T_{\text{ev}} = 1600^\circ\text{K}$.

In order to insure less than one percent of a mon. layer of impurities on the silver film during the course of a run, evaporation in UHV was required. Most of the UHV procedure utilized has been described previously by Spalvins and Keller (97). The apparatus used to attain UHV is portrayed schematically in Figure 11. The substrate for the thin film deposition was a 7.5 cm OD x 10 cm high cylindrical cell (A) of 0.022" thick OFHC copper which was silver plated on both sides with approximately 0.002 inches of silver. The substrate provided good thermal conductivity to the calorimetric fluid which surrounded the cell. In addition, the silver on the outside of the cell prevented oxidation of the copper during the bakeout cycle. The cell was attached at

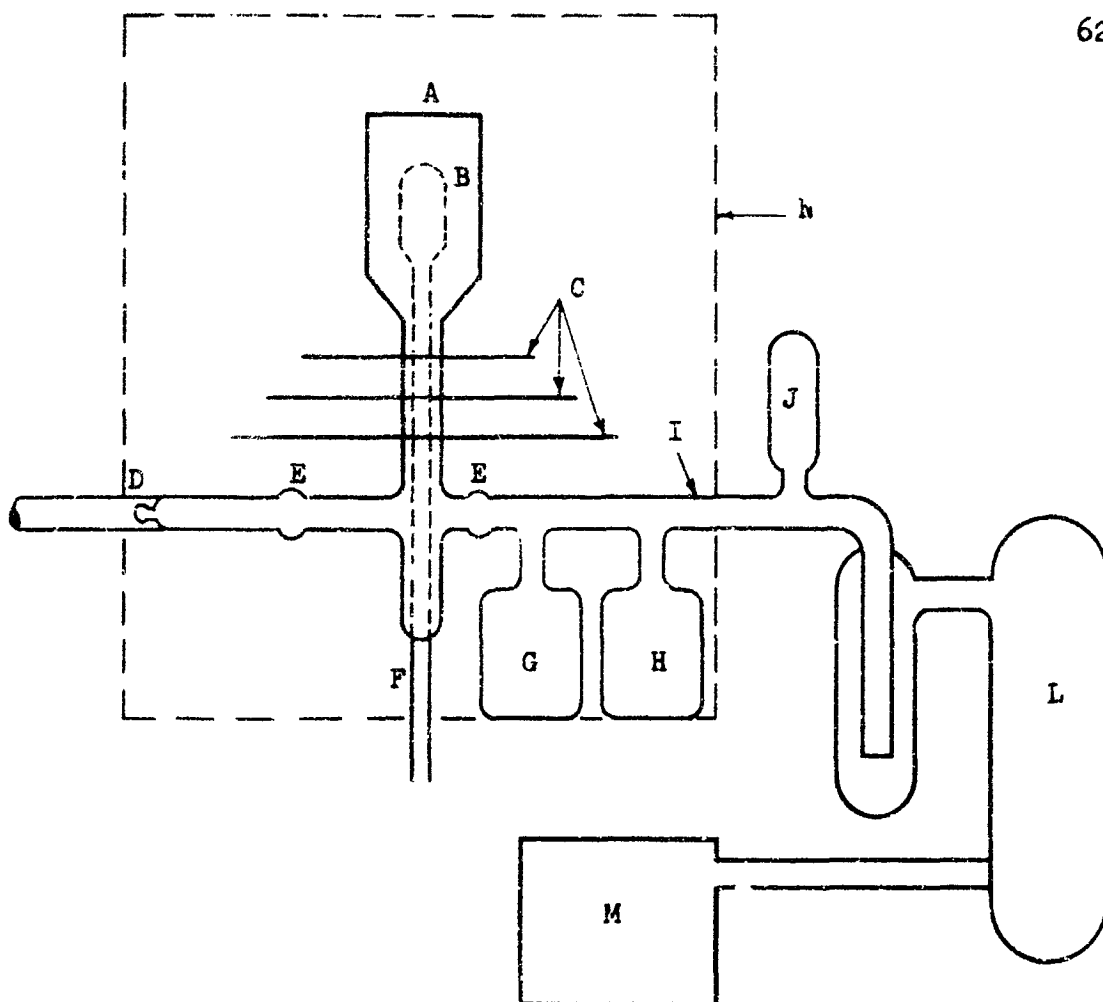


FIGURE 11 - Diagrammatic Sketch of UHV System

KEY

- A. Silver Plated Copper Cell, 3 in. diam. 4 in. High
375 cm² Surface Area, 500 cc Volume
- B. Filament Assembly
- C. Stages for Calorimeter
- D. Break-off Tip to BET System
- E. Glass-to-Metal Seals
- F. Power Leads
- G. Bayard-Alpert Ionization Gauge (range 10⁻⁴ to 10⁻¹⁰ Torr)
- H. Titanium Getter Pump
- I. The System is Sealed at this Point Before Flashing the Getter, H
- J. CVC Vacuum Gauge (range 10⁻³ to 10⁻⁷ Torr)
- K. Liquid Nitrogen Trap
- L. Mercury Diffusion Pump
- M. Mechanical Forepump
- N. Bake-out Over (removable)

one end to a 2.5 cm OD stainless steel tube leading to the UHV and BET systems. The surface area of the cell was approximately 375 cm² and since the substrate has an interface with the deposited film of silver, a small interfacial energy is involved. Even though UHV technique was utilized, the interface would involve a chemisorbed layer of gas atoms on the substrate. This problem was considered negligible, however, since the deposited silver film was granular having a much larger surface area (about 10⁴ cm²) than the interfacial area.

The pumping system included a Welch Duo-Seal mechanical fore-pump, two 3-stage mercury diffusion pumps, and a liquid nitrogen trap connected in series. The components enclosed in the bakeout oven, N, as shown in Figure 11 were baked out between 350° and 450°C for 24 to 120 hours at pressures in the neighborhood of 10⁻⁶ to 10⁻⁷ Torr as measured by an CVC discharge gauge (J). The pressure in the system at room temperature following bakeout was 5 x 10⁻⁸ Torr as measured by an NRC type 553-P ionization gauge (Bayard-Alpert type) (Q). To obtain the desired pressures careful degassing of the filament assembly (B) and of the titanium getter pump (H) was necessary. This was accomplished both during and following bakeout while maintaining the pressure in the system below 10⁻⁵ Torr. The Bayard-Alpert gauge and the filament assembly were degassed again at room temperature following bakeout. After bakeout, the system was isolated at (I) and the titanium getter flashed intermittently to attain the ultra-high vacuum range. High purity 0.010" diameter titanium wire obtained from Armetco which

was wound on 0.010" diameter tungsten filament served as the getter.

Many problems were encountered developing leak tight seals between the metal components of the ultra-high vacuum system. Cracks and porosity which developed during the bakeout period were numerous and presented the most difficulty. Most of the metal joining was accomplished using (Handy-Harmon Braze types 715 and 580) silver solders which contained no high vapor pressure constituents.

The vacuum required to limit adsorbed impurity coverage of the thin film surface can be estimated assuming ideal gas kinetic theory. The fraction of surface covered, θ , is given by:

$$\theta = \frac{3.53 \times 10^{22} \alpha s p}{MT} \quad (37)$$

where α is the sticking probability, s is the cross-sectional area of the adsorbing atoms, t is the time at pressure, p after forming a clean surface, M is the molecular mass and T is absolute temperature. To obtain a rough estimate of θ knowing that the residual gases in an ultra-high vacuum system are usually hydrogen, helium, and carbon monoxide we can use an average of the masses of these gases for M and an average molecular cross section of 10\AA^2 . For a temperature of 77°K , a sticking probability of 0.5, and a total time of three minutes, one percent of a monolayer coverage will occur at a pressure of 10^{-9} Torr. Consequently, pressures close to or better than 10^{-9} Torr were used in these experiments. The actual pressure inside the vaporization cell immediately

following the condensation of the silver vapor was probably much less than that read on the pressure gauge since at a pressure of 10^{-9} Torr there would be only about 10^{11} molecules inside the 500 cc vaporization cell. Since one monolayer of gas on the thin film surface constitutes about 10^{18} molecules and since the mean free path at 10^{-9} Torr is close to 10^7 cm most of the molecules within and close to the vaporization cell are gettered by the silver film. From the above discussion it can be seen that if a pressure below 10^{-8} is attained for an experimental run, a clean surface can be guaranteed if the sample material is thoroughly degassed.

C. Power Measurement System

The energy to form a thin film surface, γA , was shown to be a very small percentage of the total energy in the analysis given in Appendix 1. For example, to form a thin film of silver at an evaporation temperature of 1600°K , γA is about 2% of the total energy utilized ($\Delta H + W$). As a consequence, to approach a precision of $\pm 5\%$ in γA , the power required for evaporation must be measured to at least one part in 10^3 .

In order to accomplish a precision of this order a circuit as shown in Figure 12 was designed. Direct current supplied from a heavy duty battery was supplied to the evaporator filament (R_3) through a standard resistance (R_6) and a series resistance R_1 . The current passing through a calibrated* NBS standard 0.01 Ω resistor (R_6) produces a voltage drop across the resistor. This emf output activated a high speed Brown Electronic recorder (A) (1/4 sec rise

*July, 1963, to a value of 0.010033 ohms at ten amps

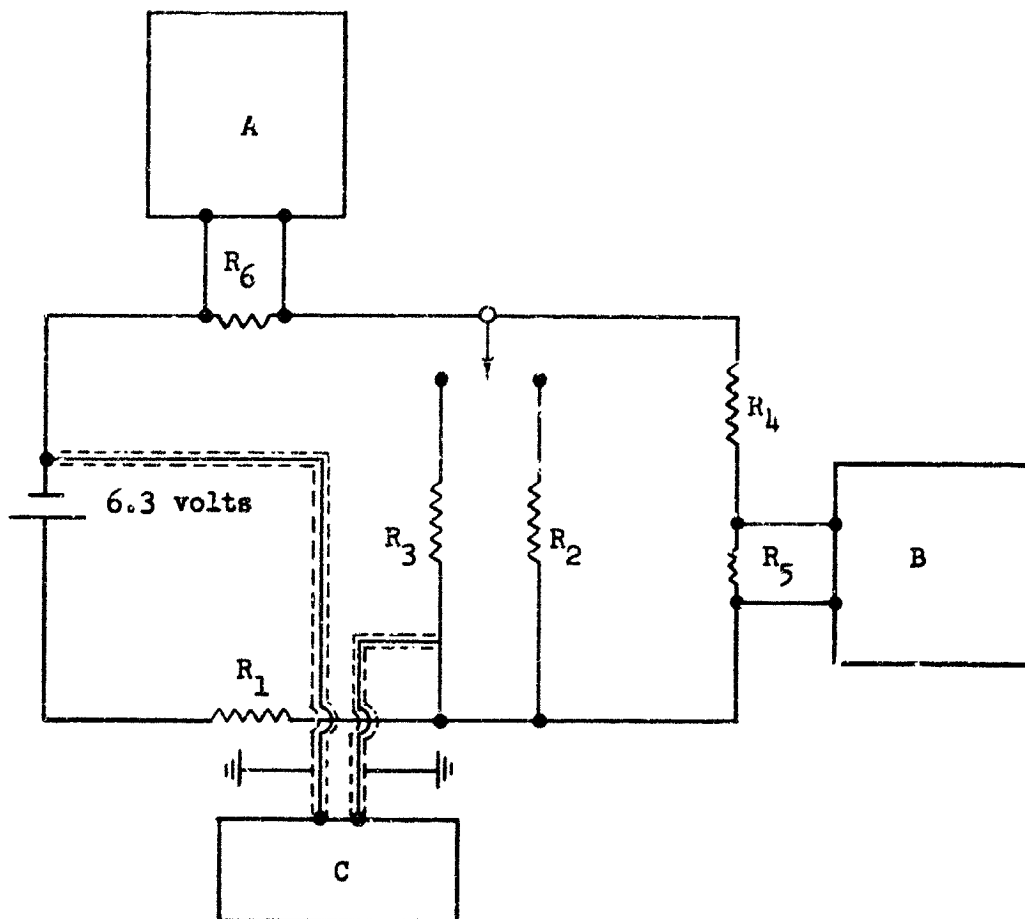


FIGURE 12 - Power Measurement Apparatus

KEY

- A. High Speed Recorder (amperage)
- B. High Speed Recorder (voltage)
- C. Time Interval Meter
- R_1 Series Resistance; Approximately 0.7Ω
- R_2 Dummy Load; Approximately 1.0Ω
- R_3 Load; Filament Assembly
- R_4 Standard $1\text{ K}\Omega$) Voltage Divider
- R_5 " 1Ω)
- R_6 0.01Ω NBS Standard

time; 4.8 in/sec chart speed) to produce a recording of the current profile during the run. The current passing through standard resistance, R_5 , which was part of a voltage divider composed of R_4 and R_5 , produced a similar voltage drop which was also plotted on a similar instrument. The emf values printed on the recorder charts were subsequently standardized by duplicating a sufficient number of data points by placing an input emf into the recorder from a Leeds and Northrup potentiometer (436634) or a Lindeck Microvolt source; thus, the recorder instrument errors could also be standardized.

The exact total time interval of the run was recorded to $\pm 2 \times 10^{-6}$ sec on a digital Berkeley Time Interval Meter (C) fixed into the circuit control.

Before starting a run, current was passed through the dummy resistor, R_2 , then switched to the filament assembly, R_3 , to initiate the run. The recorder strip charts were activated slightly before the start of a run to ensure uniform chart speed throughout the run. Upon switching the current from R_2 to R_3 , the tin was activated and a change in the plot was visible on the recorder charts. A resistance, R_1 , in series with the filament was used to decrease the large amperage variation that was due to the resistance change of the filament assembly as it increases in temperature during the first few seconds of a run. Sample strip chart recordings of the voltages recorded on the Brown Instruments are portrayed in Figure 13.

Since the total energy (E) provided to the filament assembly is a function of the product of the time, (t), voltage (v), and

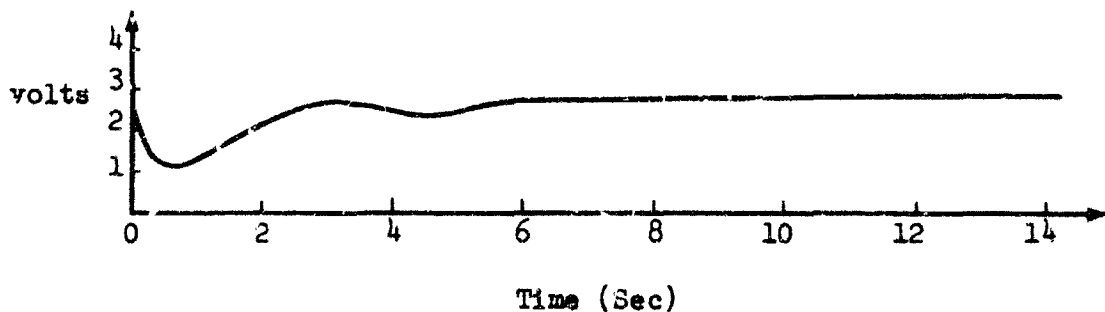


FIGURE 13a - Strip Chart Recording of Voltage From Brown Instrument emf.

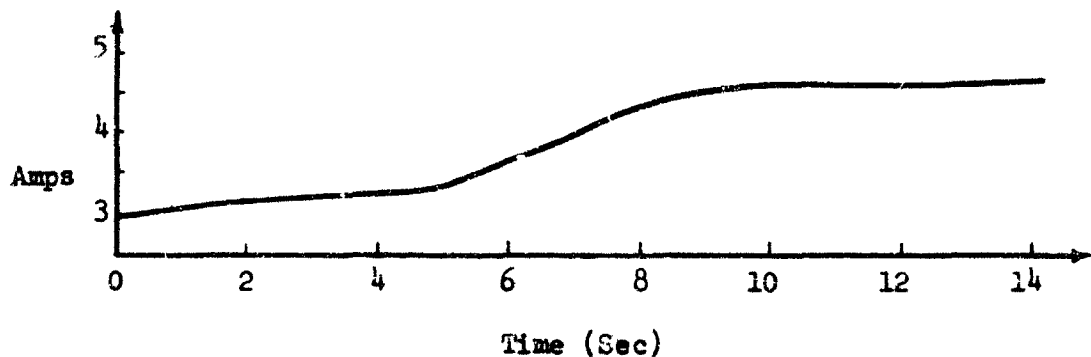


FIGURE 13b - Strip Chart Recording of Amperage from Brown Instrument emf.

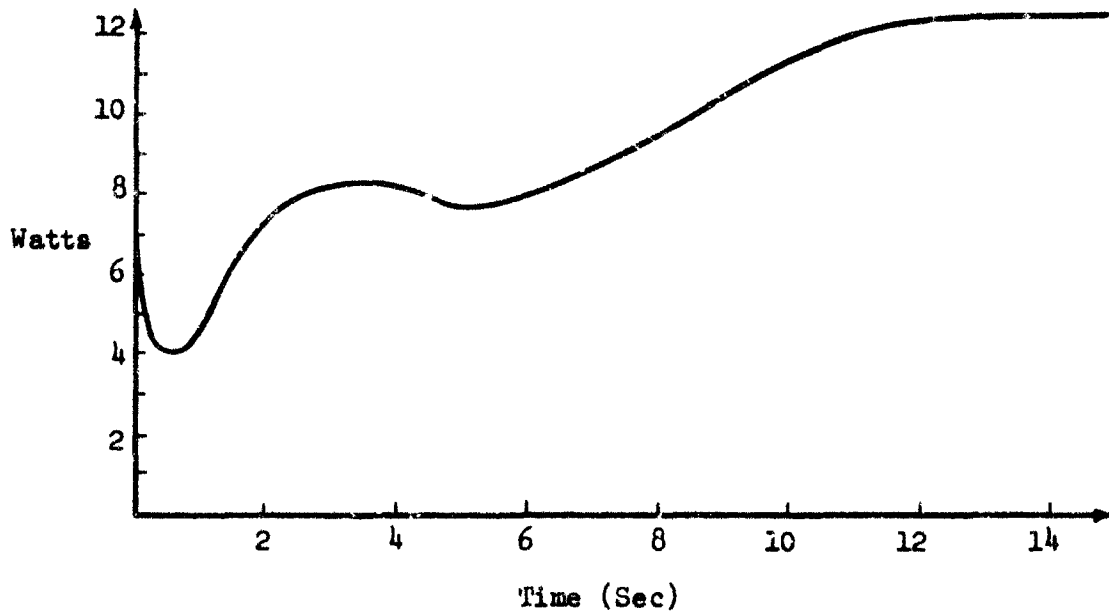


FIGURE 13c - Power Plot Taken From Curves Shown in Figure 13a and b.

current, (i), to the filament and the voltage and current vary with time the following equation would apply:

$$E = \int_0^t i(t) v(t) dt \quad (38)$$

In order to obtain an accurate determination of power from the voltage and amperage curves, a plot of instantaneous power versus time was made on 75 cm high graph paper (see Figure 13c). This was accomplished by plotting the product $v(t) i(t)$ versus time for a series of points taken from the voltage and amperage curves. The total power was then determined by the method of weighing the area of graph paper under the instantaneous power curve. The precision in power measurement obtainable with this technique was $\pm \frac{1}{40}$ watt and, if a total power of 50 watts were measured during an experimental run, this amounts to a precision of $\pm 0.05\%$.

D. Calorimeter System

In order to measure the total energy received by the substrate during the vaporization and condensation of the silver sample an isothermal calorimeter was designed which could be operated in the liquid nitrogen temperature range. An isothermal low temperature drop calorimeter such as that described by Ginnings and co-workers (98) might have been designed; however, there are numerous difficulties inherent in such a design, particularly for very low temperature operation. Since the energies to be measured in this experiment were small, i.e. less than 50 calories, and since the change in volume upon the evaporation of liquid nitrogen is large, an isothermal calorimeter was conceived which utilized liquid nitrogen at its boiling point as a calorimetric

fluid. The heat received at the calorimeter wall from the silver vapor and coincident radiation during the process would pass through the cylinder walls and convert liquid nitrogen to gas (18.3 cc gas at STP per calorie) which in turn could be collected in a gas burette at atmospheric pressure and room temperature. Glaugue and Clayton (99) have given a value of 1332.9 cal/mol for the heat of vaporization of nitrogen at a boiling point of 77.32°K; thus, with the volume of liquid nitrogen vaporized during an experiment, the heat given off to the calorimeter can be calculated.

A cross section of the liquid nitrogen calorimeter which was designed and constructed is shown in Figure 14. The system consisted of the vaporization cylinder (B) which was surrounded by the calorimetric fluid, liquid nitrogen (C), which was held in a monel container. Insulation of the calorimetric fluid from ambient temperature was accomplished by surrounding the container concentrically with a vacuum chamber and then a third concentric chamber placed outside the vacuum chamber which contained more liquid nitrogen. Each of the three concentric chambers were flanged (see insert of Figure 14) and affixed to a permanent base plate by bolts spaced approximately one inch apart and utilizing gaskets of 1/8" diameter 50% Sn - 50% In. The vacuum seal at the top of the middle container was fashioned in a similar manner. Each of the concentric shells were removed during the bakeout procedure to prevent their deterioration. The heat leak of the calorimeter was reduced considerably by polishing the containers and by utilizing a series of radiation shields (D) incorporated within the vacuum chamber (E). Various types of multiple radiation barriers have been discussed by

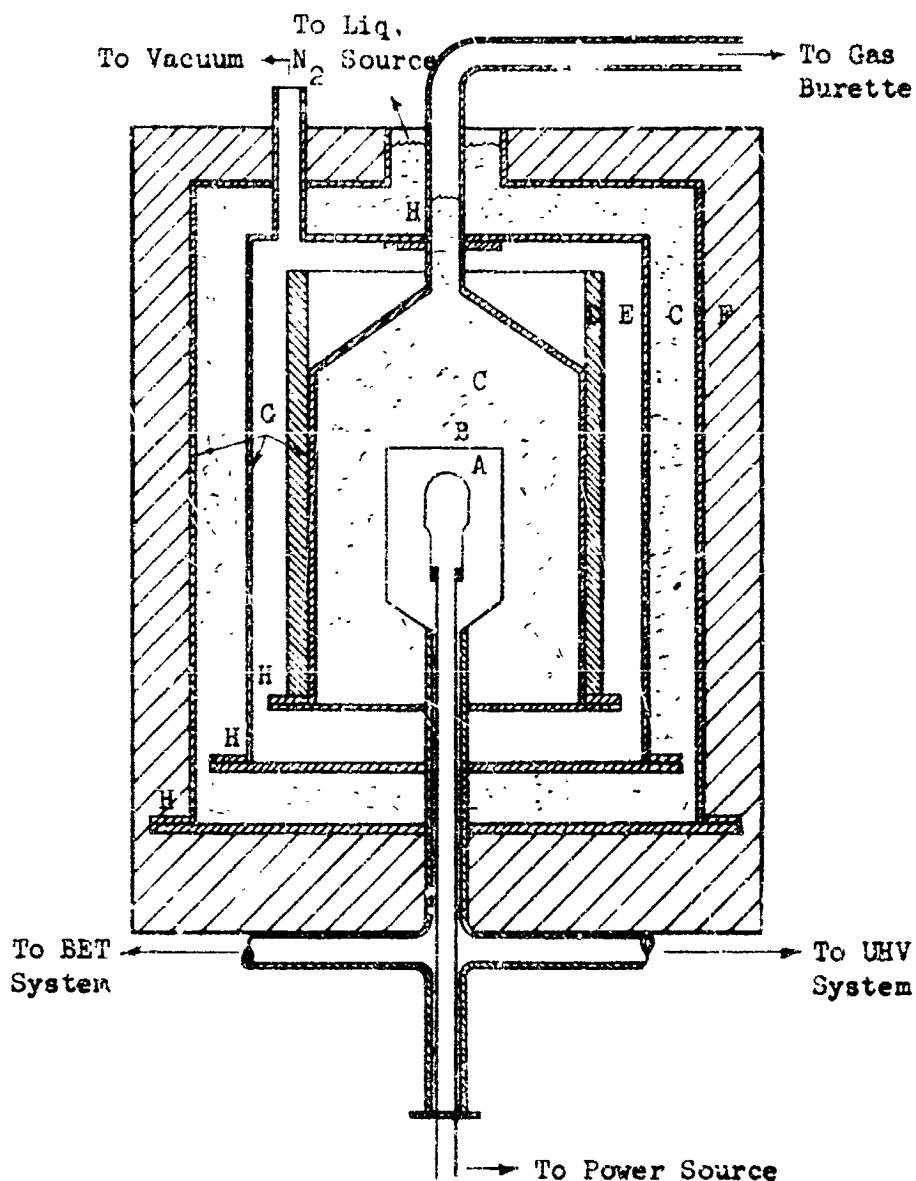
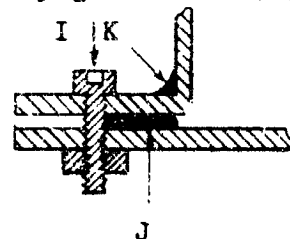


FIGURE 14 - Liquid Nitrogen Calorimeter

KEY

- A. Filament Assembly
- B. Vaporization Cell
- C. Liquid Nitrogen
- D. Radiation Shield
- E. Vacuum
- F. Polystyrene
- G. Monel Containers
- H. Cryogenic Seal (see insert)
- I. Allenhead 1/8" Bolts
- J. 50 In: 50 Sn Solder
- K. Silver Solder

Cryogenic Seal (H)



various authors for the insulation of cryogenic liquids. The type utilized in these experiments consisted of ten alternating layers of 0.001" thick aluminum foil and 0.015" thick glass fiber paper. Additional insulation for the calorimeter was provided by enclosing the outer container of liquid nitrogen in aluminum foil and a polystyrene casing (F) about 2" thick.

The normal heat leak attainable with the calorimeter was 0.05 cal/min. In order to retain a low heat leak a good vacuum (E) had to be maintained in the vacuum chamber and the level of liquid nitrogen in the outer container had to be kept constant. The latter was accomplished by adding liquid nitrogen continuously to the outer container.

The gas burette system is portrayed in Figure 15 and consisted of a gas collection vessel initially filled with distilled water and a small furnace for heating the nitrogen gas to approximately room temperature before collection within the burette. The gas was bubbled into the burette at atmospheric pressure at the tip of a bubbler near the bottom of the burette. The pressure within the container holding the calorimetric fluid was, therefore, held constant at atmospheric pressure. After the gas was collected and allowed to reach equilibrium, the temperature was read on a precision mercury thermometer to $\pm 0.05^{\circ}\text{C}$. The volume of gas collected in the burette could be ascertained to a precision of ± 0.5 cc which corresponds to ± 0.03 calories. Corrections were made for the partial pressure of water vapor mixed with the nitrogen gas in the burette. Corrections for the volume of nitrogen gas dissolved in the water were avoided by saturating

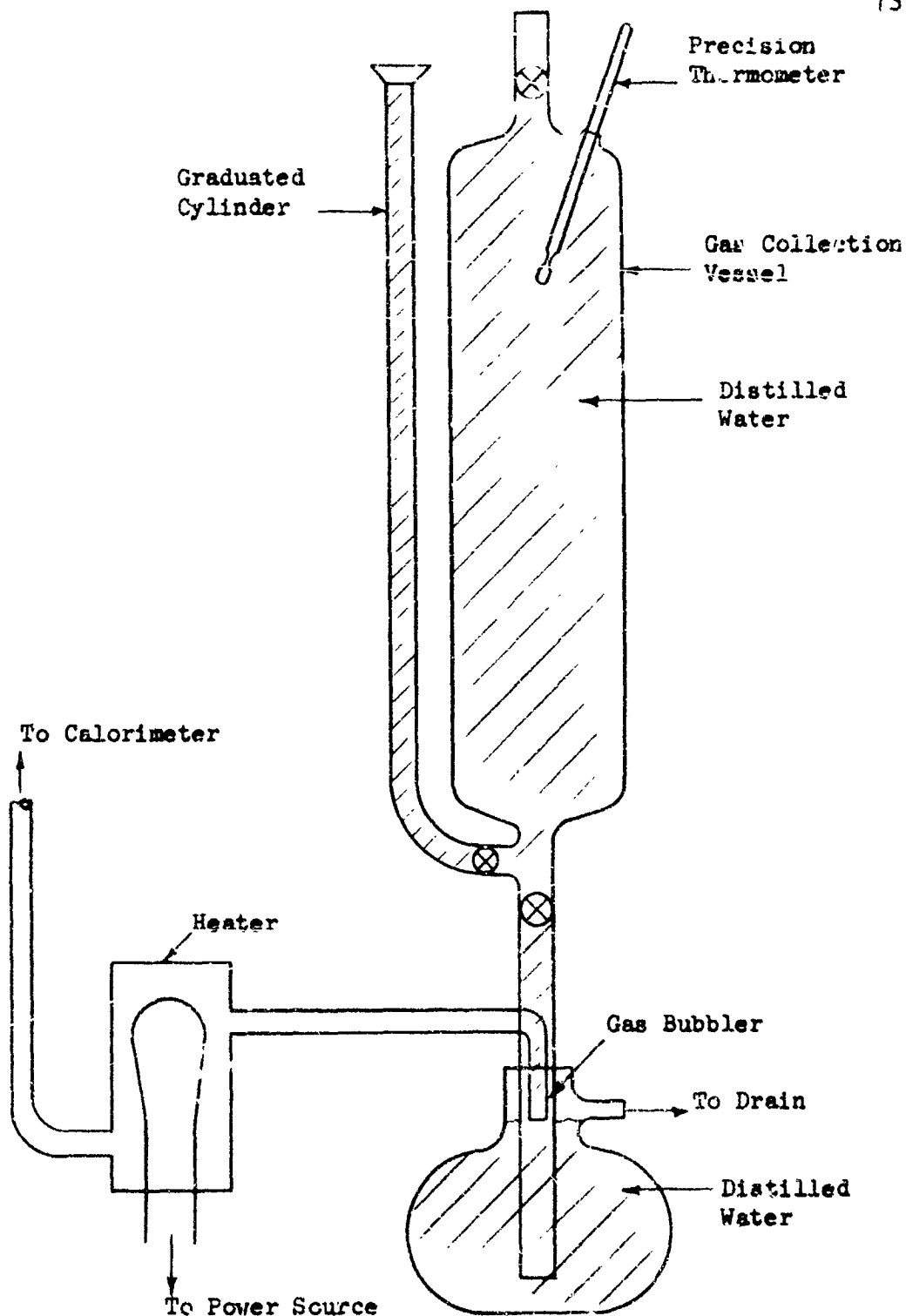


FIGURE 15 - Gas Burette

the water with nitrogen prior to a measurement. It was necessary to do this because of the poor data available concerning solubilities of nitrogen gas in water (cf. Landolt-Börnstein Zahlenwerte und Functionen (100)).

In the operation of the calorimeter and gas burette during an experimental run, the calorimeter heat leak rate was determined both prior to and following vaporization of the silver sample by counting the number of bubbles emanating from the bubbler tip in the gas burette. The leak rate was calculated from a known volume of gas per bubble and was subtracted from the total volume of gas liberated during a run.

E. Surface Area Measurement

There are many techniques in existence for the determination of the surface area of a finely divided powder or a thin film of a metal (cf. Plumb (101)). The need for a technique in this study of making the area measurements at liquid nitrogen temperature within the vaporization cell, which is a closed container, precluded the use of such techniques as the measurement of surface double layer capacitance in an electrolyte, the emission from a radioactive surface layer, or others. The technique more adaptable to this experiment was gas adsorption which has been reviewed recently by Emmett (102) and O'Connor and Uhlig (103). Of the many gas adsorption techniques devised for surface area determination, the Brunauer, Emmett, Teller (BET) (29) technique has been the most widely used and was adopted for our experimental measurement of the surface area of the thin films of silver deposited in ultra-high vacuum. Of the very large volume of literature concerning the BET

technique for surface area measurements, very little work has been reported for clean surfaces in ultra-high vacuum, e.g. cf. Allen, et al (33).

The validity of the BET technique for surface area determination has been vindicated, imposing certain limitations, by exhaustive comparisons with other techniques and by excellent agreement for different adsorbates using the proper BET method on the same adsorbent. The BET equation for adsorption on a porous solid is:

$$V = \frac{V_m C x}{(1-x)} \left(\frac{1 - (n+1)x^n + nx^{n+1}}{1 + (C-1)x - Cx^{n+1}} \right) \quad (39)$$

where V is the STP volume of gas adsorbed, V_m is the STP volume of one monolayer of adsorbed gas, x is the relative pressure, p/p_0 , where p_0 is the saturation vapor pressure, n is an empirical constant related to the number of layers of adsorbate required to fill up small pores or capillaries in the solid, and C is a constant proportional to $\exp(E_1 - E_L)/RT$ where E_1 is the heat of adsorption of the first layer and E_L is the heat of liquefaction of the adsorbate. If $n = 1$, the above equation reduces to the Langmuir adsorption isotherm:

$$\frac{x}{V} = \frac{1}{CV_m} + \frac{x}{V_m} \quad (40)$$

and if $n = \infty$, Equation (38) becomes the usual, well known, BET equation:

$$\frac{x}{V(1-x)} = \frac{1}{V_m C} + \frac{(C-1)x}{V_m C} \quad (41)$$

A method for evaluating the constant, n , as well as the constants V_m and C , and in addition, the range of applicability of each of the above three equations has been discussed by Joyner, et al (104). The importance of utilizing Equation (38) for the determination of surface areas of thin films deposited at liquid nitrogen temperature must be emphasized since the particle size of the crystallites is extremely small, (cf. Keith (105)) giving rise to the likelihood of small pore sizes. Adsorbents with small pore sizes have presented the most difficulties in surface area measurements.

The apparatus utilized to obtain the BET adsorption isotherm is portrayed in Figure 16. Methane gas of 99.94% purity as obtained from Phillips Petroleum Co. was used for the adsorbate. The melting point of methane is -182.5°C while the adsorbent temperature was -195.8°C ; therefore, the molecular area of the methane molecule in the solid state, 15.0 \AA^2 , was used, for determining the surface area once the constant, V_m , was found. The saturation vapor pressure of methane at -195.8°C was taken to be 9.55 Torr as given by Rossini (106).

Measurements were made shortly after the completion of an evaporation and after isolating the getter and ultra-high vacuum gauge from the thin film and breaking the large conductance break-off tip. Known volumes, A and/or B, were filled successively with methane from the reservoir and passed into the system by opening the appropriate valves, 3, 4, or 5. After each increment of methane had been metered into the system and adsorption had occurred, the system pressure was measured on one of the two

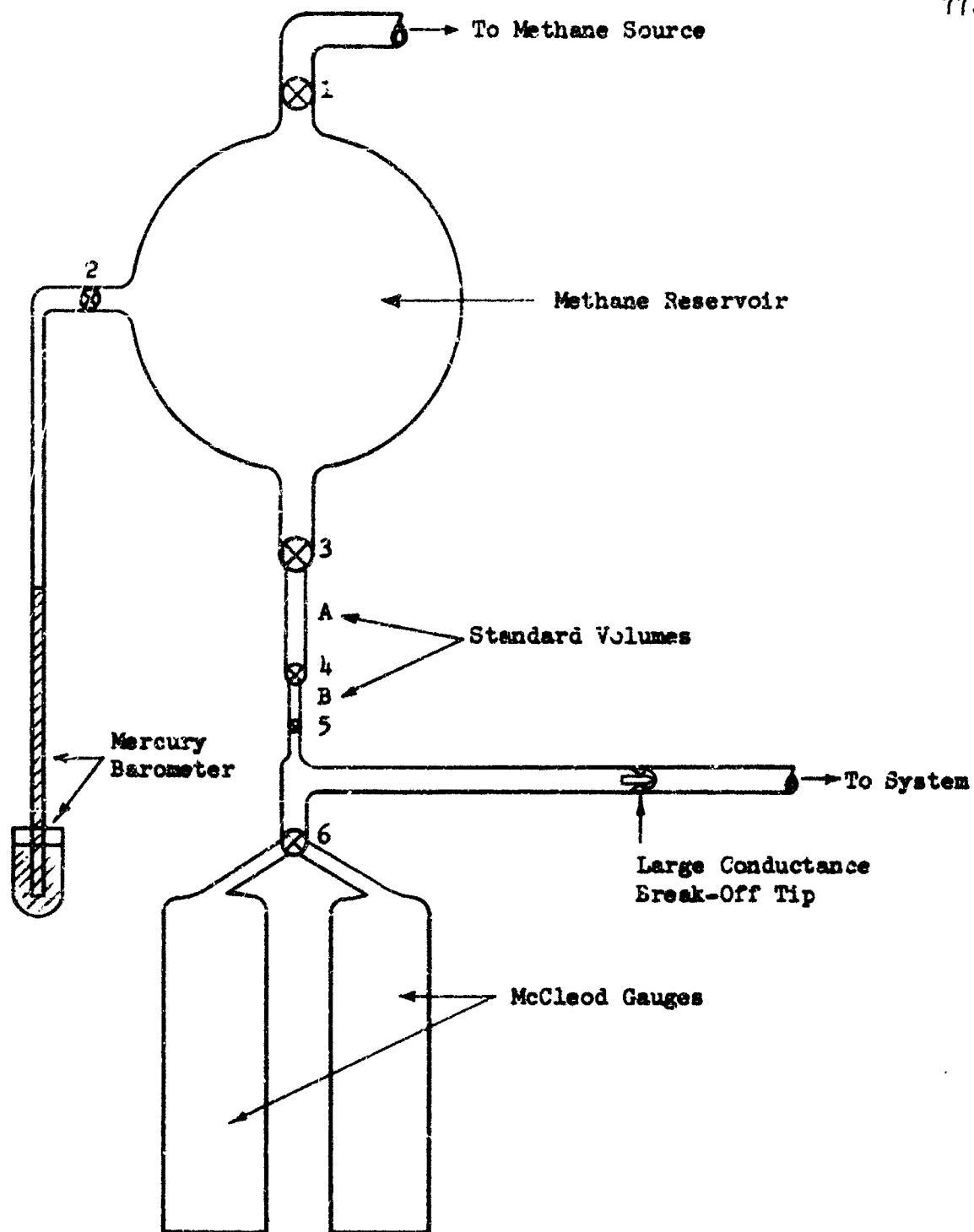


FIGURE 16 - Surface Area Measurement Apparatus (BET Technique)

McCleod gauges. One McCleod gauge had a pressure range of 10^{-5} - 10^{-1} Torr while the other gauge had a pressure range of 10^{-2} - 60 Torr. The volume of the entire system was known such that the resulting system pressure after admitting a known number of molecules would permit a calculation of the number of adsorbed molecules.

V. RESULTS AND DISCUSSION

The discussion given in the sections dealing with Theory and Other Experimental Techniques indicated that the surface tension of an atomically clean surface should be higher than that of a surface contaminated with adsorbed atoms. In addition, the effect of strain energy due to surface stress in solids was discussed. The magnitude of each of these effects is largely unknown but it is expected that both atomic cleanliness and surface stress will increase the energy of a solid surface over that of an unclean, unstrained surface. These expectations were verified by the experimental results obtained.

The experimental procedure has been outlined above and the techniques described for obtaining ultra-high vacuum and for determining the power input and heat evolved to the calorimeter were followed. Surface areas were determined by the BET technique and, for the precision obtained in these experiments, the two constant BET equation (Equation 41) was used rather than the equation involving three constants (Equation 39). The results for surface area, mass of silver evaporated and surface area per gram of thin film for one experimental run are:

<u>Area</u>	<u>Mass</u>	<u>Area per gm</u>
2490 cm ²	.015 gm	16.6 m ²

For this run, the difference between the electrical power input to the filament assembly and the heat evolved to the calorimeter was 0.203 calories. The energy used in forming the new surface was determined to be

$$\frac{0.203 \text{ cal} \times 4.185 \times 10^7 \text{ ergs/cal}}{2490 \text{ cm}^2} = 3960 \text{ ergs/cm}^2$$

for a solid silver thin film deposited on a silver substrate at 77°K in UHV. The surface tension of silver at 77°K obtained by extrapolating data given by Buttner et al (54)(who used the method of creep of thin wires in inert atmospheres) is 1675 ergs/cm^2 . Our results are a factor of 2.4 times this value and this factor is attributed to the effects of a clean surface and to the state of strain in the thin film as well as to the energies incorporated in point and line defects within the film.

From the experimental results and from known data the magnitude of each of these effects may be estimated. In order to do this, a model of the thin film deposited at 77°K must be formulated (see sections on Theory and Experimental Procedure). If the thin film is assumed to consist of small crystallites of less than about 100 Å diameter which are misoriented with respect to each other, then the extremely large surface area of the thin film compared to the substrate area indicates that the crystallites did not coalesce at this low temperature. Hence, the large dislocation densities due to the growing together of misoriented crystallites, as found in films deposited at higher temperatures, is avoided. The point defect density within the crystallites is, however, an unknown factor and could contribute to the energy of the thin film.

The energy of formation of a vacancy in silver is approximately 0.8 eV (107) which is about 18.4 kcal/mole. The weight of the thin film in this experiment was 0.015 gms or about 1.39×10^{-4} moles. Hence, the energy contribution by vacancies due to the vacancy concentration in this thin film, assuming a relatively high concentration value about 10^{-3} , would be only 0.0026 cal which would result in only a 1.3% error in the observed value.

The effect of strain energy on the energy of the surface has been

discussed above (see pp. 38 and 39). Planta, Ghey, and Piuze (108) have demonstrated that the strain in small, thermally equilibrated, silver crystallites (down to 60\AA) is quite appreciable. Using electron diffraction, they found that the lattice parameter was 1.1% smaller for crystallites of 60\AA diameter than for the bulk. From their results, they obtained a value for the surface stress of 5960 dynes/cm assuming that the entire change in lattice parameter was due to the surface stress.

It is possible to obtain a rough estimate of the strain energy within a granular thin film if the particle size and shape are known. If we assume, to start with, that a number, N , of cubic particles of side length l constitute the film, then the surface area of the film is $A = 6 l^2 N$. The number of particles, N , is equal to the volume of silver evaporated divided by the volume per particle and is $N = \frac{0.0014\text{cc}}{l^3}$. Since the surface area, A , is known, the side length is found to be about 300\AA . With a known particle size and knowing the surface stress and volume strain given by Planta et al (108) for silver, the total strain energy of the thin film can be calculated readily. If this is done for a particle size of 300\AA on edge, it is found that the strain energy is a negligible percentage of the total experimental energy, 0.203 calories. If, however, the particle size were 100\AA on edge, the strain energy is about 0.02 calories or about one tenth of the measured energy. Since the particles are most likely not cubic but elongated polyhedrons with highly stressed regions of contact between particles, and since the thin film is certainly not in thermal equilibrium, it was felt that the strain energy could easily approach a value of 0.02 calories.

Other energies involved in the condensation of the thin film are considered negligible. The interfacial energy between substrate and film

was considered very small because the surface area of the film is much larger than the interfacial area. Atomic migration energies in the film during deposition are considered negligible because of the cold substrate and, hence, short diffusion distance. Dislocation energies are insignificant since dislocation densities in such films are low and since the dislocation density in the initial sample (0.005" diameter wire) was probably high. From this discussion, it appears that most of the experimental energy measured (3960 ergs/cm^2) represents a true surface energy. If a maximum correction of 500 ergs/cm^2 is assumed in order to account for strain energy, point defect concentration, and other factors which increase the energy of the thin film, a value of approximately 3500 ergs/cm^2 is obtained for the surface energy of atomically clean silver at 77°K .

Another possible source of error was the measurement of surface area by the BET technique. A cross sectional area of 15.0 \AA^2 was used for methane assuming the solid state for the adsorbed gas. Hiza and Kidnay (109) have shown, however, for a silica gel that an adsorbed film of methane at 77°K is in a transition region ($76-88^\circ\text{K}$) between the solid and liquid states. In the liquid state, the cross sectional area of methane is 18.1 \AA^2 and, if this value is used, the surface energy is decreased by about 25%.

Although each phase of the surface energy determination technique, UHV evaporation, calorimetry, electrical analysis and BET analysis were calibrated independently there was no obvious method in which the whole series could be standardized in one continuous experiment; therefore, the observed surface energy values reported herein may be liable to an error in any one or more of the foregoing steps even though extreme

care was taken to prevent such an occurrence. Furthermore, the reported surface energy value is the result of one very successful series which correlated well with a second series. To obtain a higher degree of confidence in the technique as well as our reported values for silver a large number of runs ought to be made utilizing silver as a standard and the statistical reliability of the data determined for the technique. With the development of the apparatus used in these experiments the time necessary to conduct each run could probably be reduced from over a month to less than a week and would reduce the probability of apparatus failure in any step which normally terminates that run in failure.

VI. CONCLUSIONS AND RECOMMENDATIONS

The conclusions derived from the experimental and theoretical portions of this study include the following:

- 1) An atomic model of the solid surface was developed and the origin of surface stress explained. Surface stress and surface tension are considered in three dimensions and related to each other.
- 2) The state of equilibrium and of quasi-equilibrium in solid surfaces is developed and a relation between gradients of thermodynamic quantities in surfaces is derived.
- 3) A new direct approach to the experimental determination of surface tension in solids was developed which utilizes ultra-high vacuum.
- 4) An isothermal liquid nitrogen calorimeter was designed, constructed, and utilized in the determination of surface energies.
- 5) A surface energy value of 3500 ergs/cm^2 was obtained for atomically clean solid silver at 77°K .

Due to the success of the preliminary experiments discussed above and the numerous modifications in the apparatus that could improve the accuracy of the surface energy values, it is recommended that further development of this technique be pursued. A great deal of difficulty was encountered in obtaining ultra-high vacuum in the vaporization cell assembly due to oxidation of the cell during the bake-out cycle and subsequent formation of leaks. The maintenance of ultra-high vacuum when the cell was immersed in the calorimetric fluid, liquid nitrogen, also presented difficulties. The improvements in technique which are particularly recommended include standardization of the liquid nitrogen

calorimeter and perfection of surface area measurement technique. With further perfection of the apparatus, techniques for measuring heats of adsorption on atomically clean vapor deposited films could be very easily developed.

APPENDIX AList of Symbols

β	sticking probability
γ	surface tension
Γ	surface atomic concentration
θ	fractional surface coverage
λ	second derivatives of $\phi(r)$
μ	chemical potential
$\tilde{\mu}$	electrochemical potential
ν	stoichiometric coefficient
π	decrease in surface energy due to adsorption
σ	effective area of adsorbed molecules
$\tau_{\mu\nu}$	three dimensional surface stress tensor
ϕ	electric potential
$\phi(r)$	two-body potential energy
Φ	variable in heats immersion
a	lattice parameter
a, b	two-body potential constants
d	depth of body stresses
e, e_k	charge on k^{th} carrier, emissivity
e_s, e_{ev}	interfacial energies
σ_{ij}	two dimensional stress tensor of Herring
h	depth of surface stresses
$i(t)$	amperage
n	BET constant
p	pressure

$p_{\mu\nu}$	bulk stress tensor
q_j	unit vector components
r	radius
r_2, r_3	two and three body interatomic distances
s	molecular area
t	time
$u_{\mu\nu}$	strain tensor
$v(t)$	voltage
x	relative pressure, p/p_0
A	area
A'	area/gm of evaporated thin films
C	constant in BET equations
E	energy
F	Helmholtz free energy
\vec{F}	external forces
\vec{F}	non-electrical external forces
G	Gibbs free energy
H	enthalpy
J	scalar fluxes
\vec{J}	vector fluxes
K	first derivatives of $\phi(r)$
L	phenomenological coefficients
M	mass
N	number of atoms
P	pressure
Q	amenability to experimental technique
R	gas constant, resistances

S	entropy
T	temperature
U	energy
V	volume
V_m	STP volume of one monolayer of adsorbed gas
W	work, radiation energy
X	extensive thermodynamic variables, atomic positions, concentration
Z	evaporation rate
BET	Brunauer, Emmett, Teller adsorption isotherm and surface area measurement technique
NN	nearest neighbor
nNN	next-nearest neighbor
RT	room temperature
UHV	ultra-high vacuum
NBS	National Bureau of Standards

APPENDIX BHeats Involved In Evaporation Of The Silver Sample

In the experimental procedure electrical power heats the tungsten filament and silver sample from 77.4°K to the evaporation temperature, T_{ev} . Heat is transferred by radiation and by vaporized silver atoms from the filament to the walls of a surrounding cell, which is held in a liquid nitrogen cryogenic fluid at 77.4°K. Following the run, liquid nitrogen temperature is again attained throughout the system. If the temperature of the vaporized silver atoms can be assumed equal to the filament temperature, then the heat content of the gas between T_{ev} and 77.4°K plus the heat of sublimation will be released to the cell wall and, in turn, to the calorimeter. The total heat released, ΔH , per mole of condensed silver gas was calculated for various temperatures from data given by Hultgren et al (110) using a heat of sublimation of silver of 68,100 cal. Then the weight of silver evaporated from one cm^2 of surface area per second was taken from Dushman and Lafferty (23) and the total heat released to the calorimeter by silver atoms per second at various temperatures for the weight of silver evaporated is plotted in Figure 17.

The quantity of radiant energy received by the cell from the filament will follow the Stefan-Boltzmann law, $W = \alpha eAT^4$ where W is given in watts, α is a constant equal to 5.67×10^{-12} watts/ $cm^2 \text{ } ^\circ K^4$, e is the emissivity, A is surface area in cm^2 , and T is T_{ev} .

The sum of the radiant energy and heat released from the condensing gas per second is shown by a curve in Figure 17 which approaches the radiation curve at low temperatures and the ΔH curve at high temperatures. Thus, high temperatures are better in that radiation loss is a smaller

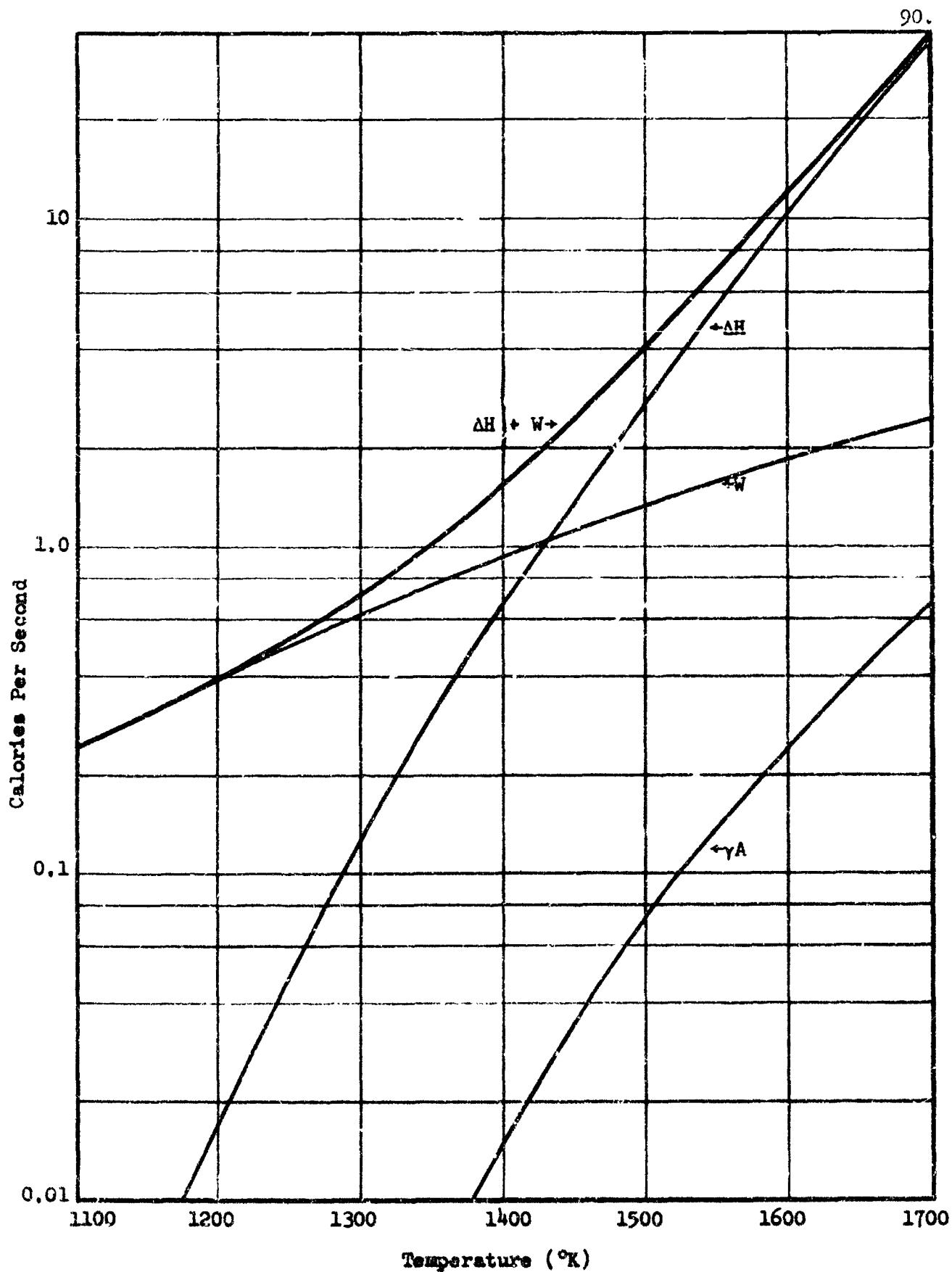


FIGURE 17 - A Plot of the Energies Involved Versus Temperature
In the condensation of a Silver Film.

percentage of the total energy and of the energy of the newly formed surface.

The total surface energy, γA , of the evaporated film is also plotted in Figure 17, again using the known evaporation rate of silver for various temperatures. This was accomplished by finding the number of grams evaporated from one cm^2 of surface area per second at each temperature and multiplying by $40 \text{ m}^2/\text{gm}$ to give an approximate area of surface of the evaporated film. This area was then multiplied by $\gamma = 1675 \text{ ergs/cm}^2$ at 77.4°K and converted to calories to give the curve shown.

The optimum temperature of operation would be the one at which the total surface energy of the deposited film was the highest percentage of the total heat evolved, $\Delta H + W$. This occurs at about 1600°K . Above this temperature, the curves separate farther apart and, in addition, data are not given for the evaporation rate of silver, so the curves were not extrapolated past 1700°K since the trend was obvious.

BIBLIOGRAPHY

- 1) Gibbs, J.W., "On The Equilibrium of Heterogeneous Substances", The Scientific Papers of J. Willard Gibbs (Dover Publications, Inc., New York, 1961) 1, 55-353
- 2) Wood, E.A., J. Appl. Phys. 35, 1306 (1964)
- 3) Mullins, W.W., "Solid Surface Morphologies Governed by Capillarity", Metal Surfaces (American Society for Metals, Metals Park, Ohio, 1963) pp. 17-66
- 4) Frank, F.C., "The Geometrical Thermodynamics of Surfaces", *ibid.*, pp. 1-16
- 5) Kaplan, H., Phys. Rev. 125, 1905 (1962)
- 6) Shewmon, P.G., and Robertson, W.M., "Variation of Surface Tension With Orientation", Metal Surfaces (American Society for Metals, Metals Park, Ohio, 1963) pp. 67-98
- 7) Herring, C., "The Use of Classical Macroscopic Concepts in Surface-Energy Problems", Structure and Properties of Solid Surfaces (University of Chicago Press, Chicago, 1953) pp. 5-72
- 8) Seeger, A., and Mann, E., Z. Naturforsch 14a, 154 (1959)
- 9) Herring, C., "Surface Tension as a Motivation for Sintering", The Physics of Powder Metallurgy (McGraw-Hill Book Company, Inc., New York, 1951) pp. 143-178
- 10) Shuttleworth, R., Proc. Phys. Soc. (London) 63, 444 (1950)
- 11) Lennard-Jones, J.E., and Dent, B.M., Proc. Roy. Soc. (London) A121, 247 (1928)
- 12) Cottrell, A.H., Dislocations and Plastic Flow in Crystals (Oxford University Press, London, 1953)
- 13) Born, M., and Huang, K., Dynamical Theory of Crystal Lattices (Oxford University Press, London, 1954)
- 14) Weyl, W.A., "Wetting of Solids as Influenced by the Polarizability of Surface Ions", Structure and Properties of Solid Surfaces, (University of Chicago Press, Chicago, 1953) pp. 147-180
- 15) MacRae, A.U., and Germer, L.H., "The Interatomic Spacings at the Surface of a Clean Nickel Crystal", Ann. New York Acad. Sci. 101, Article 3, pp. 627-633
- 16) Farnsworth, H.E., private communication

- 17) Schlier, R.E., and Farnsworth, H.E., J. Chem. Phys. 30, 917 (1959)
- 18) Lander, J.J., and Morrison, J., J. Chem. Phys. 37, 729 (1962)
- 19) Farnsworth, H.E., Marsh, J.B., and Toots, J., Proc. Interat. Conf. Phys. Semiconductors, Exeter, 1962, pp. 836-841
- 20) Haneman, D., *ibid.*, pp. 842-847
- 21) Sokolnikoff, I.S., Mathematical Theory of Elasticity (Summer Session, Brown University, Providence, R.I., 1941)
- 22) Walton, A.G., J. Chem. Phys. 39, 3162 (1963)
- 23) Dushman, S., and Lafferty, J.M., Vacuum Technique (John Wiley and Sons, Inc., New York, 1962)
- 24) MacRae, A.U., and Germer, L.H., J. Appl. Phys. 33, 2923 (1962)
- 25) Ehrlich, G. in Structure and Properties of Thin Films (John Wiley and Sons, Inc., New York, 1959) pp. 423-471
- 26) Ehrlich, G. in Metal Surfaces (American Society for Metals, Metals Park, Ohio, 1963) pp. 221-258
- 27) Hill, T.L. in Advances in Catalysis IV, 211-258 (1952)
- 28) Olivier, J.P., and Ross, S., Proc. 2nd Interat. Cong. Surface Activity, II, 46 (1957)
- 29) Brunauer, S., Emmett, P.H., and Teller, E., J. Am. Chem. Soc. 60, 309 (1938)
- 30) Hirth, J.P., and Pound, G.M., Prog. Materials Sci. 11, 1963
- 31) Moazed, K.L., and Pound, G.M., Trans. AIME, 230, 234 (1964)
- 32) Duell, M.J., and Moss, R.L., Brit. J. Appl. Phys. 12, 157 (1964)
- 33) Allen, J.A., Evans, C.C., and Mitchell, J.W. in Structure and Properties of Thin Films (John Wiley and Sons, Inc., New York, 1959) pp. 46-50
- 34) Swaine, J.W., Jr., and Plumb, R.C., J. Appl. Phys. 33, 2378 (1962)
- 35) Allen, J.A., Aust. J. Chem. 13, 210 (1960)
- 36) Ehrlich, G., Brit. J. Appl. Phys. 15, 349 (1964)
- 37) Herring, C. in Metal Interfaces, ASM Trans. 44a, 1 (1952)
- 38) Hellman, H., "Einführung in die Quantenchemie", (F. Deuticke, Leipzig and Vienna, 1937) p. 285

- 39) Feynman, R.P., Phys. Rev. 56, 340 (1939)
- 40) Tompkins, F.C., and Culver, R.V., Adv. in Catalysis 11, 67 (1959)
- 41) Cahn, J.W., and Hilliard, J.E., J. Chem. Phys., 28, 258 (1958)
- 42) Hart, E.W., Phys. Rev. 113, 412 (1959)
- 43) Prigogine, I., Thermodynamics of Irreversible Processes (Interscience Publishers, New York, 1961)
- 44) de Groot, S.R., Thermodynamics of Irreversible Processes (North-Holland Publishing Company, Amsterdam, 1958)
- 45) de Groot, S.R., and Tolhoek, H.A., Proc. K. Ned. Acad. Wet. 54(B), 41 (1951)
- 46) Inman, M.C., and Tipler, H.R., Met. Revs. 8, 105 (1963)
- 47) Nabarro, F.R.N., "Deformation of a Crystal by the Motion of Single Atoms", in Report of a Conference on the Strength of Solids (London: Physical Society, 1948)
- 48) Herring, C., J. Appl. Phys. 21, 437 (1950)
- 49) Chapman, I.C., and Porter, H.L., Proc. Roy. Soc. A83, 65 (1909)
- 50) Sawai, I., and Hishida, M., Z. Anorg. Allgem. Chem., 193, 1119 (1930)
- 51) Tammar, G., and Boehme, W., Ann. Physik. 12, 320 (1932)
- 52) Udin, H., J. Metals 3, 63 (1951)
- 53) Funk, E.R., Udin, H., and Wulff, J., J. Metals 3, 1206 (1951)
- 54) Buttner, F.H., Udin, H., and Wulff, J., J. Metals 3, 1209 (1951)
- 55) Hayward, E.R., and Greenough, A.P., J. Inst. Metals, 88, 217 (1959)
- 56) Radcliffe, S.V., J. Less Common Metals 3, 360 (1961)
- 57) Inman, M.C., McLean, P., and Tipler, H.R., Proc. Roy. Soc. (London) 273, 538 (1963)
- 58) Prenatis, A.L., and Pound, G.M., Trans. AIME, 203, 664 (1955)
- 59) Allen, J.A., Aust. J. Chem. 13, 210 (1960)
- 60) Greenhill, E.B., and McDonald, S.R., Nature, 171, 37 (1953)
- 61) Schlier, R.E., and Farnsworth, H.E., in Semiconductor Surface Physics, edited by R.H. Kingston, 1957

- 62) Farnsworth, B.E., Schlier, R.E., George, T.H., and Buerger, R.M.,
J. Appl. Phys. 29, 1150 (1958)
- 63) Griffith, A.A., Phil. Trans. Roy. Soc. (London) A221, 163 (1920-21)
and Proc. Internat. Congr. Appl. Mech. (Delft), 55 (1924)
- 64) Obreimoff, J.W., Proc. Roy. Soc. (London) A127, 290 (1930)
- 65) Orowan, E., Z. Phys. 62, 239 (1933)
- 66) Westwood, A.R.C., and Hitch, T.T., J. Appl. Phys. 34, 3085 (1963)
- 67) Westwood, A.R.C., and Goldheim, D.L., J. Appl. Phys. 34 (1963)
- 68) Gross, G., Midwest Research Institute, personal communication
- 69) Gilman, J.J., J. Appl. Phys. 31, 2208 (1960)
- 70) Bailey, A.I., Sec. Internat. Conf. Surf. Act. III, 406 (1957)
- 71) Deryogin, B.V., and Metsik, M.S., Soviet Physics-Solid State 1,
1393 (1960)
- 72) Bryant, P., Taylor, L., and Gutshall, P., Trans. Tenth Nat. Vac.
Symp., 21 (1963)
- 73) Bryant, P., Gutshall, P., and Taylor, L., to be published in the
Journal Wear
- 74) Westwood, A.R.C., and Kandar, M.H., Phil. Mag. 8, 787 (1963)
- 75) Berry, J.P., J. Appl. Phys. 34, 62 (1963)
- 76) Snowden, K.U., J. Appl. Phys. 34, 3150 (1963)
- 77) Westwood, A.R.C., Fracture of Solids, 20, 553 (1963)
- 78) Lipsett, J., Johnson, R., and Maass, P., J. Am. Chem. Soc. 50,
2701 (1928)
- 79) Jura, G., and Garland, C., J. Am. Chem. Soc. 74, 6033 (1952)
- 80) Brunauer, S., Sec. Internat. Conf. Surf. Act. II, 17 (1957)
- 81) Schubert-Birckenstaedt, M., Z. Anorg. Chem. 276, 227 (1954)
- 82) Harkins, W.D., and Jura, G., J. Am. Chem. Soc. 66, 1362, 1366
(1944)
- 83) Meissner, H., Z. Anorg. Allgem. Chem. 110, 169 (1920)
- 84) White, D.W.G., Trans. ASM, 52, 757 (1962)

- 85) Skapski, A.S., *Acta Met.* 4, 576 (1956)
- 86) Good, R.J., Girifalco, L.A., and Kraus, G., *J. Phys. Chem.*, 62, 1418 (1958)
- 87) Jarboor, J.P., Charbonnier, F.M., Dolan, W.W., Dyke, W.P., Martin, E.E., and Trolan, J.K., *Phys. Rev.* 117, 1452 (1960)
- 88) Barnes, R.S., *Phil. Mag.* 5, 635 (1960)
- 89) Amelinckx, S., Maenhout-Vander Vorst, W., and Dekeyser, W., *Acta Met.* 7, 8 (1959)
- 90) Haneman, D., U. of New South Wales, Australia, private communication.
- 91) Frazer, M.J., *Acta Met.* 8, 732 (1960)
- 92) Borel, J., *C.R. Aca. Sci. (Paris)* 257, 1847 (1963)
- 93) Shewmon, P.G., *Trans. AIME*, 227, 400 (1963)
- 94) Bailey, G.L.J., and Watkins, H.C., *Proc. Phys. Soc.* B63, 350 (1950)
- 95) Brennan, D., Hayward, D.O., and Trapnell, B.M.W., *Proc. Roy. Soc. (London)* A256, 81 (1960)
- 96) Rock, H.L., and Plumb, R.C., *Appl. Phys. Letters* 1, 11 (1962)
- 97) Spalvins, T., and Keller, D.V., in *Trans. Vac. Met. Conf.*, edited by R.F. Bunshah, 1962, pp. 149-155
- 98) Furukawa, G.T., Ginnings, D.C., McCoskey, R.E., and Nelson, R.A., *J. Res. Nat. Bur. Stds.*, 46, 195 (1951)
- 99) Glaue, W.F., and Clayton, M., *J. Am. Chem. Soc.* 55, 4875 (1933)
- 100) Landolt-Bornstein Zahlenwerte und Functionen, II Band, 2 Teil, Bandteil b (Springer-Verlag; Berlin, 6 Auflage, 1962) s. 1-22
- 101) Plumb, R.C., *J. Electrochem. Soc.* 105, 502 (1958)
- 102) Emmett, P.H., in *Advances in Catalysis*, Vol. I, edited by W. G. Frankenburg, V.I. Komarevsky and E.K. Rideal (Academic Press, Inc., New York, 1948)
- 103) O'Connor, T.L., and Uhlig, H.H., *J. Phys. Chem.* 61, 402 (1957)
- 104) Joyner, L.G., Weinberger, E.B., and Montgomery, C.W., *J. Am. Chem. Soc.* 67, 2182 (1945)
- 105) Keith, H.D., *Proc. Phys. Soc. (London)* 69B, 180 (1956)

- 106) Rossini, F.D., "Selected Values of Properties of Hydrocarbons",
Am. Pet. Inst., Project 44 (1953)
- 107) Fumi, F.G., Phil. Mag. 46, 1007 (1955)
- 108) de Planta, T., Grey, R., and Piuze, F., Helv. Phys. Acta 37, 74
(1964)
- 109) Hiza, M.J., and Kidnay, A.J., Adv. in Cryogenic Engr. 6, 457 (1961)
- 110) Hultgren, R., Orr, R.L., Anderson, P.L., and Kelley, K.K.,
"Thermodynamic Properties of Metals and Alloys", (John Wiley and
Sons, Inc., New York, 1963)

BIOGRAPHICAL NOTE

Name: Wilbur Mitchell Franklin, Jr.

Date and Place of Birth: February 28, 1933; Berlin, Germany

Elementary Schools: Public School No. 19, Patterson, New Jersey
St. Clairsville Elementary School,
St. Clairsville, Ohio

Junior High School: North Junior High School, Newburgh, New York,
Graduated 1947

High School: Newburgh Free Academy, Newburgh, New York,
Graduate 1950

Colleges: The College of Wooster, Wooster, Ohio, B.A.,
1954
Case Institute of Technology, Cleveland, Ohio,
B.S., 1957

Graduate Work: Yale University, New Haven, Connecticut,
Holder of Kaiser Aluminum Fellowship, M.S.,
1962
Syracuse University, Syracuse, New York
Graduate Assistant

N64-29219

PART II

FORCES OF ADHESION BETWEEN
CLEAN METALLIC SOLIDS

by

Daniel Hauser

(In Part - Master's Thesis)

TABLE OF CONTENTS AND ILLUSTRATIONS

	Page
I. Introduction	1
II. Theory of Metallic Adhesion	2
Table 1 - Adhesion Data	4
Figure 1 - Mean Coefficient of Adhesion Versus Melting Point ..	10
III. Experimental	18
Figure 2 - UHV Analytical Balance	19
Figure 3 - Balance Knife-Edge Fulcrum	20
Figure 4 - Solenoid Circuit Resistance Versus Wire Mass	22
Figure 5 - Indenter Assembly	23
Figure 6 - Balance Assembly	25
Figure 7 - Glass Valve	26
IV. Discussion	29
V. Bibliography	31

I. INTRODUCTION

Previous research on solid adhesion and its mechanism has provided a great deal of data and insight into the mechanism of this phenomena. Indenter-plate contact, twist-compression bonding, and roll bonding have been the major experimental techniques of study; permitting the correlation of adhesion tendencies with various physical, mechanical, and chemical properties of the materials under consideration. Several authors have suggested that adhesion between metals will not occur unless combined normal and tangential stresses are applied to the surfaces in contact.

An atomistic approach to the problem, however, suggests a mechanism for metallic adhesion in which the application of either normal or tangential forces is unnecessary provided the surfaces are atomically clean when they are brought into contact.

An analytical balance for measuring adhesion forces between clean surfaces in ultra-high vacuum was designed, constructed and tested. Several alterations in design of the equipment have been made following preliminary experiments.

II. THEORY OF METALLIC ADHESION

Metallic adhesion, or the cold welding of metal surfaces when they are brought into contact, can be considered (1,2,3) to arise from both mechanical and chemical processes. The mechanical process involves the interlocking of surface irregularities, intrusion or extrusion of one phase into or around the other. This process is a function of the mechanical properties of each of the phases and not their inherent chemical or electrical properties. The latter processes, which are of particular interest in this study, are a function of the surface chemistry of the phases and their relation to one another. In a hypothetically ideal situation, atomically clean and planar surfaces of the same material could achieve bonding (autohesion) without the application of an exterior mechanical force (26). If the two surfaces meet in crystallographic coincidence, the resulting adhesion energy should be equivalent to twice the surface energy (2γ) (28). The presence of crystallographic misorientation or of surface impurities in such an ideal contact, however, would tend to reduce the adhesion energy with an accompanying excess energy at the interface which is often called an "interfacial energy".

Dissimilar metal couples, while displaying analogous phenomena in varying intensities, also display chemical reactions of one surface with the other, diffusion of one into the other, and electrical quasi-equilibrium phenomena at the interface. As a consequence, a simple interpretation of interfacial behavior during adhesion presents a most difficult problem.

Before considering the more specific details of adhesion or autohesion between metal couples as presented by several authors, two factors ought to be presented which seem to be constant throughout all of the

investigations, i.e. the interruption of adhesion by surface impurities; and secondly, the high interfacial strengths observed in metal-metal adhesion as opposed to those bonding strengths of oxide-oxide or metal-oxide systems. Since only solid state adhesion is under consideration, the two factors are often involved simultaneously. For example, adhesion of one metal with another under impure conditions (low vacuum or atmospheric) requires relatively high, normal or tangential forces to insure a stable weld.

The underlying chemical principles which seem to fit the experimental observations arise from the ability of the free metal atom in a crystal to retain a high percentage of its original atomic bond strength even while undergoing a considerable amount of mechanical strain, i.e. the placement of atoms away from their equilibrium lattice positions. Covalent solids, on the other hand, though capable of a degree of mechanical strain, are far more apt to cleave under such a strain than metallic materials which suggests that atomic displacement of covalently bound materials will promote bond fracture rather than the absorption of strain. An extension of this view into the adhesion process suggests that covalent or ionic solids require rather exact positioning of nearest neighbor atoms at the interface before strong atomic bonds can be formed, whereas metals will accept a more liberal positioning of their nearest neighbors. The former is characterized by the inability of covalent solids, e.g. diamond, graphite, silicon, etc., to form stable powder compacts when subjected to briquetting tests below the diffusional temperature range. Degassed nickel powder, on the other hand, will adhere under its own weight below 400°C.

The presence of van der Waals forces during any surface to surface

contact procedure is expected to contribute as well as the metallic and valence forces. The magnitudes of van der Waals attractive forces between solid plates of some oxides have been measured (31) but very little data is available for these forces in metal-oxide or metal-metal (29) systems.

As a consequence, the interference of surface contamination, including adsorbed gases, in a metallic adhesion experiment would behave as an unknown, uncontrollable variable interrupting the metal-metal contact via metal-oxide and oxide-oxide junctions. Because the area of each type of contact and its corresponding bond strength is unknown, an accurate analysis of the interface would be impossible. One approach to the separation of these variables was presented by Spalvins et al (2) in which the metallic samples were cleaned of their oxide coatings and of their adsorbed gases by argon ion bombardment and electron bombardment treatments in ultra-high vacuum (UHV) before each test was made. They presumed the surfaces to be ideally clean, i.e., at least 90% of the atoms in contact were metallic. The results of these experiments are shown in Table I in which adhesion occurred between miscible metal pairs and no adhesion between immiscible pairs (3).

TABLE I

<u>Adhesion Observed</u>	<u>No Adhesion Observed</u>
Iron-Aluminum	Copper-Molybdenum
Copper-Silver	Silver-Molybdenum
Nickel-Copper	Silver-Iron
Nickel-Molybdenum	Silver-Nickel

In an analysis of these data they suggested that adhesion was observed if the two metals produced a negative heat of mixing, i.e. they formed a solid solution or intermetallic phase. If, however, the metals

displayed a positive heat of solution, no adhesion was observed. The latter criterion is normally indicated by a complete immiscibility gap in the equilibrium phase diagram at the temperature of testing. Emphasis ought to be made of the fact that after an adhesion junction is formed, and for that matter even after diffusion has been allowed to take place, thermodynamic equilibrium cannot be achieved at the interface until the diffusion fluxes, both mass and electronic, have equilibrated. For example, after contact a junction potential ought to be present with its associated thermoelectric properties (25, 27). Under conditions of increased temperature ($> 0.75 T_m$ where T_m is the melting temperature) the chemically isolated interface will begin to diffuse over a distance perpendicular to the interface and exhibit phenomena related to the Kirkendall effect (32,33,34), e.g. porosity (32,34), Matano interface (33), and possible compound formation (21) depending on the system in question.

Since the examination of some of these phenomena and their correlation with an atomistic mechanism of adhesion is the purpose of this investigation, a review of several related studies dealing with the mechanical aspects of the adhesion junction and its formation seem pertinent. According to Bowden et al (4,5,24), two factors prevent the occurrence of adhesion under atmospheric or low vacuum conditions. As previously discussed, the interference of surface oxides or adsorbed gases will prevent metal-metal contact unless a tangential stress of sufficient magnitude is applied to cause disruption of these protective impurities. The second factor suggests that a reduction in adhesion results from the release of elastic stresses at the interface when the normal compressive load is removed. For example, elastic stresses produced upon removal of the compressive load during adhesion are

minimal in ductile metals with low elastic limits such as indium (24) and, therefore, do not significantly hinder adhesion. Most other metals do not adhere as readily as indium since they are less ductile, have higher elastic limits, and their surfaces oxidize or become contaminated in air more rapidly. An apparatus (24) was constructed for the investigation of the influence of surface contamination, ductility, temperature, and combined tangential and normal stresses on adhesion. Specimens were heated in vacuum (10^{-6} mm Hg) to a temperature near their evaporation point, cooled to room temperature, and pressed together with a normal force. Adhesion was observed although the bond strengths in tension were not very reproducible. An increase in adhesion was observed, however, when a tangential prestressing force was applied to the specimen which did not cause macroscopic sliding of the specimens across one another. The adhesion was roughly proportional to the prestressing force and is explained by the increased cleanliness of the surfaces and the growth of the contact junctions under combined stresses (18). The authors developed and discussed an equation based on plasticity theory (5) which related the tangential force coefficient (μ) to the adhesion coefficient (σ) and included the effect of elastic recovery upon release of the applied normal compressive load:

$$1 + \alpha\mu^2 = \left(\frac{\sigma}{\sigma_0}\right)^{4/3}$$

where α and σ_0 are constants. The tangential force coefficient is related to the experimental parameters through: $S = \mu \frac{W}{A}$, where: S is the tangential stress, A is the area of contact, and W is the normal load. The adhesion coefficient was defined as the ratio of the adhesion force

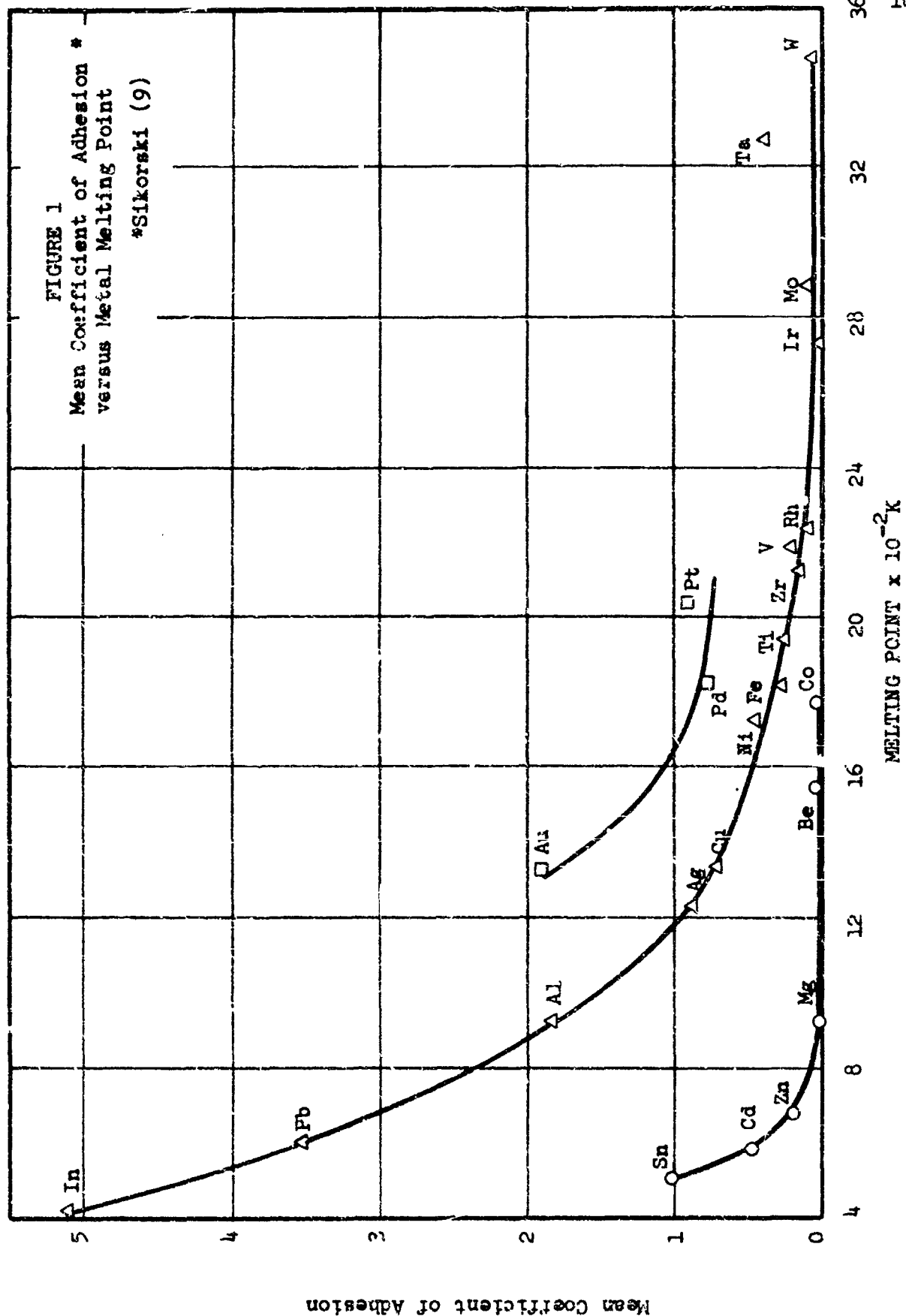
to the joining load. In order to study the effect of ductility on adhesion, experiments were performed wherein the time for applying a load was equal to the time to rupture the adhesive bonds. When performed in the annealing temperature range of the specimens, the constant σ_0 , evaluated graphically, was greater than at room temperature as a result of the increased ductility of bonded regions at elevated temperatures. It was suggested that annealing may also improve the bond strength by removing some of the structural imperfections and promoting diffusion within the interfacial region.

Several major problems appear to still remain unanswered in a consideration of Bowden's investigations. The first and probably most crucial is the behavior of contaminating films at the interface prior to adhesion. A number of investigators (35,38) have shown that the possibility of preparing an atomically clean metal surface by thermal evaporation or cycling techniques is very small. For example, Farnsworth (38) held silver at red heat in a pressure of 10^{-8} Torr for over 2000 hours and was still able to report the presence of a sorbed layer, capable of interference with the work function experiments. Therefore, the questions at hand are: is this sorbed layer, which no doubt lowers the surface energy (28), capable of hindering adhesion processes and secondly, are tangential stresses necessary to disturb this interfering layer in order to permit metal-metal contact? Closely related to these questions and forming another unanswered problem is the proposed necessity for a normal force in order to produce an adhesion junction. According to Debye (26), two surfaces do have an attractive force for each other when they are separated by a few hundred angstroms of vacuum space and should possess a bond strength without the aid of an

applied normal force. The dispersion forces involved in the surface contact of oxides (26) is quite small and certainly not the entire bond strength developed in an adhesion weld; however, such forces do provide a mechanism for intimate contact of metallic atoms if no foreign atom interference is present. In experiments involving real surfaces, which are not entirely clean, the normal force may be necessary for enlarging the contact area through plastic deformation of surface asperities such that immediate macro-adhesion forces can be observed by an experimenter. The presence of such normal forces may not, however, be necessary in the development of an adhesion mechanism.

A great deal of valuable data regarding the behavior of one metal in contact with another has been generated by Anderson and Sikorski et al (6-11,16) and Milner et al (19-23) in which the contact junctions were formed between metals by the "brute force" approach to adhesion. Their technique generally utilized an extreme normal force accompanied by transverse forces of a magnitude great enough to expand the contact interface under atmospheric conditions such that extended metal-to-metal contact was eventually obtained. Residual oxide and sorbed gases were reduced by mechanical filing or brushing in air prior to forcing the surfaces together. The twist-compression bonding techniques developed by Anderson (6,7) and extended by Sikorski (9-11) involve the placement of a 1/4" rod of material in compression with a 1/4" O.D. - 1/8" I.D. tube of the same material and rotating one specimen 180° while holding the other rigidly. A coefficient of adhesion was defined as the ratio of the adhesion force to the force used to make the junction. The large degree of scatter in the data necessitated statistical analysis of the results for each sample pair. The median coefficient was found to be reproducible.

The authors related the median coefficient of adhesion to surface contamination, crystal structure, work hardening coefficient, specimen purity, hardness, elastic modulus, melting point, recrystallization temperature, atomic radius, and surface energy. These factors except for the latter two are considered to be mechanical rather than physiochemical and, therefore, represent influences on the ability to place clean metallic surfaces in contact. The effect of surface contamination is essentially the same as that presented by Bowden (5) in that it prevents metal-to-metal contact and may be largely overcome by the application of tangential stresses. The most noticeable influence of crystal structure was the low coefficients of adhesion observed for hexagonal close-packed metals as compared to cubic structures as shown in Figure (1). These results are probably due to differences in plastic deformation behavior as a result of divergent dislocation mechanisms. While body-centered cubic crystals may slip or glide on several planes ($\{110\}$, $\{112\}$, and $\{123\}$) and face-centered cubic on four sets of $\{111\}$ octahedral planes, the hexagonal close-packed structures glide predominately on the basal $\{0001\}$ planes so their deformation is comparatively restricted, whereby removal of surface contamination and attainability of surface conformity are correspondingly hindered. The work hardening coefficient, defined as the slope of the true stress versus true strain curve and evaluated by tensile testing, is intimately related to structure (12). The HCP metals, with only one easy glide system do not work harden readily and have a low work hardening coefficient compared to the cubic metals. Work hardening during plastic flow also strengthened the contact junctions once they had formed. Decreased sample purity increased adhesion by interfering with dislocation motion, thereby resisting plastic



deformation at the interface. It was shown that the median coefficient of adhesion decreased as the specimen hardness increased, the hardness being measured on the sample faces after the junction was broken. The effect of a large elastic modulus was to inhibit plastic deformation and thus lower the adhesion coefficient. Large values of the median coefficient of adhesion were associated with large atomic volumes, which was ascribed to decreased cohesive forces between larger atoms (13). The melting point of a metal, also a measure of cohesive forces, (13) was relatively lower for greater median adhesion coefficients. The recrystallization temperature, at which grain growth occurs and strength and internal stress decreases (14) was a measure of the resistance to adhesion. A low recrystallization temperature implies that asperity junctions would be ductile and able to withstand elastic recovery effects at the interface when the normal load was removed. The mechanical aspect of surface energy dictated that high surface energies, corresponding to high hardnesses, resulted in low median coefficients of adhesion. The physicochemical aspect of surface energy was considered in an ideal experiment where the specimens of a single metal were atomically clean and planar and were brought into contact in ultra-high vacuum. The adhesive force was a function of the surface energy and metal couples with high surface energies would exhibit greater adhesion than those with low surface energies. High surface energy implies high hardness so that the competing factors (surface energy and hardness) tend to complicate the picture. When dissimilar metal couples contact one another, interfacial energy plays a role. Solid-solubility, considered a general trend setting factor by Keller and Spalvins (1-3) and others, is supported by Sikorski and Courtney-Pratt (10) who report that atomic size factors and

crystal structures of rare earth metals suit them well for uses requiring low adhesion. Hume-Rothery (14) illustrated the correlation between size factor (percentage difference in atomic diameters), crystal structure, and extent of solid solution.

Milner et al (19-23) have investigated the processes of adhesion through a roll bonding technique in which two metals were bolted together and compressively rolled to some predetermined degree of deformation. In effect the rolling process serves to expand the interface in the absence of contaminant gases to a degree in which metal-metal atoms are brought into contact. In a discussion of the mechanism (23) of roll bonding the effect of the variables of surface preparation, surface contamination, roll pressure, time and temperature were considered.

Experimentally, 4" x 4" metal composites were passed through compressive rolls and regions of the bonded couple were tested in tensile shear after the amount of deformation had been calculated. The effect of adsorbed contaminants was evaluated by applying various surface preparations and measuring the shear strength of the composites as a function of percent deformation. The preparations included machining, scratch-brushing followed by degreasing, degreasing followed by scratch-brushing, and electropolishing the surfaces. In one case aluminum specimens were preheated to 500°C and cooled in a desiccator to prevent readsorption of impurities, while in the other this preliminary step was omitted. The results indicated that, for unheated samples, degreasing followed by scratch-brushing was superior; the shear strength for a given deformation was greater than for the other preparations. The minimum deformation required to produce a measurable bond strength

(40% for aluminum) was lower. The heated specimens, electropolished or machined, displayed higher bond strengths than those not preheated but not as high as scratch-brushed composites. The authors attribute the effect of heating and cooling in a desiccator to the removal of adsorbed contaminants. Baking-out the specimens in air or vacuum (5×10^{-3} mm Hg) to as high as 600°C indicated that the bake-out atmosphere (air or vacuum) had little influence on bond strength at a constant 60% deformation, although the higher temperatures produced greater bond strengths. Bake-out at 600°C and 60% deformation produced a bond shear strength (4.5 tons/sq.in.) less than that of similarly prepared but scratch-brushed aluminum specimens (6 tons/sq.in.), implying factors other than contamination play an important role. Samples of anodized aluminum (thick oxide layer) would not bond even with 80% deformation. If, however, these were baked at 500°C and cooled in a desiccator, they indicated a good bond above a threshold deformation of about 50%, but not as good as that achieved after scratch-brushing. Thick oxides do not completely deform as one as illustrated by microscopic examination while thin oxides do after scratch brushing, and thick oxides therefore result in a lower percentage area of metal-to-metal contact and a lower strength. Similarly it was observed that the other sample preparations, without final scratch-brushing, produced thin oxide layers which broke up independently and reduced the area of metallic aluminum contact. Parallel studies of surface preparation and oxide formation were made using copper to correlate with the results on aluminum. Generally the same results were obtained. However, with thick oxide layers, the threshold deformation was about 60% compared to about 45% for a scratch-brushed copper couple, a difference of 15%. This same difference for

anodized versus scratch-brushed aluminum was about 10%. The disparity between the changes in threshold deformations of copper and aluminum couples was ascribed to irregular fracture characteristics of massive copper oxide which effectively reduced the area of metallic copper contact to a greater extent than for the aluminum. In the anodized aluminum, the thick oxide fractured into separate, rectangular blocks. When the interfacial oxides broke up as a single layer, metallographic inspection showed the total length of the fractured oxide particles along the interface equalled the original length of the specimens. In another study (22) the authors examined the effect of temperature. The specimens were cleaned, scratch-brushed, and seam-welded along the outside edge of the composites to prevent high temperature oxidation. Bond strength as a function of deformation was determined for aluminum, Armco iron, magnesium, and zinc. For aluminum, the threshold deformation decreased from 40% at room temperature to 5% at 600°C. Further, at room temperature, the oxide broke up with the hard, worked, scratch-brushed layer and bonding of relatively soft bulk aluminum occurred whereas at elevated temperatures, bonding occurred between the work hardened surfaces resulting in higher shear strengths. Armco iron achieved a bond strength equal to the strength of the solid metal at 900°C and 14% deformation and metallographically displayed recrystallization and grain growth of the scratch-brushed region during the heating period prior to rolling. Inexplicably low bond strengths were developed with magnesium between 400 and 600°C. Similar results were obtained with zinc as with magnesium and at room temperature the scratch-brushed layers displayed brittleness in some regions and ductility in others. The authors suggest that the weaker bonding of the hexagonal metals,

magnesium and zinc, is due to independent break-up of the oxide layer. This independent fracture tendency is related, by the authors, to relative motion of the surfaces during rolling caused by the strongly orientation-dependent deformation behavior of the hexagonal metal structures.

It is suggested that the ease of solid welding is related to atomic mobility, and therefore to a reduced or homologous temperature (ratio of a welding temperature to the melting temperature, T_m). For the metals studied, the threshold deformation decreased with increasing temperature until about one-half of the melting point ($0.5 T_m$) where, for the scratch-brushed cubic metals, the threshold deformation decreased rapidly with further increase in temperature. This follows from the fact that above $0.5 T_m$, fine grained and ductile layers bonded. This behavior was not seen with the hexagonal metals.

In a study of pressure welding of dissimilar metals (21), Milner et al review their earlier work and inject the metallurgical variable into their studies. It was found that, for single metal composites, longer times of bonding (lower roll speeds), greater oxygen solubilities of the metals at elevated temperatures (effectively increasing the area of metallic juncture), and increased metal purity all enhance the weld strength. Heat treatment after rolling generally improved the bond although with magnesium and silver, the weld was inexplicably destroyed by this procedure. When dissimilar metals were roll bonded, relative movement occurred at the interface due to differing hardnesses and deformation behavior of the specimens. This tended to lower the threshold deformation but did not affect the bond strength at high deformations. Therefore, high deformations were used for roll bonding of dissimilar

metal couples. Roll bonding of miscible metals produced strong welds, but with subsequent heat treatment at elevated temperatures several systems (Cu-Ni, Fe-Ni) were considerably weakened by development of diffusional porosity near the interface. Immiscible cubic metal systems bonded readily, approaching the strength of the weaker metal at high deformations. A hexagonal metal in the couple (Cd-Fe) resulted in lower strength as experienced in autogenous bonding. Immiscible systems Cu-Pb and Cu-Mo displayed an increase in bond strength when subjected to post-heating. Couples forming intermetallic compounds produced divergent behavior depending on the nature of the compound. Brittle intermetallic layers were detrimental to the bond when thick but had little influence when thin. If the compound was ductile, the weld was strong, independent of thickness, and failure occurred in the weaker metal. In a more recent paper (20) the effects of surface contamination on roll bonding of aluminum couples at room temperature were considered in greater detail. These impurities, principally oxide and water vapor, are prime factors for the inability to weld by roll bonding techniques. This is proven, for example, by an experiment where high purity aluminum was baked out in vacuum at 500°C for 12 hours, machined in vacuum, and passed through the rolls (within 5 seconds after machining) in a vacuum of better than 10^{-4} mm Hg. The threshold deformation was 10% compared to 40% in earlier experiments in the atmosphere after scratch-brushing. It is believed that the threshold deformation is required in order to disrupt surface contaminants and allow metallic contact. Also suggested is the possibility of reaction bonding of aluminum and oxygen (of the water molecules) at the interface with the hydrogen entering into solution in solid aluminum. Milner and Rowe (19) have published an

excellent review on the state of the art of solid phase welding with 118 references.

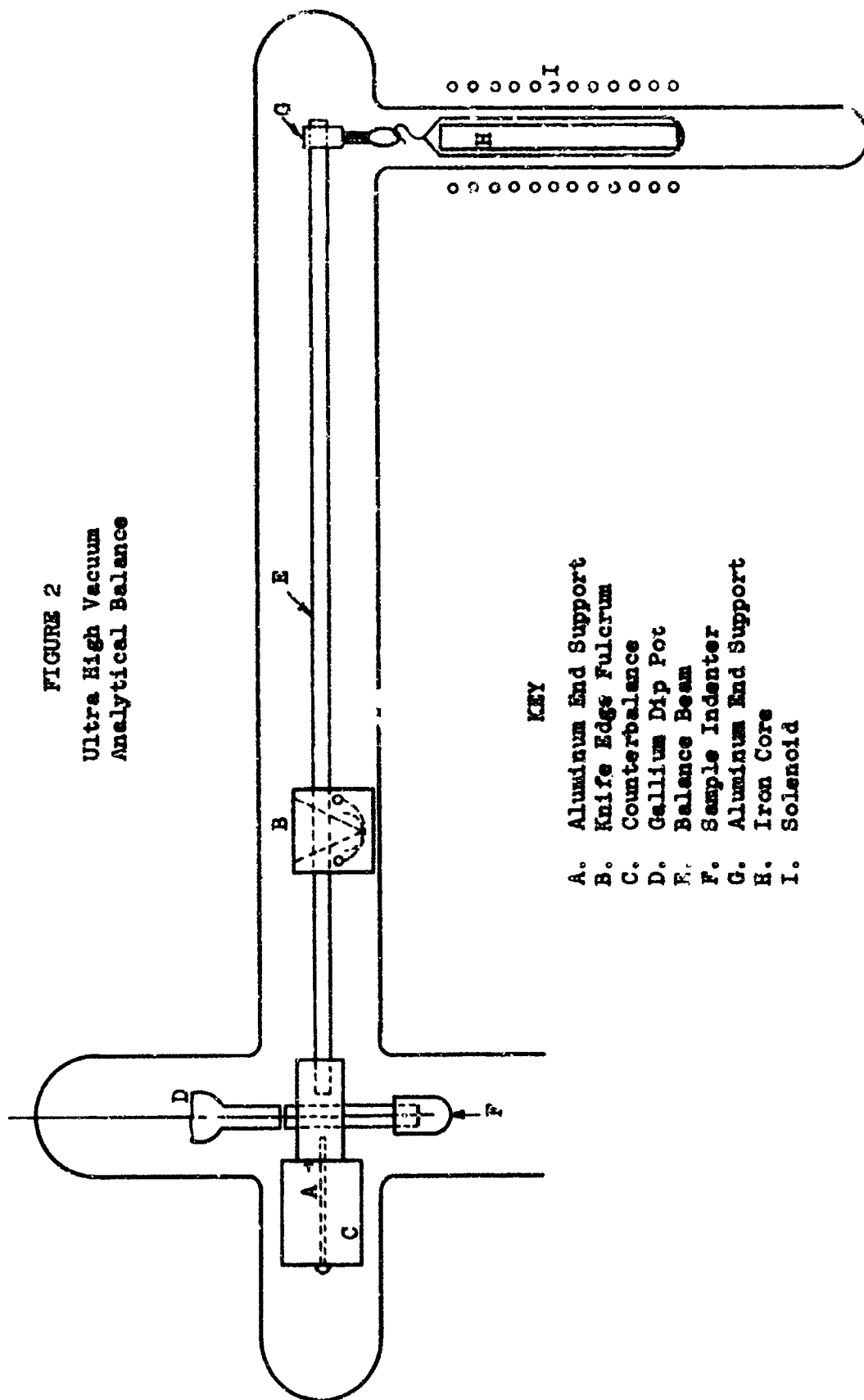
Although the data cited above does provide excellent information on the behavior of metal-metal contacts under the conditions of large normal or transverse loads which is invaluable for further correlation to wear and friction phenomena, the data does not lend itself to a clear interpretation which will be ultimately necessary for the development of a mechanism of adhesion. The existence of uncontrollable parameters due to surface contamination and macro-mechanical forces during the performance of an experiment to determine whether or not some variable is a significant factor in an adhesion mechanism could readily reverse the true outcome and provide a totally erroneous interpretation. In order to avoid these pitfalls an experiment was designed which involves the contact of atomically clean surfaces under a minimum of normal and tangential contact force, such that the electrical properties of such a junction could be measured and correlated with the normal load. Such information may provide a measurable quantity which could in turn be used to ascertain interfacial changes as time and temperature are varied.

III. EXPERIMENTAL

An apparatus to measure adhesion forces between atomically clean metallic surfaces with a minimum of compressive normal and tangential force, in ultra high vacuum, was designed and constructed as shown in Figures 2-7. The analytical balance (39,40) used to measure the forces of adhesion consisted of a $9/32'' \times 12''$ pyrex rod beam (E) as shown in Figure 2. Affixed to one end of this beam was an aluminum attachment (A) which supported the specimen indenter (F) and a 304 stainless steel counter weight (C). The other aluminum end fixture (G) supported an iron solenoid core (H) which was in turn sealed in a glass tube and hung from a 6 mil. tungsten wire. The balance beam was secured to a 304 stainless steel knife-edge fulcrum (B) which rested on a $1/2''$ semi-circular cylinder of pyrex tube (A) to reduce the rocking friction between the knife-edge (B) and the $5/8''$ stainless steel semi-circular cylinder support (C) as shown in Figure 3. The axis of the stainless steel support (C) was held in a fixed position normal to the beam axis by spot welding to a $1-1/2''$ stainless steel semi-circular cylinder (D) which was in turn secured concentrically to the vacuum cell housing (F) by its spring tension.

The heavy counterweight(C)of Figure 2 fastened to the balance beam, was included such that the fulcrum could be located nearer the sample while still retaining balance of the system. The fulcrum was positioned so that the sample end of the balance beam was only slightly heavier than the end supporting the solenoid core. This placement accomplished several objectives. Force multiplication through the solenoid-core magnetic coupling was improved, lateral movement of the sample due to similar motion of the core in the magnetic field was reduced, and the

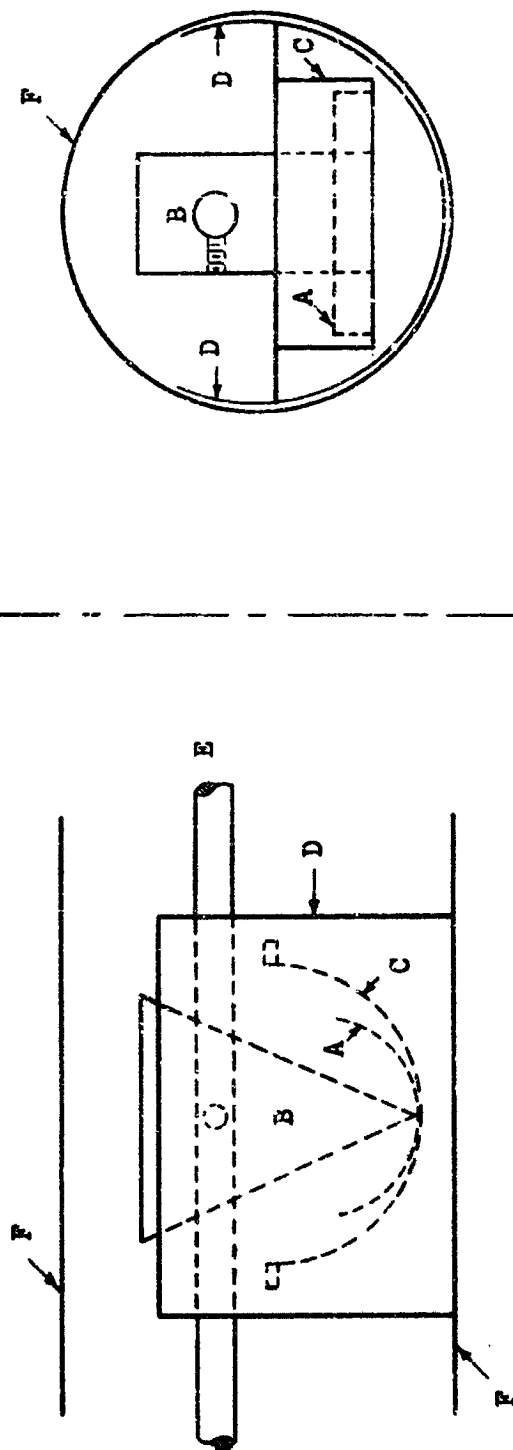
FIGURE 2
Ultra High Vacuum
Analytical Balance



KEY

- A. Aluminum End Support
- B. Knife Edge Fulcrum
- C. Counterbalance
- D. Gallium Dip Pot
- E. Balance Beam
- F. Sample Indenter
- G. Aluminum End Support
- H. Iron Core
- I. Solenoid

FIGURE 3
Balance Knife-Edge Fulcrum



KEY

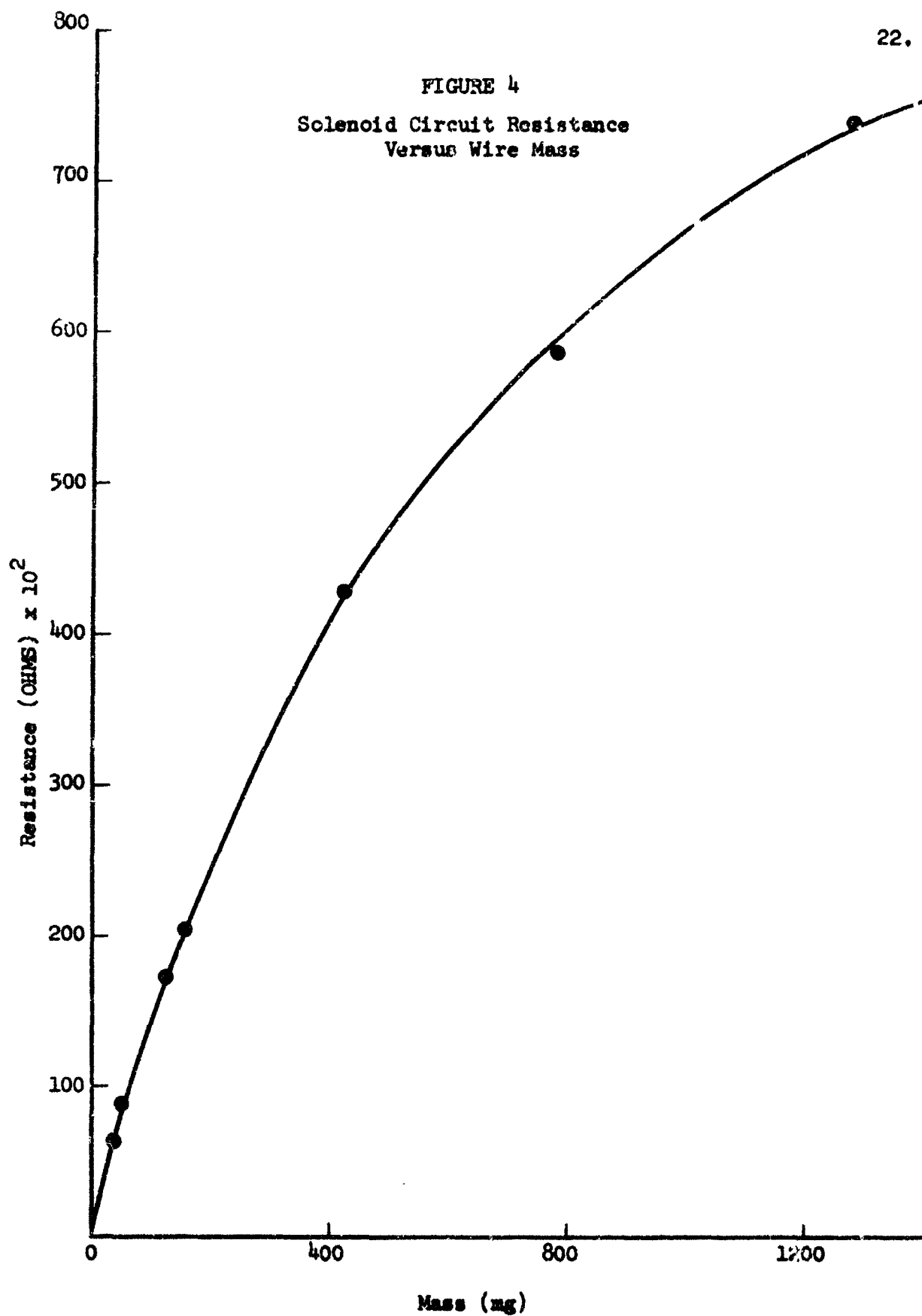
- A. Pyrex Bearing
- B. Stainless Steel Fulcrum
- C. Stainless Steel Bearing
- D. Stainless Steel Housing
- E. Balance Beam
- F. Vacuum Tube

stability of the beam assembly was enhanced. The greater mass somewhat reduced the sensitivity of the balance.

In its operation, the vertical force and motion of the indenter specimen in the balance assembly was controlled by magnetic coupling of a core within the system and an external solenoid. The solenoid was constructed of a $3/4$ " I.D. x 4 " thin walled brass tube wound with #24 Formvar coated copper wire to a total resistance of 5.206 ohms. The simple electrical circuit consisted of a 6 volt D.C. storage battery, switch, Model A ten turn-ten ohm precision Helipot potentiometer, and the solenoid connected in series. The Helipot was affixed with a turns-counting duo-dial which registered from 1 to 1000 as the circuit resistance was varied. Initially, the position of the solenoid relative to the core was adjusted such that the balance beam was horizontal and the indenter specimen vertical. The only physical contact of the balance beam assembly and the other apparatus at this stage was along the knife-edge of the fulcrum. Since the purpose of the balance was to measure contact force, the balance was calibrated by suspending wires of known mass from the indenter specimen and recording the corresponding circuit resistance required to return the balance beam to the initial balance position. A typical calibration curve is shown in Figure 4. After the specimens were brought into touch contact (as described in detail below) the Helipot resistance was slowly decreased from 10 ohms until the adhesion bonds were broken, the resistance value recorded, and the applied force read from the calibration curve.

The specimen plate (G), shown in Figure 5, was attached to an aluminum cylindrical platform (C) which was connected to the monel bellows vertical motion assembly (A) by a pyrex rod (B). In an earlier

FIGURE 4
Solenoid Circuit Resistance
Versus Wire Mass



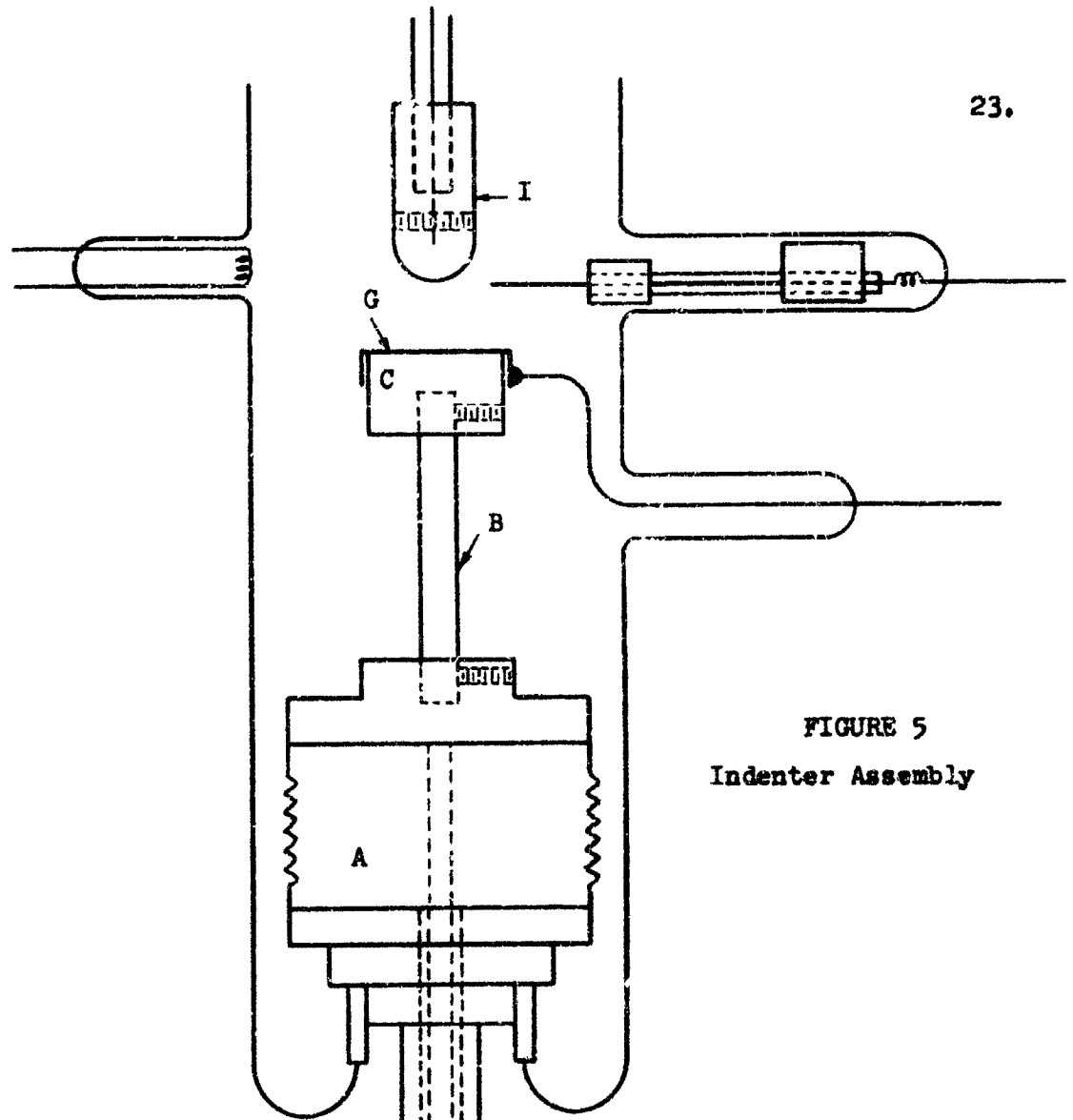
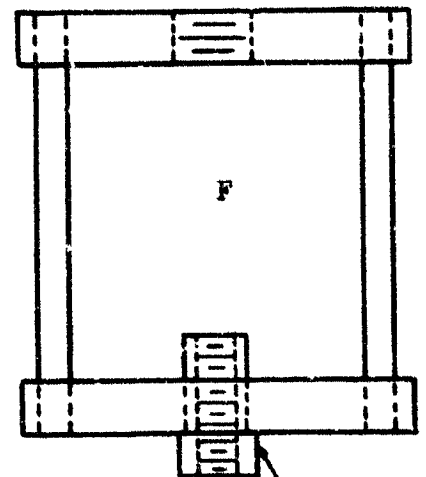


FIGURE 5
Indenter Assembly

KEY

- A. Monel Bellows
- B. Pyrex Rod
- C. Aluminum Platform
- D. Stainless Steel Tube
- E. Stainless Steel Rod
- F. Aluminum Frame
- G. Nickel Plate Sample
- H. Tension Nut
- I. Sample Indenter



experiment, the specimen holder consisted of a pyrex cup rather than a platform because the sample was indium (low-melting point) instead of nickel. Electrical contact to the outside of the vacuum cell was made by silver soldering a 30 mil OFHC copper wire to the nickel plate sample (G) and to the nickel wire of an electrical through seal.

A frame (F) was attached to the upper threaded tube (D) in the bellows unit and a tension nut (H) was screwed onto the threaded rod (E) which held the bellows in compression. Loosening the nut raised the specimen by allowing expansion of the bellows to its equilibrium length. If the specimen had to be moved closer to the indenter, a 1" micrometer head could be fastened into the frame by a set screw and extended to expand the bellows vertically. The total distance over which the specimen could be moved was about $3/4$ ".

The vacuum pumping system as shown schematically in Figure 6 consisted of a Welsh Duo Seal mechanical pump (A), a two stage CVC oil diffusion pump (B) with a liquid nitrogen trap (T_1), and a three stage Kontes (Model No. K-92475) mercury diffusion pump (C) which also had a built-in liquid nitrogen trap (T_3). The pressure between the diffusion pumps was measured with a CVC (GPH-100A) discharge gauge (D), capable of measuring to 1×10^{-7} Torr and separated from the mercury diffusion pump by a liquid nitrogen trap (T_2). Bakeable liquid nitrogen traps (T_4 and T_5), 2" O.D. by 11" long, led to a standard ball and socket ground glass valve (H) enlarged in Figure 7, which could be opened or closed by coupling to a magnetic rod (A) sealed in a glass tube which in turn was attached to the upper portion of the valve. The valve was held in an open position by a second magnetic bar (B), also sealed in pyrex and resting in a horizontal side arm.

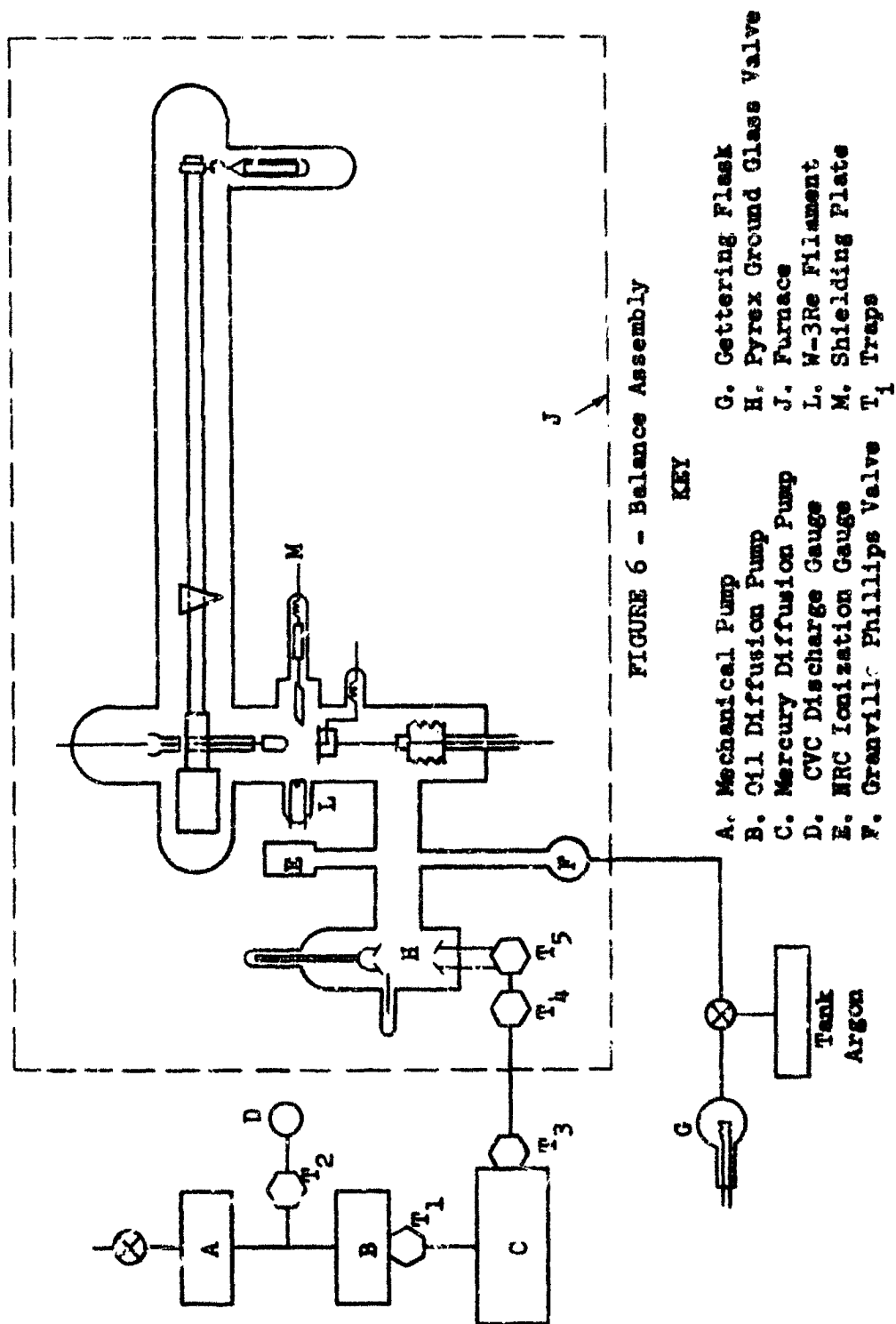
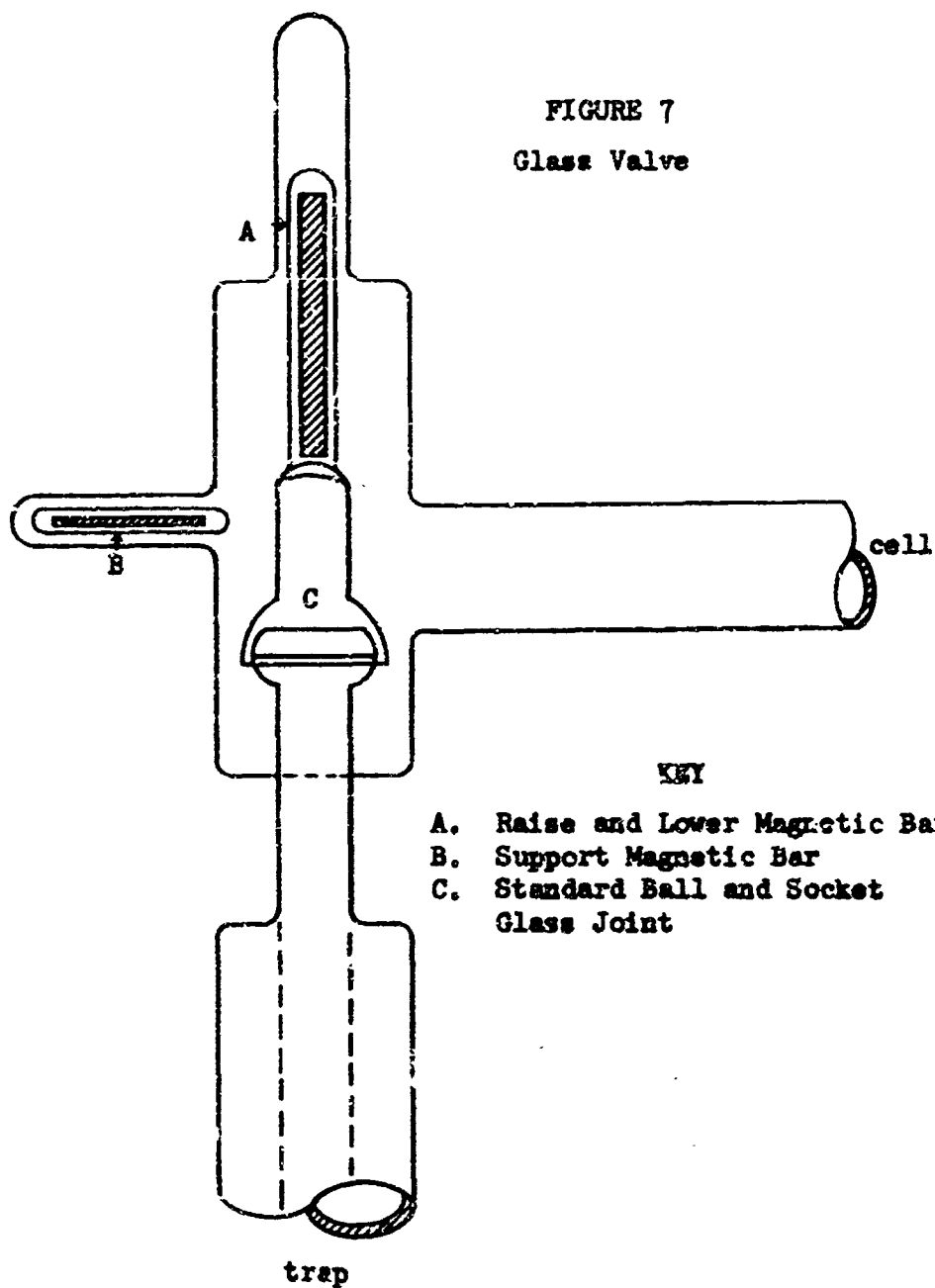


FIGURE 7
Glass Valve



During an experimental run, the system was evacuated with the mechanical pump for a few minutes after which time the oil diffusion pump was turned on when the pressure was reduced to below 1×10^{-5} Torr. The mercury diffusion pump was then slowly heated to its operating temperature which usually required several hours. At this point the discharge gauge (D) pressure was below 1×10^{-6} Torr and the pressure near the glass valve as measured by a hot cathode Bayard-Alpert type gauge (E) (ERC 553-P and 753), was usually below 1×10^{-5} Torr. For outgassing the components of the apparatus, as shown in Figure 6, an 18" x 18" x 24" furnace (J) was constructed of ground glass insulation material held in an aluminum frame and covered internally with a triple layer of aluminum foil. Heating was accomplished by ten 230 volt, 500 watt Chromalox strip heaters connected in parallel to a 220 volt line through a 230 volt Variac (Type W5CHM) autotransformer. The system, with all of the vacuum pumps in full operation, was then baked out for at least 10 hours at 450°C . After the furnace was turned off and removed, dewars were filled with liquid nitrogen and placed around traps (T_4) and then (T_5) while the glass was still warm. The type C Granville-Phillips valve (F), also baked out, was then closed.

Tank argon was admitted to a 500 ml. gettering flask (G) following the evaporation of pure barium from Barex getters (King Laboratories, Syracuse, N.Y.). Gettering of the argon for several hours over barium removed active gases, water, and other active impurities by chemical reaction and sorption. When the cell pressure was at least 1×10^{-8} Torr, and the glass valve (H) was closed, the pure argon was admitted continuously through the Granville-Phillips valve (F) to a constant system pressure of about 8×10^{-4} Torr. The specimens were then argon

ion bombarded at 3 KV and less than 50 ma. with an Allen Jones rectified D.C. power supply by attaching the negative lead to the specimen and the positive lead to a magnetically movable shielding plate (M), placed between the specimens in order to prevent surface contamination of one specimen while the other was being bombarded. This cleaning process was continued until each specimen had a brilliant appearance. Visual observation of the specimens was impaired by metal atoms which condensed on the pyrex cell wall. Following bombardment, the Granville-Phillips valve was closed and the system re-evacuated to below 1×10^{-8} Torr. An AC potential was then supplied to a tungsten - 3% rhenium coiled filament (L) and the specimens were stripped of adsorbed argon ions by electron bombardment. When both samples had cooled and the pressure returned to 1×10^{-8} Torr or lower, the indenter and plate were brought into nearly forceless contact with the balance beam visually horizontal and the plate raised with the vertical motion assembly. The current was slowly raised in the solenoid until contact was broken. Following each run, visual and metallographic inspection was made of the indenter and plate and the balance was re-calibrated.

IV. DISCUSSION

The first experiment, using an electropolished aluminum hemispherical indenter and a pyrex cup of indium, failed for two reasons. During the bake-out cycle, in which a temperature of 460°C was achieved, a leak developed after approximately 15 hours in a welded portion of the bellows unit. The bellows was successfully repaired by silver soldering. Secondly, after the furnace had been turned off, the indenter was found to be grossly deformed, having an enlarged appearance. Subsequent sectioning of the specimen provided no clues to the cause of this deformation. In the second experiment, using a conical aluminum indenter and indium, several new problems arose. It was found that the fluoride flux used for silver solder joining of the copper wires in the vacuum cell outgassed heavily leaving an evaporated deposit on the walls of the cell which caused undue contamination in the system. It was decided, therefore, to silver solder without flux or to fusion weld with a reducing oxygen-acetylene flame in future work. Argon ion bombardment cleaning of the aluminum was rather unsuccessful and ion bombardment of the indium could not be completed due to melting of the 10 mil OFHC copper wire electrical lead. 30 mil wire was installed following in the run. The long, semi-circular shaped, coiled tungsten-3% rhenium electron bombardment filament sagged when heated and cracked the cell wall. Improvement was made by incorporating a shorter coiled filament.

The second experiment did show, however, that the glass valve arrangement could be operated successfully at system pressures below 8×10^{-9} Torr. For the present experiment, a copper (99.999%) indenter and a nickel (99.97%) plate are being studied. The copper was electropolished and the nickel polished on 4/0 paper just prior to their

installation into the vacuum cell. Both metals have been shown to be easier to clean than aluminum by argon ion bombardment. Also the nickel-copper phase diagram displays complete solid solubility (36) and should adhere on the basis of a solid state miscibility criterion. The related concept of atomic size factor (13) is favorable to adhesion in this situation (about 3%). The applicability of this factor was mentioned before in consideration of the research by Keller (1,2,3) and Sikorski and Courtney-Pratt (10) and is supported additionally by Johnson (37).

In the current experiment, a mixture of dry ice and methanol is used to cool methanol which in turn is circulated through the water cooling chambers of the mercury diffusion pump instead of cold water. Tasman (41) has shown that through this procedure the efficiency of the diffusion pump is increased significantly and the ultimate pressure capability of the pumping system is improved.

A description of the construction of the balance beam assembly was presented earlier; however, a discussion of this portion of the apparatus is in order. It was found that when a magnetic field was applied to the solenoid core, the core, as well as being pulled vertically downward, was drawn laterally against the tubular glass cell wall. Consequently, vertical motion of the indenter specimen was impeded and tangential forces would also be applied to the specimens in contact. After several trials of various magnetic coupling arrangements and geometries were tested without satisfactory results, the original design of the solenoid and core components was selected with the inclusion of the counterweight. This design reduced lateral motion to negligible amounts and improved the balance performance as mentioned earlier.

V. BIBLIOGRAPHY

- 1) Keller, D.V., "Adhesion Between Atomically Clean Surfaces", NASA, Technical Note D-2228, 1963
- 2) Spalvins, T., and Keller, D.V., "Adhesion Between Atomically Clean Surfaces", Trans. Vac. Met. Conf. 1962, ed. R. Bunshah, Pub. Amer. Vac. Soc., Boston (1963)
- 3) Keller, D.V., "Adhesion Between Solid Metals", Wear, 6 (1963) 353-365
- 4) Bowden, F.P., "The Adhesion of Metals and the Influence of Surface Contamination and Topography", Adhesion and Cohesion, 1961, ed. P. Weiss, Elsevier Pub. Co., N.Y., 1962
- 5) Bowden, F.P., and Tabor, D., "The Friction and Lubrication of Solids", Part II, Oxford University Press, 1964
- 6) Anderson, O.L., "Laws of Adhesion", Journal of Applied Physics, 30, 4 (April, 1959) 593-4
- 7) Andreatch, P., and Anderson, O.L., "New Device for Measuring the Adhesion Between Metallic Rods", The Review of Scientific Instruments, 30, 6 (1959) 458-9
- 8) Anderson, O.L., "The Role of Surface Shear Strains in the Adhesion of Metals, Part I", Wear, 3 (1960) 253-73
- 9) Sikorski, M.E., "Correlation of the Coefficient of Adhesion With Various Physical and Mechanical Properties of Metals", Transactions of the ASME, Journal of Basic Engineering, Ser. D 85 (June, 1963) 279-285
- 10) Sikorski, M.E., and Courtney-Pratt, J.S., "Adhesion of Rare Earth Metals", ASLE Transactions, 1 (1964) 73-81
- 11) Sikorski, M.E., "The Adhesion of Metals and Factors that Influence It", Bell Tel. Labs, Inc., Murray Hill, N.J., 1963
- 12) Cottrell, A.H., "Dislocations and Plastic Flow in Crystals", The International Series of Monographs on Physics, Oxford University Press, 1953, p. 157
- 13) Hume-Rothery, W., "Atomic Theory for Students of Metallurgy", The Institute of Metals, London, 1960, p. 361
- 14) Clark, D.S., and Varney, W.R., "Physical Metallurgy for Engineers", D. Van Nostrand Co., Inc., Princeton, N.J., 1959, p. 343
- 15) Hume-Rothery, W., and Raynor, G.V., "The Structure of Metals and Alloys", The Institute of Metals, London, 1962

BIBLIOGRAPHY (Cont'd.)

- 16) Anderson, O.L., "Adhesion of Inorganic Solids", Bell Tel. Labs, Inc., Murray Hill, N.J.
- 17) Rabinowicz, E., "Influence of Surface Energy on Friction and Wear Phenomena", Journal of Applied Physics, 32, 8 (1961) 1440-4
- 18) Tabor, D., "Junction Growth in Metallic Friction: Role of Combined Stresses and Surface Contamination", Proc. Roy. Soc., A251 (1959) 378-93
- 19) Milner, D.R., and Rowe, G.W., "Fundamentals of Solid Phase Welding", Metallurgical Reviews, 7, 28 (1962) 433-480
- 20) Nicholas, M.G., and Milner, D.R., "Roll Bonding of Aluminum", British Welding Journal, 9 (1962) 469-75
- 21) McEwan, K.J.B., and Milner, D.R., "Pressure Welding of Dissimilar Metals", British Welding Journal, 9 (1962) 406-20
- 22) Nicholas, M.G., and Milner, D.R., "Pressure Welding by Rolling at Elevated Temperatures", British Welding J., 8 (1961) 375-83
- 23) Vaidyanath, L.R., and Milner, D.R., "Significance of Surface Preparation in Cold Pressure Welding", British Welding J., 7 (1960) 1-6
- 24) Bowden, F.P., and Rowe, G.W., "The Adhesion of Clean Metals", Proc. Roy. Soc., A233 (1956) 429-42
- 25) MacDonald, D.K.C., "Thermoelectricity: An Introduction to the Principles", John Wiley and Sons, Inc., New York, 1962
- 26) "Adhesion and Cohesion", Ed. P. Weiss, Elsevier Pub. Co., Amsterdam, The Netherlands, 1962
- 27) Domenicali, C.A., "Irreversible Thermodynamics of Thermoelectricity", Reviews of Modern Physics, 26, 2 (April, 1954) 237-275
- 28) Gregg, S.J., "The Surface Chemistry of Solids", Reinhold Publishing Corp., N.Y., 1961
- 29) Sparsnaay, M.J., Physica, 24 (1958) 751
- 30) Black, W., de Jongh, J.G.V., Overbeek, J.T., and Sparsnaay, M.J., "Measurements of Retarded van der Waals Forces", Trans. Faraday Soc., 56 (1960) 1597-1608
- 31) Kitchenor, J.A., and Prosser, A.P., "Direct Measurement of the Long-Range van der Waals Forces", Proc. Roy. Soc., 242 (1957) 403-9

BIBLIOGRAPHY (Cont'd.)

- 32) Dekker, A.J., "Solid State Physics, "Prentice-Hall, Inc., Englewood Cliffs, N.J., 1958
- 33) Darken, L.S., and Gurry, R.W., "Physical Chemistry of Metals", McGraw-Hill Book Co., Inc., N.Y., 1953
- 34) Kittel, C., "Introduction to Solid State Physics", John Wiley and Sons, Inc., 1961
- 35) "The Surface Chemistry of Metals and Semiconductors", Edited by H.C. Gatos, John Wiley and Sons, Inc., N.Y., 1960; Symposium, Columbus, Ohio, 1959
- 36) Hansen, M., "Constitution of Binary Alloys", Second Edition, Metallurgy and the Metallurgical Engineering Series, McGraw-Hill Book Co., Inc., N.Y., 1958, p. 601
- 37) Johnson, R.L., "NASA Design Criteria", NASA, Lewis Research Center, Cleveland, Ohio, 1963
- 38) Farnsworth, H.E., and Winch, R.P., "Photoelectric Work Functions of (100) and (111) Faces of Silver Single Crystals and Their Contact Potential Difference", Physical Review, 58 (Nov. 1, 1940) 812-19
- 39) Gordon, S., and Campbell, C., "Automatic and Recording Balances", Analytical Chemistry, 32, 5 (April 1960) 271R-289R
- 40) Kraus, D.L., Petrocelli, A.W., and Price, J.C., "An Inexpensive Null Reading Torsion Balance", Anal. Chem., 33, 3 (March, 1961) 479-80
- 41) Tasman, H.A., and Babeliowsky, T.P.J.H., Rev. Sci. Instr., 33, 872 (1962)